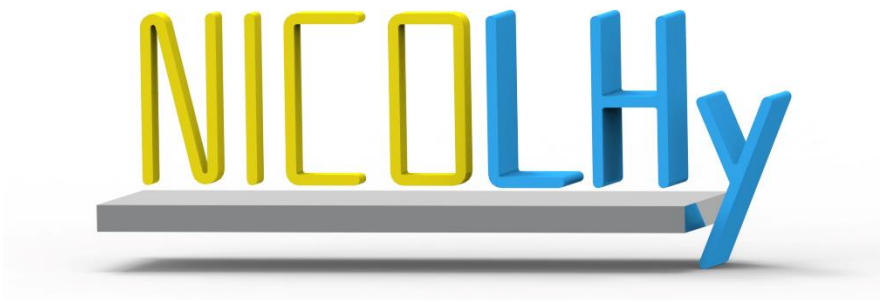

NICOLHy - Novel Insulation Concepts for LH_2 Storage Tanks

Project deliverable

D1.1 LH_2 storage tank and insulation technologies, applications, and standards

Project duration	January 2024 – December 2026
Contractual date of delivery	31/12/2024
Date of delivery	30/12/2024
Reporting class	Public (PU)
Editor:	Alessandro Campari (NTNU)
Contributors	Hederson Nascimento (NTNU), Lucas Claussner (NTNU), Davide Rescigno (NTNU), Federico Ustolin (NTNU), Agnieszka Dzielendziak (DLR), Bright Okpeke (DLR), Robert Eberwein (BAM)
Deliverable status	Approved

Co-funded by the European Union

Clean Hydrogen Partnership

NICOLHy project No. 101137629 is funded by the European Union. Views and opinions expressed are however those of the author(s) only and do not necessarily reflect those of the European Union or Clean Hydrogen JU. Neither the European Union nor the granting authority can be held responsible for them.

Document Revisions:

Version	Date	Editor	Overview
1.0	08.12.2024	Alessandro Campari	First Draft
2.0	18.12.2024	Robert Eberwein	Review
3.0	26.12.2024	Federico Ustolin	Review
4.0	27.12.2024	Alessandro Campari	Final Draft

Approvals:

Version	Date	Name	Organization
1.0	30.12.2024	Consortium	BAM, UniBo, DLR, NTNU, NTUA

The NICOLHy Consortium:

Participant No.	Short name	Country
1 (Coordinator)	BAM	Germany
2	UniBo	Italy
3	DLR	Germany
4	NTNU	Norway
5	NTUA	Greece

Content

Abbreviations:

ANSI	American National Standards Institute
BAM	Bundesanstalt für Materialforschung und -prüfung
BCC	Body-centered cubic
BM	Base metal
BOG	Boil-off gas
BOR	Boil-off rate
CEN	European Committee for Standardization
CGA	Compressed Gas Association
CSP	Cryogenic spillage protection
DBT	Ductile-to-brittle transition
DBTT	Ductile-to-brittle transition temperature
DLR	Deutsches Zentrum für Luft- und Raumfahrt
DN	Diameter nominal
EIGA	European Industrial Gases Association
EN	European Standard
EP	Expanded perlite
EPM	Ethylene propylene rubber
EPS	Expanded polystyrene
EU	European Union
FCC	Face-centered cubic
FCGR	Fatigue crack growth rate
GCT	Graphite covering tapes
GHG	Greenhouse gases
GWP	Global warming potential
HAZ	Heat-affected zone
HAZID	Hazard identification
HCP	Hexagonal close-packed
HE	Hydrogen embrittlement
HFC	Hydrofluorocarbon
HFO	Hydrofluoroolefin
HGM	Hollow glass microsphere
HIFD	High-insulation fire doors
HySTRA	Hydrogen energy Supply-chain Technology Research Association
HSN	Hollow silica nanospheres
IMO	International Maritime Organization
IRAS	Integrated refrigeration and storage
ISO	International Organization for Standardization
JU	Joint Undertaking

KSOE	Korea Shipbuilding & Offshore Engineering
LH_2	Liquid hydrogen
LN_2CS	Liquid nitrogen-cooled shield
LNG	Liquefied natural gas
LPG	Liquefied petroleum gas
MAWP	Maximum allowable working pressure
MLI	Multi-layer insulation
MLVI	Multi-layer vacuum insulation
MS	Milestone
NASA	National Aerospace Agency
NASDA	National Space Development Agency of Japan
NNT	Normalization, normalization, and tempering
NTNU	Norwegian University of Science and Technology
NTUA	National Technical University of Athens
ODP	Ozone depletion potential
PCTFE	Polychlorotrifluoroethylene
PGM	Porous glass microsphere
PN	Pressure nominal
PIR	Polyisocyanurate
PRV	Pressure relief valve
PS	Polystyrene
PSV	Pressure safety valve
PTFE	Polytetrafluoroethylene
PU	Polyurethane foam
PWHGM	Hollow glass microspheres with porous walls
QLT	Quenching, lamellarizing, and tempering
QT	Quenching and tempering
RBI	Risk-based inspection
RCS	Regulations, codes, and standards
RLG	Refrigerated liquified gas
SDO	Standard development organization
SGM	Solid glass microsphere
SOFI	Spray-on foam insulation
SPF	Spray polyurethane foam
TPS	Thermal protection system
TVS	Thermodynamic ventilation system
UniBo	Alma Mater Studiorum - Università Di Bologna
UTS	Ultimate tensile strength
VCS	Vapor-cooled shield

VDMLI	Variable density multi-layer insulation
VIP	Vacuum insulation panel
WP	Work package
WZ	Weld zone
XPS	Extruded polystyrene
YAS	Yttrium-aluminosilicate glass
YS	Yield strength

1 Introduction

As the world transitions toward sustainable energy sources, hydrogen has emerged as a key player in the clean energy landscape due to its versatility and potential for widespread application [1]. Liquid hydrogen (LH_2) offers a promising solution for large-scale energy storage and transportation, owing to its high energy density. However, the storage and transport of LH_2 pose significant technical challenges, primarily due to its extremely low boiling point of –253 °C [2], which demands advanced cryogenic storage systems. Large-scale LH_2 storage is crucial for establishing a robust hydrogen economy. However, upscaling the storage technology poses several hurdles. The existing technologies used in small and medium-sized storage systems are not suitable for large-scale applications due to long production times, low failure tolerance, and the limitations of spherical tank designs, which can reduce payload efficiency by up to 50 % [3].

The NICOLHy project is at the forefront of addressing these challenges by developing a novel insulation concept based on vacuum insulation panels (VIP). This innovative approach aims to enable the safe, cost-effective, and energy-efficient storage of large quantities of LH_2, with capacities ranging from 40’000 m³ to over 200’000 m³. This project seeks to overcome the existing limitations of LH_2 tanks by developing a modular, open-form storage system that is time- and cost-efficient across production, operation, and service phases. The system is designed to be multi-failure tolerant and applicable for both onshore and offshore installations [3].

Deliverable D1.1 provides a comprehensive state-of-the-art analysis of LH_2 storage systems, with a focus on their application in long-distance delivery, such as in the shipping sector, and large-scale onshore storage. The analysis encompasses a variety of insulation techniques, tank construction methods, and the various components that contribute to the overall efficiency and safety of LH_2 storage systems. Additionally, the document reviews existing standards and guidelines relevant to the design, operation, and safety of these systems.

The document is structured as follows. Section 7 provides various examples of existing large-scale LH_2 storage tanks, indicating the facilities under construction and in the design phase. In particular, it explores the critical role of large-scale vessels in enabling long-distance transportation and large-scale hydrogen storage. Section 3 deals with the technical characteristics of LH_2 tanks, specifying the design characteristics and technical and operational requirements of stationary tanks and maritime vessels. Considering the importance of proper material selection for safety-critical applications, a comprehensive overview of the materials suitable for hydrogen environments at cryogenic temperatures. Section 4 discusses both passive insulation and active cooling systems. It includes detailed analyses of common insulating materials such as perlite, glass bubbles, aerogel, spray-on foam insulation, multi-layer insulation, and vacuum-insulation panels. In addition, this section outlines the main benefits and limitations of vapor-cooled shields. Section 5 is dedicated to the ancillary components for LH_2 storage tanks, such as cryopumps, valves, pressure relief devices, pipes, and flexible hoses. This equipment, whether permanently or temporarily connected to the tank, allows the safe and efficient operations of the storage system. Finally, Section 6 thoroughly reviews the standards and guidelines governing LH_2 storage systems. This includes guidelines and codes related to the design and operation of storage tanks, accessories used in cryogenic systems, the material requirements for these components, and specific regulations for large-scale storage systems for refrigerated liquified gases and vacuum insulation panels. By

examining these standards, the document aims to highlight the regulatory framework that must be adhered to in the development and operation of the novel insulation concepts for LH_2.

The insights gathered in this document aim to inform other work packages within the NICOLHy project, supporting the development of a more efficient, cost-effective, and safer LH_2 storage solution.

2 Applications of large-scale LH_2 storage tanks

Large-scale liquid hydrogen storage tanks can be classified into two main categories based on their field of application:

- Tanks for stationary storage
- Tanks for mobile storage and transport

The former category refers to applications where the tank's location remains unchanged for the entire operating life of the equipment. The latter mostly refers to maritime applications, where the tank is moved from one location to another to transport LH_2. This section addresses the existing, under construction, and development LH_2 tanks with volumes larger than 500 m^3, highlighting their main characteristics and focusing on the thermal insulation systems and their performance [4].

Two identical spherical double-walled vessels with capacity of 540 m^3 and diameter of 12.6 m are located at the Tanegashima Space Center in Japan. They were developed by Kawasaki Heavy Industry in the 1980s and operated for more than 30 years without any signs of degradation in the thermal insulation performance. These tanks are insulated with vacuumed perlite. The shapes and positions of the support structures were optimized to minimize the contact surface between the inner and outer shell and reduce the conductive heat transfer [5].

Currently, two identical liquid hydrogen storage tanks are located at the Launch Complexes 39 A and B of the Kennedy Space Center (Florida, USA) to support the Apollo Program. These tanks, built by Chicago Bridge and Iron in 1965, are spherical, double-walled structures with perlite powder insulation kept under high-vacuum conditions. These tanks offer a storage capacity of 3'800 m^3 each. The outer jacket, made of carbon steel, has an inner diameter of 21.6 m, while the inner shell, made from austenitic stainless steel, measures 18.7 m in diameter [6]. The ullage reduces the usable LH_2 storage volume to 3'200 m^3. The tanks are designed to maintain a maximum boil-off rate of 0.0625 mass% per day at an operating pressure of 6.2 bar [7]. In 2001, an increased boil-off rate was detected and attributed to a perlite void in the annulus (most likely due to an error during construction). In response, NASA's Cryogenics Test Lab conducted extensive research on developing economic and reliable superinsulation materials [8]. A system based on glass bubbles demonstrated a 46 % boil-off rate reduction compared to perlite during field testing. Due to their durability against vibration and thermal cycling, the glass bubbles have been chosen for the new LH_2 storage tank currently being built at NASA [9][10].

The new 4'700 m^3 spherical LH_2 storage tank is currently under construction and will support the Artemis mission to the moon. The inner shell, exposed to cryogenic temperatures, is made of SA240 Grade 304 stainless steel, while the outer jacket is constructed from SA516 Grade 70 carbon steel. This advanced tank incorporates two innovative, energy-efficient technologies: an insulation system based on hollow glass microspheres under high-vacuum and an integrated refrigeration and storage (IRAS) heat exchanger. The hollow glass microsphere insulation replaces the traditional perlite powder. Although not yet operational, the IRAS system should integrate a heat exchanger within the tank to remove heat from the stored hydrogen, thanks to an external helium cryocooler. This combination of highly effective passive thermal insulation and active cooling will achieve the target of zero boil-off storage [11].

In 2020, Kawasaki Heavy Industry completed the construction of a 2'500 m^3 spherical LH_2 storage tank with 10 % ullage and a usable capacity of 2'250 m^3 in the HyTouch terminal

located at Kobe Airport Island (Japan). This infrastructure was developed in the CO_2-free Hydrogen Energy Supply-chain Technology Research Association (HySTRA) project. This facility is the first LH_2 receiving terminal in the world and enables the unloading of large amounts of liquid hydrogen shipped from the delivery terminal in Hastings (Australia). This pilot plant proves the techno-economic viability of a long-distance and large-scale LH_2 supply chain. The tank employs a conventional perlite insulation system. The space between the inner shell and the outer jacket is filled with perlite powder before being evacuated to create a vacuum [12][13]. Schiaroli et al. [14] conducted a preliminary consequence assessment on this facility, highlighting how an instantaneous release from the liquid hydrogen storage tank is the worst-case scenario. Campari et al. [15] developed a risk-based inspection (RBI) plan for this plant and proved that the probability of failure of the LH_2 handling equipment remains almost constant over time.

In 2020, Kawasaki Heavy Industries revealed the completion of the basic design for an 11'200 m³ spherical LH_2 storage tank with 10 % ullage, capable of holding approximately 10'000 m³ of cryogenic fuel. The tank will feature a double-shell vacuum-insulated structure and is expected to achieve a daily boil-off rate of lower than 0.1 %. It was also announced that no cryogenic pumps will be required since the fuel transfer will be guaranteed by the self-pressurization of the tank, similarly to the existing technology at the HyTouch terminal [16].

In 2021, Shell, Chicago Bridge and Iron, and NASA have completed the design of three different double-walled, spherical storage tanks for liquid hydrogen with capacities of 20'000, 40'000, and 100'000 m^3 but has not provided additional detail regarding the characteristics of the tank and the insulation performance [17][18].

Figure 1 shows two spherical double-walled tanks for the stationary storage of LH_2, located at the Kennedy Space Center in Florida and the HyTouch plant in Japan and owned by NASA and Kawasaki Heavy Industry, respectively.

Figure 1: a) 3800 m^3 LH_2 tank at the Kennedy Space Center and b) 2500 m^3 LH_2 tank at the HyTouch facility in Kobe (adapted from [4]*)*

Maritime carriers are typically employed for long-distance, high-capacity transportation of liquid hydrogen. As part of the HySTRA project, Kawasaki Heavy Industries completed the construction of Suiso Frontier, the first ship designed specifically for LH_2 transport. The vessel is equipped with a cylindrical, double-walled LH_2 tank with a capacity of 1250 m³ [13]. The insulation system is based on MLI under high vacuum. Notably, the onshore storage system in the port of Kobe has a maximum capacity that is two times higher than that of the maritime

carrier. It can therefore store LH_2 for a period equivalent to two deliveries from Australia to Japan. Glass-fiber-reinforced plastic was used for the support structures to minimize heat transfer. The reported boil-off rate is under 0.4 mass% per day. Moreover, the boil-off gas is efficiently recondensed to avoid venting into the atmosphere [12].

In 2021, Kawasaki obtained the approval for a cargo containment system built on the design and safety technologies of the Suiso Frontier. The new 160'000 m³ LH_2 carrier will feature four 40'000 m³ storage tanks with self-supporting structures capable of withstanding thermal contractions. Notably, the tank capacity is comparable to that of conventional LNG carriers. The spherical tanks will be thermally insulated with a newly developed system capable of mitigating boil-off formation. Furthermore, the evaporated gas will efficiently power the ship through a dual-fuel propulsion system and a hydrogen-powered steam turbine. This large-scale vessel satisfies the requirements of the International Maritime Organization (IMO) specified in the Interim Recommendations for Carriage of Liquefied Hydrogen in Bulk. A risk assessment has already been conducted through the hazard identification method (HAZID) [19]. Additionally, Kawasaki recently released new information about this liquid hydrogen shipping vessel. The dimensions of the CC61H type carrier and the insulating materials were adapted to match the technical requirements of existing vessels. The integrity of the welded parts, the assembly, and the insulation system's performance were assessed. In addition, Kawasaki conducted tests by injecting, cooling, and heating inert gas using a tank prototype, achieving the expected performance [20]. As a result, the LH_2 carrier will become operational by the second half of the 2020s.

Several countries, including South Korea, France, Germany, and the Netherlands, have made significant progress in developing large-scale liquid hydrogen maritime carriers, gaining expertise in the technology for LNG cargos, and working to establish global technical standards [4]. In particular, Korea Shipbuilding and Offshore Engineering (KSOE) developed the concept of a ship with a capacity of 20'000 m^3 and is expected to build a fleet of 20 ships in the 2030s. In the early stage, these carriers will be fueled by LNG, but they will be powered by evaporated hydrogen once the technology is mature [21]. In addition, a new tanker is expected to transport green hydrogen from Scotland to Germany from 2027. The storage tank will have a capacity of 37'500 m^3 and a trapezium-shaped hull design. The carrier will be directly powered by hydrogen, achieving the zero-emission target [22].

As an example of LH_2 carriers, Figure 2 illustrates the Suiso Frontier carrier and the cargo container Kawasaki is currently developing and testing.

a) b)

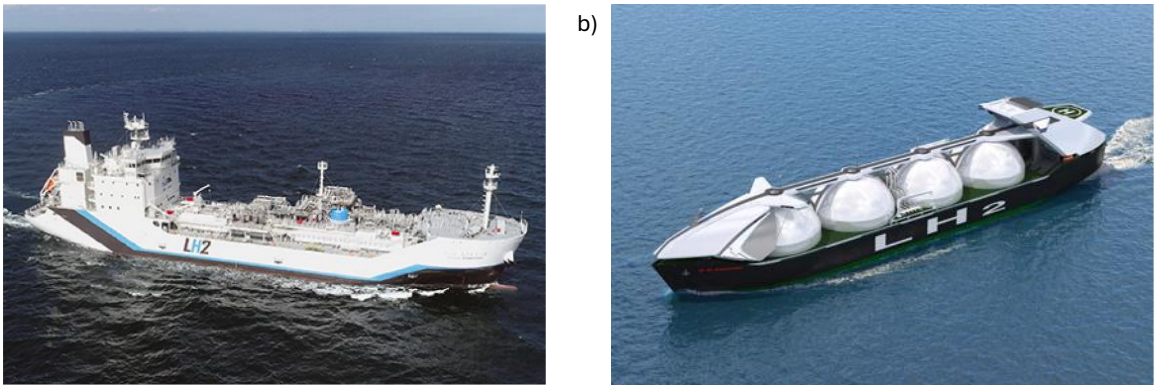

Figure 2: a) Suiso Frontier LH_2 carrier and b) the large-scale LH_2 carrier under development (adapted from [4] [19]*)*

Table 1 summarizes the LH_2 storage tanks currently available, in construction, and under development, specifying the location, size, boil-off rate (BOR), technical characteristics, and operational status.

Table 1: Summary of the existing large-scale LH_2 storage tanks for stationary and maritime applications

Location	Owner	Size [m^3]	BOR [mass%/d]	Characteristics	Status
Tanegashima Space Center, Japan	NASDA	540	-	Double-walled Spherical Inner tank 12.2 m in diameter Perlite powder under vacuum	Operative
Kennedy Space Center, USA	NASA	4’700	0.05	Double-walled Spherical Inner tank made of SA240 Grade 304 stainless steel Outer tank made of SA516 Grade 70 carbon steel Hollow glass microspheres at 1.3 Pa 10 % ullage Operating pressure of 6.2 bar IRAS heat exchanger to achieve zero boil-off External helium cryocooler	In construction
Kennedy Space Center, USA	NASA	3’200	0.0625	Double-walled (with gap 1.5 m thick) Spherical Inner tank made of stainless steel, 18.7 m diameter Outer tank made of carbon steel, 21.6 m diameter Perlite powder at 2 Pa	Operative
Kobe Airport Island, Japan	Kawasaki Heavy Industries (HyTouch)	2’250	-	Double-walled Spherical 10% ullage Perlite powder under vacuum	Operative
-	Kawasaki Heavy Industries	10’000	< 0.1	Double-walled Spherical Vacuum-insulated 10 % ullage	Design phase
-	Shell, McDermott, NASA	20’000	-	Double-walled Spherical Vacuum-insulated	Design phase
-	Shell, McDermott, NASA	40’000	-	Double-walled Spherical Vacuum-insulated	Design phase
-	Shell, McDermott, NASA	100’000	-	Double-walled Spherical Vacuum-insulated	Design phase

From Australia to Japan	Kawasaki Heavy Industries (Suiso Frontier)	1’250	0.4	Double-walled Cylindrical MLI under vacuum Supports of glass-fiber-reinforced plastic System to recondense boil-off gas	Operative
-	Kawasaki Heavy Industries	160’000		Double-walled Spherical Dual-fuel propulsion system Hydrogen-powered steam turbine	Testing phase
South Korea	KSOE	20’000		Double-walled Spherical Dual-fuel propulsion system (LNG and LH_2)	Design phase
From Scotland to Germany	-	37’500		Double-walled Trapezium-shaped Hydrogen-powered engine	Design phase

3 Description and design of LH_2 storage tanks

Large-scale storage tanks for liquid hydrogen are vital components in sectors like aerospace, maritime, energy, manufacturing, and process industries. The design of these tanks focuses on maintaining structural integrity and operational safety under extreme cryogenic conditions. Single and double-walled configurations are commonly used depending on the specific requirements of the storage system. Both configurations must account for the low-density nature of liquid hydrogen and the resulting high storage volumes, necessitating robust designs that can safely manage the large capacities involved. Section 3.1 is dedicated to the design criteria for large-scale cryogenic storage tanks. Section 3.1.3 delves into the hydrogen-metal compatibility requirements at cryogenic temperatures.

3.1 Design criteria and requirements

The storage of cryogenic fuels poses unique challenges, necessitating carefully designed tanks to ensure safety, efficiency, and sustainability. This section provides an in-depth description of the large-scale vessels currently used for cryogenic storage. It is organized into three subsections that focus on distinct applications: spherical tanks for stationary applications, large-scale cylindrical tanks for LNG, and maritime tanks intended for the large-scale transport of cryogenic fuels. Subsection 3.1.1 explores the design criteria for spherical LH_2 tanks, highlighting the importance of robust structural integrity and advanced thermal insulation techniques. It also outlines the operational requirements necessary to ensure safety in the handling and storage of hydrogen. Subsection 3.1.2 addresses large-scale LNG tanks, detailing the specific design elements that maintain structural integrity alongside operational protocols that enhance safety and monitoring. Finally, Subsection 3.1.3 investigates the unique considerations for maritime tanks.

3.1.1 Spherical tanks for stationary applications

Spherical tanks are frequently used for cryogenic storage due to their favorable thermal performance and structural integrity characteristics. In many applications, these features make them the preferred choice over other geometries, such as cylindrical and prismatic. One of the primary advantages of spherical tanks is their surface-to-volume ratio. They have the lowest surface area for a given internal volume compared to other shapes, significantly minimizing heat transfer with the external environment and reducing boil-off losses. Nevertheless, the surface-to-volume ratio changes dramatically with the sphere radius. As a result, a spherical shape is crucial to minimize the heat transfer in small tanks, but for larger systems this requirement progressively loses importance. [23], [24]. When operated at atmospheric pressure, spherical tanks exhibit much lower boil-off rates for LH_2 compared to cylindrical tanks. This efficiency derives from their reduced heat absorption under near-equilibrium conditions, mainly attributed to the smaller surface area [24].

Additionally, the stress distribution in spherical tanks is uniform across their surface, allowing them to withstand high internal pressures even with relatively thin walls. This uniform stress distribution enhances structural integrity and reduces the likelihood of failure [25]. Moreover, pressure rise rates in self-pressurized spherical tanks, whether vertically or horizontally

oriented, are lower than in cylindrical tanks. This is due to reduced heat ingress, which minimizes LH_2 vaporization and pressure buildup [24]. Despite the thermal and mechanical advantages, specific design considerations must be addressed. For example, cylindrical tanks may require less space for support structures, and the manufacturing costs of spherical tanks are often higher [24].

A careful material selection ensures compatibility with cryogenic conditions. Austenitic stainless steels, such as 304 and 316 grades, are commonly used due to their characteristics as strength, toughness, and ductility. Additionally, the tank material should exhibit low hydrogen permeability to minimize gas leakage and associated safety issues [23], [24]. A detailed analysis of the metallic materials used for cryogenic applications in hydrogen-rich environments is reported in Section 3.2.

Effective insulation systems are essential to limit heat transfer and maintain cryogenic temperatures within the tank. The state-of-the-art technologies for spherical storage tanks include vacuumed perlite, multi-layer insulation, and hollow glass microspheres. MLI systems are composed of thin reflective layers separated by vacuum and are particularly effective in reducing radiation and conduction heat transfer in spherical tanks [26]. Another promising approach lies in hollow glass microspheres within the tank's double wall with vacuum. These microspheres offer low thermal conductivity and are lightweight, making them suitable for cryogenic applications [8]. A thorough description of the passive insulation materials and systems for cryogenic applications can be found in Section 0. Additionally, vapor-cooled shields (VCS) and liquid nitrogen-cooled shields (LN_2CS) can further enhance insulation performance. VCSs utilize vaporized LH_2 from the tank as a refrigerant, while LN_2CS employs liquid nitrogen to cool the shield, mitigating the latent heat transfer within the tank and allowing for sensible heat transfer between the cold hydrogen vapor and the environment [26]. Specific information about vapor-cooled shields can be found in Section 4.7.

Dedicated support systems are required for spherical tanks. They are intended to accommodate not only the tank weight but also the thermal expansion and contraction the system may experience. Therefore, these supports must be designed to minimize heat transfer while allowing for mutual movements, ensuring both efficiency and structural integrity [23], [24].

Figure 3 illustrates the 3D model of the spherical storage tank for liquid hydrogen in the NASA Kennedy Space Center. It shows the inner and outer shells, as well as the support structures in greater detail. Figure 4 illustrates the cross-section of the 4700 m^3 LH_2 storage tank, which is currently under construction.

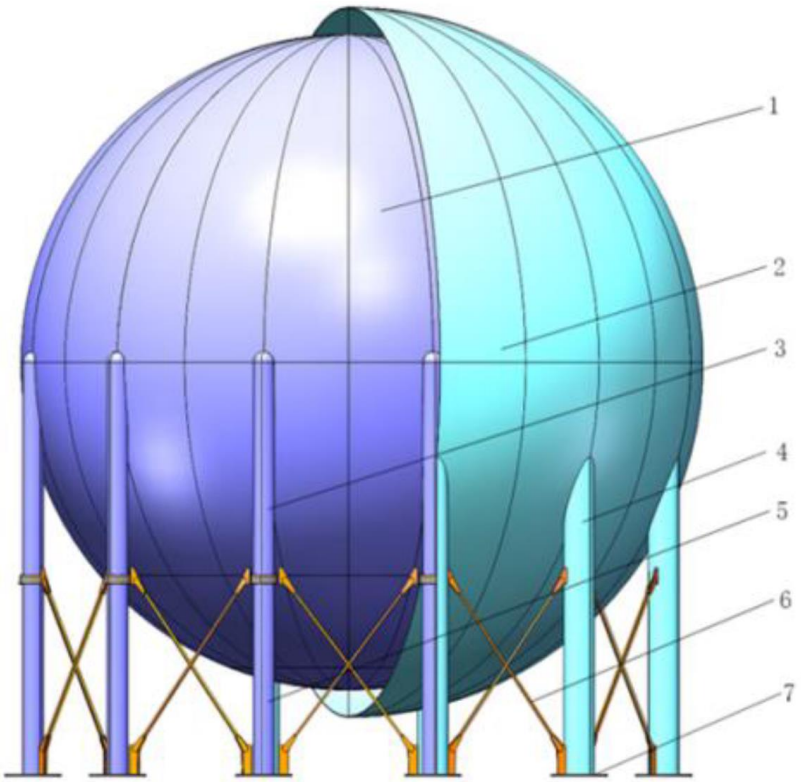

Figure 3: Model of the 3200 m^3 LH_2 spherical tank at the Kennedy Space Center. 1. Inner tank; 2. Outer tank; 3. Inner upper strut; 4. Outer upper strut; 5. Inner lower strut; 6. Pull rod; 7. Pedestal [26]

Figure 4: Schematic of the 4700 m^3 LH_2 spherical tank under development at the Kennedy Space Center [27]

Specific procedures must be followed to ensure efficiency and safety during the draining and filling of LH_2 spherical tanks. These processes involve managing thermal stresses, controlling filling rates, and ensuring proper evacuation and pre-cooling of the system. Thermal management is crucial during the filling of LH_2 tanks. Significant temperature gradients can develop in the initial stages, especially at the tank's bottom, leading to thermal stresses. To mitigate this, it is essential to control the filling rate. A low filling rate helps minimize the risk of increased thermal stress and deformation, which can occur at higher rates. Additionally, pre-cooling the system and properly evacuating the receiver tank are critical steps to effectively manage internal pressure and temperature, ensuring smooth operations [28]. Improper adherence to these procedures can result in significant risks. Failure to manage thermal gradients may cause excessive thermal stresses, leading to structural failures [28]. During draining, the discharge rate must align with the system's vaporization capacity to prevent cavitation and excessive tank emptying, which can cause overheating [29]. Additionally, pressure management is another vital aspect. The tank's internal pressure must remain within safe limits during loading and unloading operations, typically below 0.5 barg. Controlled venting or re-liquefaction of boil-off gas is necessary to avoid overpressure and minimize losses [30].

Regular inspections are essential to ensure the integrity of the tank, with their frequency depending on several factors, such as regulatory requirements, operational history, and environmental conditions. Engineering standards often establish minimum inspection intervals to comply with national and international guidelines. Tanks that had structural issues or accidents in the past, such as leaks or unintended releases, usually require more frequent inspections to mitigate potential risks. Additionally, tanks exposed to harsh environmental conditions, such as high humidity, maritime environment, or extremely low temperatures, may necessitate more frequent evaluations to maintain structural integrity and fitness for service [29], [31]. In the current LH_2 tank's technology, the thermal insulation efficiency relies on maintaining a high vacuum in the annular space for MLI systems and medium vacuum for perlite and microspheres. Therefore, continuous monitoring of the vacuum, along with procedures to detect and repair leaks, is critical to ensuring optimal performance and safety [30].

In normal operations, thermal stratification can increase evaporation rates and the internal pressure of the tank. Higher initial liquid levels or mixing devices can help mitigate this issue [24], [29]. When implementing safety measures for cryogenic storage tanks, it should be remembered that LH_2 is a flammable and cryogenic fluid. Safety measures should include fire detection and suppression systems, proper ventilation, and emergency procedures to address leaks or spills [29], [31].

3.1.2 Large-scale LNG tanks for stationary applications

The standard EN 14620 [32]–[36] regulates the design and manufacturing of vertical, cylindrical, flat-bottomed tanks for the storage of refrigerated liquefied gases with operating temperatures between 0 °C and –196 °C. The cylindrical design is one of the most prevalent for such equipment due to its efficiency in space utilization. These cryogenic tanks typically consist of a vertical cylindrical shell with a flat or slightly sloped bottom. The tank wall must be

fabricated from materials that can withstand cryogenic temperatures, commonly involving stainless steel or carbon steel with specific alloying elements to enhance toughness and reduce brittleness. The shell thickness depends on the tank size, operational pressure, and environmental factors. Two design methodologies are employed:

- Limit state theory for concrete components.
- Allowable stress theory or limit state theory for metallic components and insulation elements.

Steel components must achieve liquid and vapor tightness through precise design requirements. Concrete tightness depends on compression zones and moisture barriers, with polymeric alternatives acceptable if they match steel's performance. Bunds must contain the entire tank volume and be liquid-tight. Vertical anchors stabilize tanks against uplift forces due to internal pressure while accommodating thermal expansion.

Foundations must accommodate settlement, seismic loads, and frost-related hazards. Heating systems are required to maintain the foundation above freezing in cold climates. A thermal protection system (TPS) may be necessary to prevent cracking in concrete containers exposed to leaks. Minimizing openings in primary and secondary containment systems enhances structural integrity. Openings in concrete walls or bottoms are prohibited, and thermal protection systems prevent condensation and ice buildup.

The tank must contain liquids and vapors under cryogenic conditions. To minimize heat transfer, an efficient insulation system is paramount. Common insulation solutions include vacuum insulation or polyurethane foam, which encases the tank walls. The insulation must be designed to prevent thermal bridging, thus optimizing the system's efficiency and minimizing the boil-off gas formation. Moreover, insulation systems should include purging or drying mechanisms where vapor circulation is unavailable. By way of illustration, Figure 5 depicts the schematic of a vertical, cylindrical flat-bottom LNG tank.

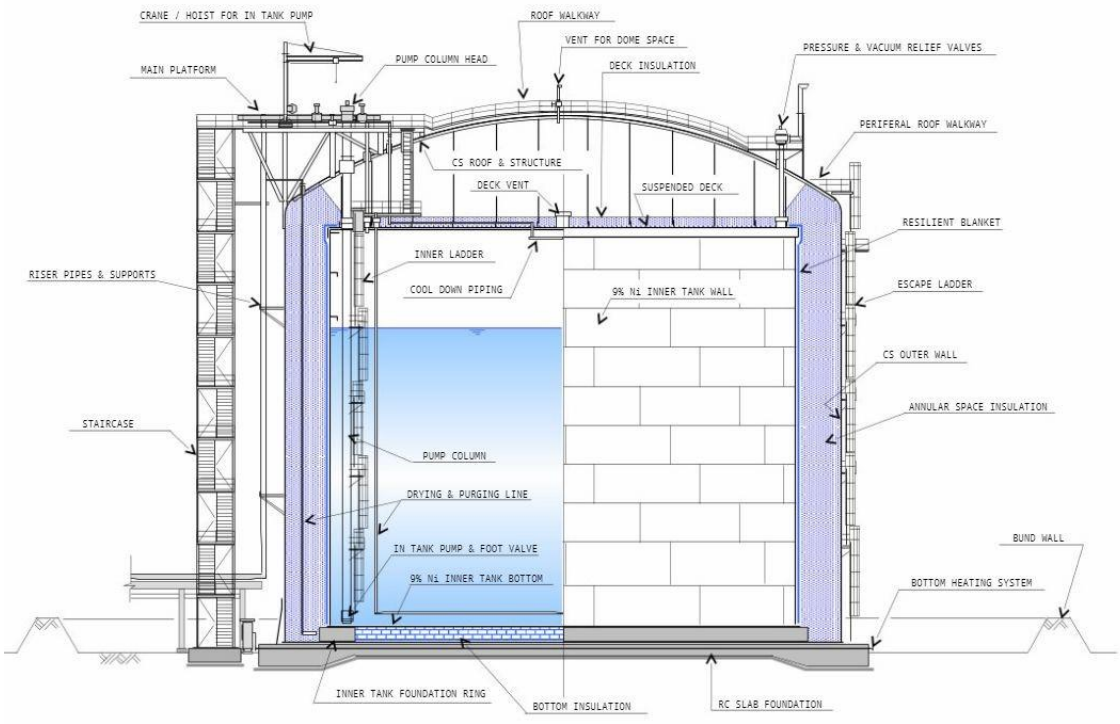

Figure 5: Schematic of a cylindrical flat-bottom tank for LNG (adapted from [37]*)*

Safety is important in the design of such cryogenic tanks. These components are equipped with several safety systems, including pressure relief valves, which prevent the tank's overpressurization by venting excess gas. Additionally, secondary containment systems are necessary to mitigate leakage risks. Piping penetrations are limited to specified areas, prohibiting bottom penetrations, and using internal shut-off valves. Advanced monitoring systems play a crucial role in the real-time assessment of the tank's conditions. They commonly include:

- Redundant liquid level gauges with height alarm and overflow cutouts.
- Independent pressure and temperature sensors.
- Systems to prevent rollover by monitoring temperature and density and maintaining circulation in stratified tanks.

In addition, measures must be in place to prevent air and moisture ingress, frost formation, condensation, and frost heave. Dedicated systems must limit damage from accidental events, avoid uncontrolled vapor release, and ensure that structural degradation remains within safe limits. The analysis of seismic hazards is mandatory for these tanks. Regional seismicity, geological conditions, and response spectra are taken into account.

The design of cylindrical flat-bottom tanks also considers operational accessibility, including loading and unloading systems, emergency response access, and maintenance routes. As local regulations dictate, the layout must allow efficient handling of cryogens during transfer operations while adhering to safety separation distances from adjacent infrastructure.

Cylindrical tanks are unusual for LH_2 stationary storage. However, an ongoing project led by Kawasaki Heavy Industries is considering the development of large-scale cylindrical flat-bottom tanks for LH_2, similar to those used for LNG storage. In fact, the advantage in terms of low surface-to-volume ratio of spherical shapes becomes more limited as the tank size increases. These tanks will have hydrogen gas between the inner shell and the outer jacket. It will be kept at atmospheric pressure to prevent the issues associated with a loss of vacuum between the tank walls. Barrier materials will protect the insulation to avoid hydrogen permeation [38]. A preliminary structural design is shown in Figure 6.

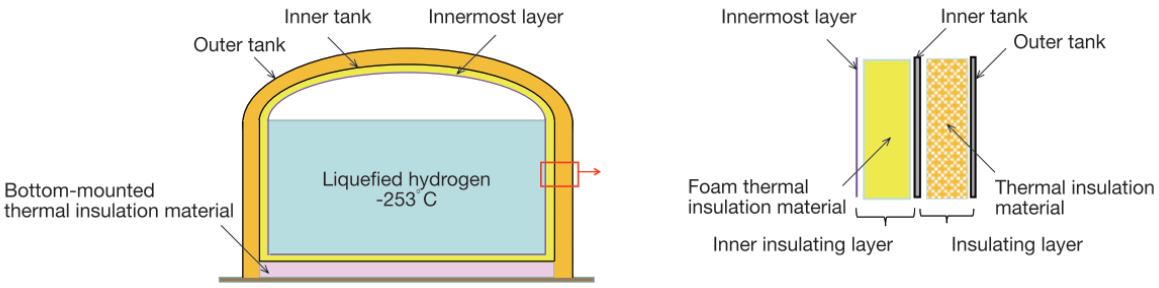

Figure 6: Structural design of a large-scale cylindrical flat-bottom tank for LH2 [38]

3.1.3 Tanks for maritime applications

Liquid hydrogen tanks for marine applications can be cylindrical with hemispherical heads, spherical, prismatic, or configured as multiple arrays of smaller and separate tanks. As shown in Figure 7, tanks can be positioned in various areas of the ship depending on the different

geometries. Drube et al. [39] examined the feasibility of multiple small and high-performing LH_2 tanks arranged within the ship's hull to optimize fuel storage and adaptability. The approach aimed to exploit the storage space as much as possible by minimizing the volume occupied by other essential systems, such as connection and ventilation equipment. However, even under the most optimistic assumptions, the total LH_2 storage capacity was 5–9 % less than that of a single large tank, suggesting the limited potential of further research on multiple LH_2 small tanks. In fact, this reduction in storage capacity significantly undermines the practicality of multiple small tanks, especially for maritime applications where maximizing fuel storage is critical. A comparative evaluation with two identical LH_2 cylindrical tanks was conducted in the same study. The tanks considered are manufactured by Chart Industries. The original design features an inner vessel 11 mm thick. However, the authors reduced the inner vessel thickness to 5.5 mm to increase the space between the two tanks and reduce the overall weight by approximately 3'600 kg. The materials evaluation for mechanical strength and thermal cycling ability when subjected to filling and emptying cycles was not conducted for the configuration with reduced thickness. The large cylindrical tanks are equipped with a multi-layer insulation, with layers made of low emissivity aluminum foil alternated with layers of glass fibers. This design ensures a nominal boil-off rate of 0.30 mass%/day. Conversely, the configuration with multiple-tanks is equipped with 25 mm of MLI under high-vacuum conditions and achieves nominal boil-off rates ranging from 0.49 to 0.70 mass%/day.

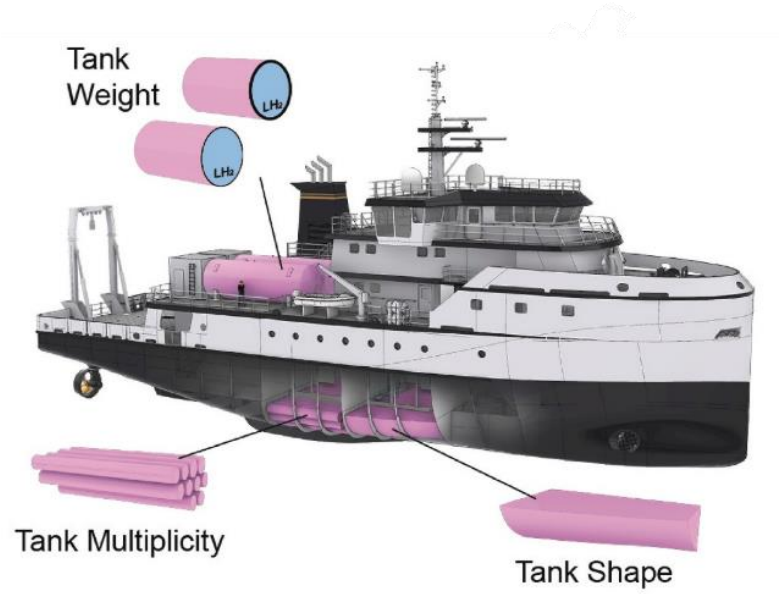

Figure 7: Placement of different LH_2 tanks: cylindrical, prismatic, and arrays of smaller tanks [39]

Table 2 summarizes the features of the LH_2 tank in the baseline configuration, considering the original tank design (i.e., the vessel without thickness reduction on the inner shell).

Table 2: Attributes of the LH_2 tank in the baseline vessel

Attributes of the baseline LH_2 tank	**Unit**	**Value**
Inner vessel material	-	SA 240 T304 stainless steel
Inner vessel thickness	mm	11
Inner vessel diameter	m	2.7
Inner vessel length	m	8.6
Outer jacket material	-	SA 36 carbon steel

Outer jacket thickness	mm	12.7
Outer jacket diameter	m	2.9
Outer jacket length	m	9.2
Inner vessel water volume	m^3	45.5
Weight empty tank	kg	17’230
Weight full tank	kg	20’450
Maximum storage capacity	kg	3’220
Consumable LH_2 (64 – 5%)	kg	1’900
Maximum allowable pressure	bar	10
Insulation	-	50 mm of MLI under high vacuum
Nominal boil-off rate	% / day	0.30
Estimated holt time to 5 barg	day	32

Alkhaledi et al. [40] presented a liquid hydrogen tanker named JAMILA, illustrated in Figure 8. The wall of the cylindrical tank is 168 cm thick and composed of three layers: 100 cm of rigid open-cell polyurethane foam, 43.4 cm of aluminum, and 24.6 cm of liner made from an aluminum alloy (i.e., Al-Mg 5086). The authors provided a preliminary design for a potential LH_2 tanker. The tonnage of the fully loaded cargo ship is 230’000 tons, with a maximum capacity of 20’000 tons of liquid hydrogen.

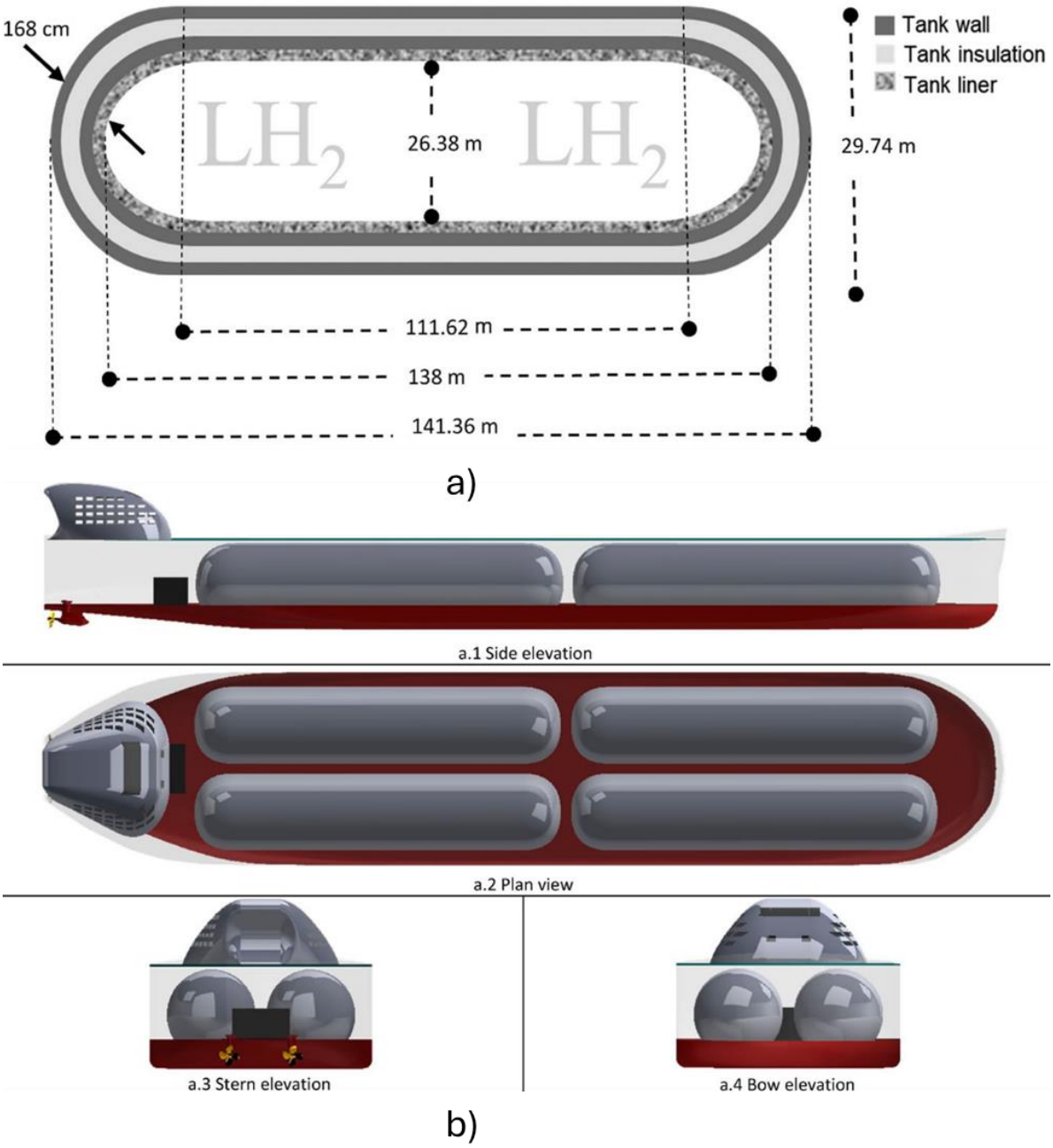

Figure 8: Overview of JAMILA: a) Cross-section of the LH_2 tank and b) 3D model of the cargo ship with tank allocations [40]

The authors dimensioned the tanks using the approach proposed by Colozza and Kohout [41] for hydrogen storage on aircraft. Furthermore, the tank was designed to achieve a boil-off of 0.1 mass%/day, using polyurethane foam as insulation. However, the study did not address the tank's feasibility in terms of static mechanical stress and fatigue performance. The design parameters of the tank and its insulation system are summarized in Table 3.

Table 3: Technical characteristics of the model of LH_2 storage tank [40]

Design parameters	Unit	Value
Mass of LH_2	t	5'000

Internal pressure	MPa	0.5
Internal temperature	K	20
Density of LH_2	kg/m^3	71
Excess volume	%	0.252
Length of the cylinder	m	111.6
Total internal length (hemisphere + cylinder)	m	138
Total external length (hemisphere + cylinder)	m	141.36
Yield strength of aluminum	MPa	410
Safety factor	-	54
Aluminum density	kg/m^3	2‘800
Volume of LH_2	m^3	70‘600
Inner radius	m	13.19
Wall thickness	m	0.434
Weight of the empty tank	t	14‘226
Boil-off rate	mass%/day	0.1
Inner insulation radius	m	13.624
Outer insulation radius	m	14.624
Mass of polyurethane foam	t	14.5
Mass of tank liner	t	7‘715
Weight of the full tank	t	21‘955

Another study conducted by Abe et al. [42] pointed out that prismatic tanks are more compact than spherical ones but require careful design to accommodate shrinkage and thermal stress. Figure 9 schematically illustrates hydrogen tankers equipped with spherical and prismatic tanks. The support system is rigid and specifically designed to minimize the heat ingress through the connections (i.e., thermal bridges), often necessitating thermal breaks. In contrast, prismatic tanks offer a more flexible support system that allows for free contraction and reduces thermal stresses. Additionally, prismatic tanks minimize heat ingress since there is no direct metallic connection between the tank and the hull. However, data on the insulation performance are not provided. Instead, the researchers presented a preliminary study exploring the use of polyurethane foam panels in vacuumed and non-vacuumed hold spaces, vacuum insulation panels, and super-insulation within a vacuumed hold space. However, the choice of the insulation type and tank geometry (i.e., spherical, cylindrical, and prismatic) depends on the specific requirements of the vessel design, balancing factors such as weight, flexibility, heat management, and space utilization efficiency.

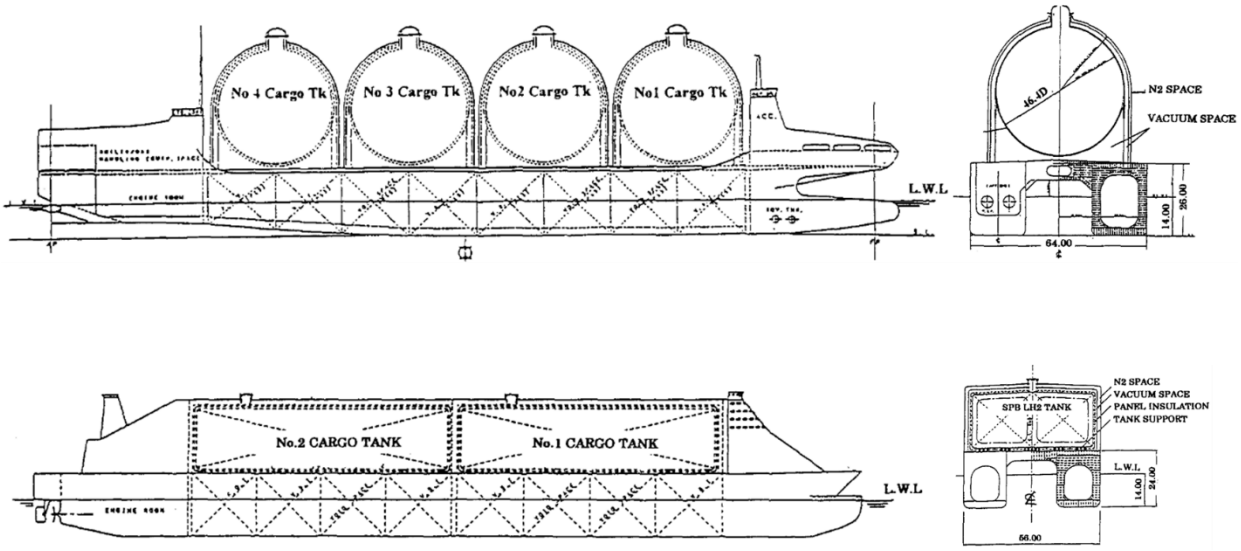

Figure 9: Conceptual design of 200'000 m^3 hydrogen tanker (adapted from [42]*)*

Kawasaki Heavy Industries conducted a feasibility study on establishing a hydrogen supply chain from Australia to Japan [43]. To achieve this target, Kawasaki developed the conceptual design for two LH_2 carriers: a cargo ship with a capacity of 160'000 m^3 for the full-scale supply chain and a smaller carrier with a capacity of 2'500 m^3 for the pilot supply chain, illustrated in Figure 10. The large-scale carrier is equipped with four vacuum-panel MOSS-type spherical tanks, each with a capacity of 40'000 m^3. These tanks have a nominal boil-off rate of 0.2 mass%/day or less and exhibit thermal insulation performance nearly ten times better than conventional LNG carriers. In contrast, the small-scale LH_2 carrier is equipped with two cylinder-type multi-layer vacuum-insulated tanks, each with a capacity of approximately 1'250 m^3. The expected boil-off rate is not reported for these tanks.

In maritime applications, it is crucial to consider the impact of mechanical loads from sloshing, which is one of the most significant factors affecting structural integrity. On the one hand, the fluid motion caused by the ship's rolling increases the boil-off gas formation by transferring heat to the tank through the kinetic energy dissipation and expanding the interface between liquid and vapor phases [44]. On the other hand, sloshing of LH_2 does not damage the tank due to its significantly lower density compared to liquefied natural gas [45]. However, different perspectives emerged, with Baeten et al. [46] arguing that the increased boil-off rate in LH_2 tankers results in higher impact pressures compared to LNG, leading to more significant deformations of the tank's structure. Additionally, they suggested that the impact forces exerted on the tank walls can be significantly mitigated if the walls exhibit elastic rebound behavior. This can be achieved using a lightweight membrane, which is technically feasible by incorporating fiber-reinforced structural layers and insulation layers arranged in a carefully designed stacking sequence [44], [47].

Items	
Class pf ship	Large ship (Spherical tank)
Type of Ship	Monohull ship
Tank capacity	160,000 m^3 (40,000m^3 x 4 unit)
Tank method	Spherical tank ,Type-B
Thermal insulation	Vacuum panel
BOG(Boil off gas rate)	0.2%/day
Propulsion system	Hydrogen gas engine

a)

Items	
Class of ship	Small accumulated ship
Type of ship	Monohull
Tank capacity	2500m^3 (1250m^3 x 2 unit)
Tank method	Cylindrical tank ,Type-C
Thermal insulation	High vacuum multilayer
BOG	0.2%/day
Propulsion system	Diesel engine

b)

Figure 10: Conceptual design for two LH_2 carriers from Kawasaki Heavy Industries: a) large and b) small [43]

The experience acquired on LNG handling equipment could be crucial in accelerating the adoption of LH_2 systems. As a reference of LNG systems that could be adapted to hydrogen applications, Banaszkiewicz et al. [48] designed the structure of a C-type LNG tank for maritime applications, shown in Figure 11. Three types of insulation materials were investigated for this application: vacuumed perlite powder, multi-layer insulation, and polyurethane foam. The proposed design can be applied to LH_2 tanks, considering variations such as material selection to counter hydrogen embrittlement and incorporating an appropriate relief unit system.

Another system that was proposed for LH_2 storage in the maritime sector is the MARK III insulation system. This technology was developed to ensure LNG's safe and efficient storage and transportation. The main structure of the MARK III system includes a thin steel membrane, a layer of plywood, two layers of foam separated by a second steel membrane, and a second layer of plywood beneath them [49]. MARK III utilizes advanced insulation materials to minimize the boil-off rate and ensure the minimal energy loss during transport [50]. In addition, this system could minimize sloshing and the resulting boil-off increase.

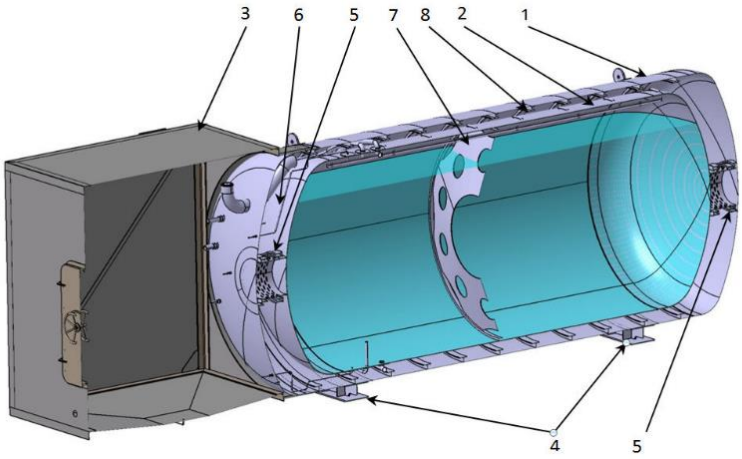

Figure 11: The main elements of the LNG tank: 1) outer jacket; 2) inner tank; 3) tank connection space; 4) external supports; 5) internal supports; 6) pipes; 7) sloshing plate; 8) ribs [48]

3.2 Material selection

Cryogenic storage tanks demand materials with a unique combination of properties. They must have elevated toughness to ensure the safety and reliability of the hydrogen handling equipment. In addition, high strength is a primary requirement for structural materials since it allows for thinner sections and reduces the weight and cost of the components [51][52]. Figure 12 shows the typical ranges of yield strength and fracture toughness for steels for cryogenic service.

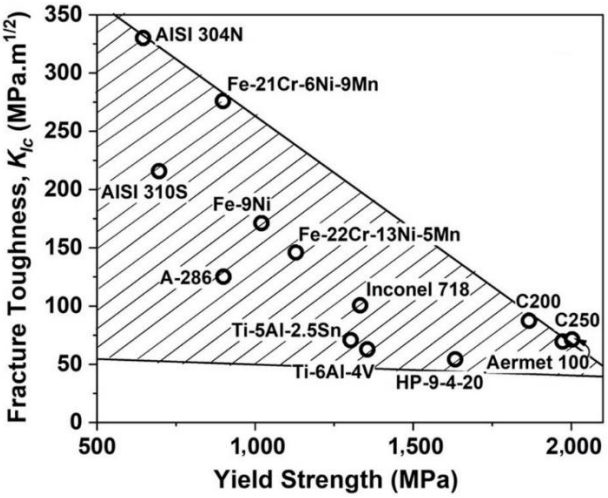

Figure 12: The range of yield strength and fracture toughness for alloys for cryogenic applications [53]

Along with yield strength and fracture toughness, density, specific heat, coefficient of thermal expansion, and thermal conductivity significantly impact the tank's performance, design, and cost-effectiveness. The density is critical in transportation applications, such as large-scale shipping. Specific heat is a crucial physical property that influences the heat input required to increase the temperature of the system, thus affecting the heat extracted during the cooldown process and filling operations. This property is significant for systems that undergo multiple

cooling and heating cycles, directly impacting operational costs. For most metals, specific heat remains relatively constant from ambient temperature to 77 K but decreases rapidly with further temperature reduction. The temperature variation in a solid determines a change in its volume, known as thermal expansion. When this expansion is constrained, it can induce mechanical stresses, residual stresses, or both. If not adequately considered in the design phase, these stresses can cause distortions in cryogenic storage tanks, thus compromising their safety and fitness for service. The coefficients of thermal expansion of different materials can vary by an order of magnitude [54]–[56].

Additionally, thermal conductivity is a critical property in selecting materials for cryogenic systems. All structural materials have high thermal conductivity, thus requiring an insulation system to limit the heat transfer between liquid hydrogen and the surrounding environment. It should be mentioned that metallic alloys generally exhibit a decrease in thermal conductivity at low temperatures [56]. By way of illustration, Table 4 reports the specific heat capacity (c_p), coefficient of thermal contraction (δL/L), and thermal conductivity (k) of AISI 304 stainless steel (typical reference material) measured at room and cryogenic temperatures.

Table 4: Specific heat, coefficient of thermal contraction, and thermal conductivity of AISI 304 stainless steel at temperatures ranging from 4 K to 300 K [56]

Properties	4 K	20 K	40 K	77 K	100 K	150 K	200 K	300 K
c_p [J/g·K]	$2.00\cdot10^{-3}$	$2.10\cdot10^{-2}$	$9.60\cdot10^{-2}$	$1.97\cdot10^{-1}$	$2.75\cdot10^{-1}$	$2.00\cdot10^{-3}$	$4.16\cdot10^{-1}$	$4.71\cdot10^{-1}$
δL/L [%]	$2.96\cdot10^{-1}$	$2.96\cdot10^{-1}$	$2.96\cdot10^{-1}$	$2.00\cdot10^{-1}$	$2.00\cdot10^{-1}$	$2.00\cdot10^{-1}$	$2.00\cdot10^{-1}$	$6.60\cdot10^{-2}$
k [W/cm· K]	$2.70\cdot10^{-3}$	$2.20\cdot10^{-2}$	$6.20\cdot10^{-2}$	$7.90\cdot10^{-2}$	$2.00\cdot10^{-3}$	$9.20\cdot10^{-2}$	$1.30\cdot10^{-1}$	$1.50\cdot10^{-1}$

Exposure to cryogenic temperatures modifies the mechanical properties of all materials. Most steels increase in strength and decrease in ductility and toughness when the temperature rises. The ductile-to-brittle transition (DBT) indicates the shift from ductile to brittle fracture behavior, often with minimal or no yielding, at low temperatures [54][55]. The DBT phenomenon is characterized by a significant drop in the absorbed impact energy below a specific temperature, known as ductile-to-brittle transition temperature (DBTT) [57]. The mechanical performance at cryogenic temperatures and the presence of DBT depend substantially on the steel's microstructure. Alloys with a body-centered cubic (BCC) structure show a sharp reduction in toughness as the temperature decreases. In contrast, metals with a face-centered cubic (FCC) structure do not undergo DBT and keep their toughness and ductility even at cryogenic temperatures. Metals with a hexagonal close-packed (HCP) structure exhibit behavior between BCC and FCC metals, depending on specific structural features and interstitial impurities [58].

The yield strength (YS) generally increases at low temperatures. The relationship between YS and the breaking stress determines the material's susceptibility to DBT. When the YS exceeds the breaking strength at a specific temperature, the material can fail without yielding, showing a brittle behavior. Accurate control over the material microstructure and chemical composition can reduce the DBTT. In particular, removing interstitial impurities, enhancing grain boundary cohesion, and facilitating delamination perpendicular to the crack path are effective preventive methods [54].

The low-temperature deformation behavior of BCC metals exhibiting ductile-to-brittle transition is marked by a sharp increase in YS and a minimal rise in ultimate tensile strength (UTS), which reduces the gap between YS and UTS. In contrast, FCC metals show low sensitivity of YS to temperature and more significant strain hardening, resulting in a larger gap between YS and UTS, which results in a higher toughness at low temperatures. Due to the absence of DBT, FCC alloys are inherently safer for cryogenic applications [54][55].

Austenitic stainless steels have been used for various cryogenic applications due to their absence of DBT, excellent mechanical properties, and good formability. However, their yield strength is lower than that of many alloy steels. Grades AISI 304 and 316 have been extensively studied for cryogenic uses, but for LNG storage tanks, different materials can meet the requirements of higher strength and cost-effectiveness. One of the most widely used materials for this purpose is 9% nickel steel [59][60]. Table 5 summarizes the suitable materials for hydrogen storage tanks of different sizes.

Table 5: Summary of the suitable materials for various hydrogen storage vessels

Cryogenic vessels	Metallic materials for cryogenic service		
	Nickel steels	Austenitic stainless steels	Copper alloys
Inner vessel of large transportable tanks		×	×
Outer jacket of large transportable tanks	×		×
Inner vessel of small transportable tanks		×	×
Outer jacket of small transportable tanks	×		×
Inner vessel of large static tanks		×	×
Outer jacket of large static tanks	×		×
Inner vessel of large transportable tanks		×	×
Outer jacket of large transportable tanks	×		×

3.2.1 Ferritic stainless steels

Ferritic steels typically contain 10.5–30.0 $\%_{wt}$ of chromium with small amounts of microalloying elements like molybdenum, aluminum, titanium, niobium, and copper to adjust their properties as needed. They exhibit elevated strength at room temperature and are relatively inexpensive. However, their BCC structure makes their mechanical properties susceptible to temperature [61]. Therefore, their use at low temperatures is generally limited. Nickel is added in the 1.5–9 $\%_{wt}$ range to increase the austenite phase stabilization, increase the resistance to transgranular cleavage fracture, and make them suitable for temperatures down to 77 K [62][63]. As the nickel content increases, the DBTT decreases. As shown in Figure 13, the drop in impact energy at 77 K completely disappears for 9 $\%_{wt}$ Ni steel [64]. In addition, small amounts of boron can be added to mitigate the occurrence of intergranular brittle fracture and strengthen the grain boundaries [65].

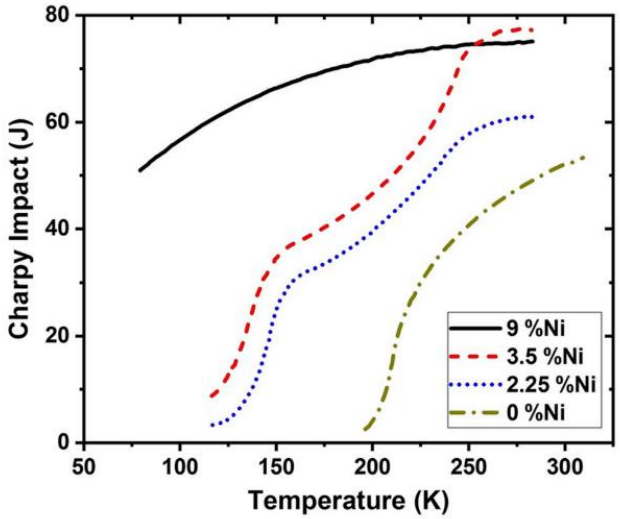

Figure 13: Effect of nickel content on impact energy of 12.5-mm-thick plate of low-carbon steel [64]

Appropriate heat treatments can further enhance the mechanical performance of 5–9 $\%_{wt}$ Ni ferritic steels. Thick or welded plates can undergo thermomechanical processing to obtain ultrafine grain sizes [66]. The quenched and tempered (QT) treatment lowers the ductile-to-brittle transition temperature below 77 K. For lower nickel content steels (5–6 $\%_{wt}$), a three-step heat treatment of quenching, lamellarizing, and tempering (QLT) is used for grain refinement. Double normalization and tempering (NNT) treatments are typical for formed components like tank heads [52].

Weldability is a crucial factor when working with 9 $\%_{wt}$ Ni steel, especially since it is commonly used for welded plates. Nickel alloy austenitic filler wire allows for excellent cryogenic toughness and a coefficient of thermal expansion close to that of the base metal. For welding thicker components, overmatched filler wire ERNiCrMo-3 is typically used. In fact, a lower heat input during the welding process ensures a thin heat-affected zone (HAZ), which helps maintain the nominal material's properties [67].

In general, these steels offer a good balance of strength and toughness, making them suitable for plates, tubes, wrought pipe fittings, forged flanges, valve parts, and LNG tanks. Nevertheless, LH_2 is stored at a significantly lower temperature. Even if they cannot be used for components directly exposed to liquid hydrogen (e.g., inner vessels), they are potentially suitable for outer jackets of LH_2 storage tanks.

3.2.2 Austenitic stainless steels

Austenitic stainless steels are the most used materials for cryogenic applications. The microstructure is composed of an austenite matrix with a face-centered cubic lattice structure, thus resulting in the absence of a ductile-to-brittle transition. These steels are characterized by excellent strength and fracture toughness at cryogenic temperatures [61]. Notably, the austenite phase undergoes spontaneous transformation into martensite when exposed to temperatures lower than the martensite start temperature (M_s) without requiring any deformation. The Eichelmann and Hull's correlation in Eq. 1 can empirically predict the M_s temperature based on the chemical composition of the steel [68]:

$$Ms = 1.320 - 61\ \%Ni - 42\ \%Cr - 33\ \%Mn - 28\ \%Si - 1.667\ (\%C + \%N) \quad (1)$$

In nearly all austenitic stainless steels, the martensite start temperature is significantly lower than the ambient temperature. However, in class-300 austenitic steels, martensitic transformation can occur with the application of mechanical deformation (deformation-induced martensitic transformation) at temperatures given by the Angel correlation in Eq. 2 [69]:

$$Md\left(\frac{30}{50}\right) = 413 - 462\ (\%C + \%N) - 9.2\ \%Si - 9.5\ \%Ni - 13.7\ \%Cr - 8.1\ \%Mn - 18.5\ \%Mo \quad (2)$$

where $Md\left(\frac{30}{50}\right)$ indicates the temperature at which 50 % of the material has transitioned to martensite when deformed at 0.3 strain.

Compared to AISI 304 and 304 L, austenitic grade 316 L exhibits higher stability and does not show spontaneous martensitic transformation at low temperatures, although DIM transformation still occurs. Consequently, grade 316 L is the preferable choice for thin-walled shell structures. AISI 301 can achieve tensile strengths exceeding 2’000 MPa due to the transformation of unstable austenite into martensite. Leaner grades, such as 301, 304, and 304 L, are often subjected to extensive cold work to enhance strength while maintaining ductility. Additionally, grade 200 austenitic stainless steels have a remarkable combination of toughness, corrosion resistance, and cost-effectiveness [70].

At ambient temperature, austenitic stainless steels do not show a distinct yield point and have quasi-elastic behavior. Deformation under stress levels below half of the yield strength is fully elastic, while stresses below two-thirds of the yield point result in minimal plastic deformation [71]. Both the yield and ultimate tensile strength increase as the temperature decreases. While the enhancement in UTS is modest, the YS shows a significant rise. However, there can be unusual behavior in terms of percentage elongation. For instance, 21Cr-12Ni-5Mn steel shows a sharp increase in percentage elongation between 4 and 77 K, followed by a decrease at room temperature [72]. These steels maintain sufficient toughness at cryogenic temperature. Even if the impact strength decreases as temperature drops, it remains above 20 J (a standard threshold for cryogenic applications) [73]. The enhanced ductility at low temperatures is also effectively utilized in cryo-forming processes. Figure 14 shows the yield strength, ultimate tensile strength, elongation at failure, and reduction of area of austenitic stainless steels as functions of temperature.

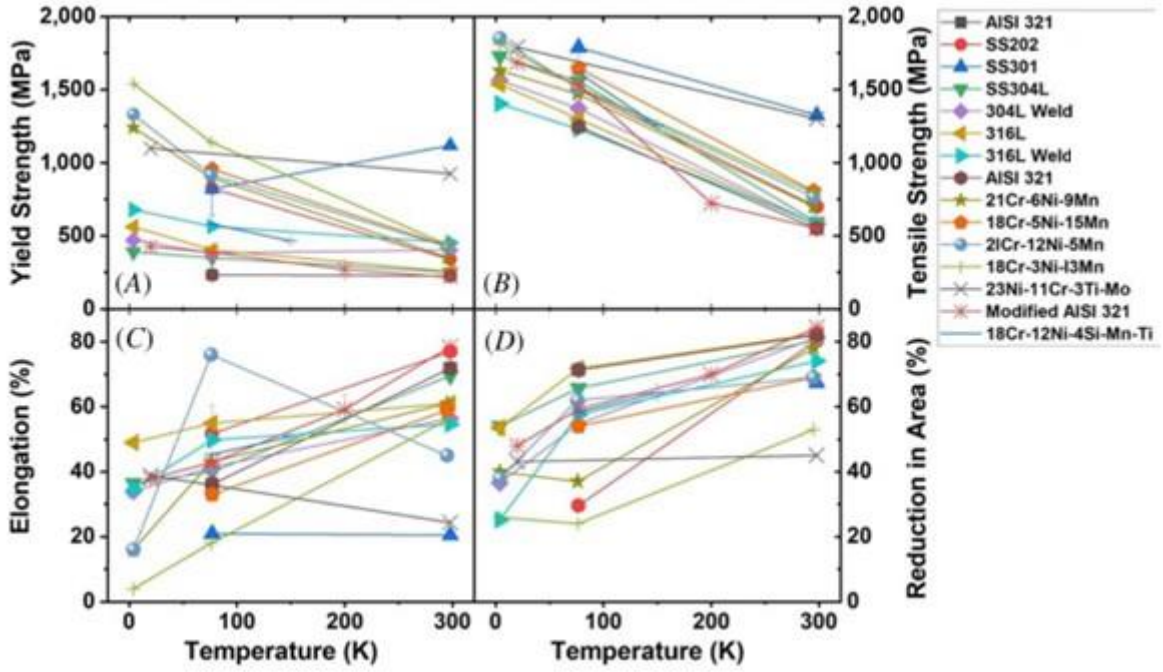

Figure 14: Effect of temperature on the tensile properties of austenitic steels (A) yield strength, (B) ultimate tensile strength, (C) elongation, and (D) reduction of area [61]

Figure 15 illustrates YS versus percentage elongation for various steels at 20 K. Austenitic steels are preferred due to their strength-elongation balance. Cr-Ni and Cr-Ni-Mo-Cu steels display high YS and elongation, justifying their use at 20 K.

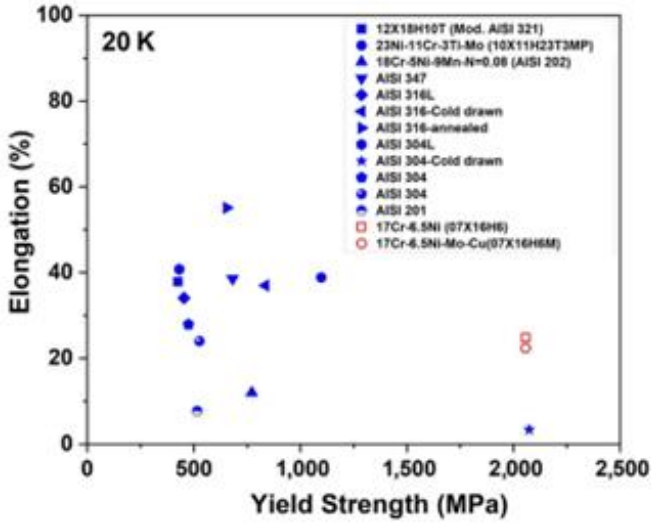

Figure 15: Percentage elongation and corresponding YS of steels at 20 K [61]

Austenitic stainless steels have strict limits on carbon content. While carbon increases the material's strength and stabilizes the austenite phase, it can also form chromium carbides, which cause sensitization. In addition, titanium and niobium are added to avoid the formation of chromium nitride [61].

All fabricated components contain minor flaws and geometrical defects. These initial microcracks can propagate under dynamic loading, potentially causing catastrophic failures [74]. When materials undergo cyclic loads below their UTS, fatigue failure may eventually occur. In general, the fatigue life of components tends to increase at low temperatures and decreases at low frequencies (typical conditions for LH_2 storage equipment). Fatigue resistance of AISI 304 L and 304 N at 20 K is slightly higher than at room temperature. The stress range necessary for failure at 10^6 cycles is approximately half of the UTS for AISI 304 N. Similar considerations also apply to AISI 304 L, 310, and 316. AISI 310 and AISI 316 demonstrate superior fatigue resistance compared to AISI 304 L in low-cycle fatigue (less than 10^4 cycles), except at the highest strain ranges [75][76].

The fatigue behavior of 21Cr-6Ni-9Mn at 4 K is similar to that of 300-series steels: in the high-cycle regime, fatigue resistance improves with decreasing temperature, whereas in the low-cycle regime, fatigue strength declines. 21Cr-6Ni-9Mn alloy has a higher fatigue strength than AISI 304 L but is lower than AISI 316, as shown in Figure 16 [75]. The greater strength of nitrogen-strengthened grades does not correspond to a significant improvement in fatigue life. In another study, a cold-rolled AISI 301 sheet (YS of 1530 MPa) demonstrated better fatigue resistance at room temperature compared to annealed AISI 347 sheet (YS of 255 MPa) [77]. However, at 20 K, AISI 347 outperformed AISI 301, indicating that the latter steel grade is unsuitable for fatigue-critical applications at cryogenic temperatures. Tests on high and low-cycle fatigue response of base and weld materials for SUS 304 L and SUS 316 L allowed to assess the long-term reliability of liquid hydrogen storage tanks [78]. In low-cycle fatigue, welds exhibited slightly shorter fatigue lives than base materials.

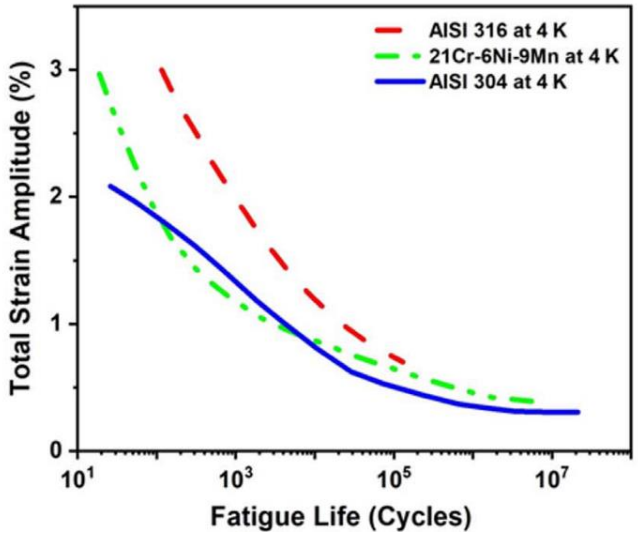

Figure 16: Fatigue behavior of three austenitic stainless steel: AISI 304, AISI 316 and 21Cr-6Ni-9Mn alloy at 4 K [75]

Stable alloys typically show enhanced resistance to fatigue crack growth at cryogenic temperatures. For AISI 310 S, the fatigue crack growth rate (FCGR) is lower at 77 K and 4 K compared to room temperature, with no significant difference within the cryogenic temperature range. Fe-25Ni-20Cr and Fe-25Ni-14Cr stainless steels exhibit a similar pattern. Metastable austenitic steels experience martensitic transformation, which generally improves fatigue crack growth resistance since it relieves the stress field at the crack tip [79]. High-manganese steel 18Mn-5Ni-16Cr-0.02C-0.22N shows similar FCGRs at 4 K and 77 K over a stress-intensity

factor range of 20–70 MPa·m$^{1/2}$ and is significantly lower than AISI 304 LN at 4 K [80]. SUS 304 exhibits greater fatigue life than high-manganese steel [81].

When cooled or stressed, unstable austenitic stainless steels transform into HCP and BCC phases. Depending on the alloy composition, this transformation can impact fatigue crack growth rates, either positively or negatively. Studies on Fe-Cr-Ni stainless steels AISI 304 and AISI 316 show no significant difference in FCGRs at 4 K. In contrast, AISI 304 L shows lower crack propagation rates at cryogenic temperatures, while AISI 304 N displays the opposite behavior [79]. Austenite stability significantly impacts the fatigue crack growth for nitrogen-strengthened stainless steels. Therefore, AISI 304 N and 304 LN have four to five times higher FCGRs at 4 K than AISI 304 or 304 L [82].

The base metal (BM), heat-affected zone, and weld zone (WZ) show minimal reduction in absorbed energy as temperature decreases. The WZ displays significantly higher absorbed energy than the BM and HAZ from room temperature to 77 K [83]. Therefore, welded austenitic stainless steel pipes are well-suited for cryogenic applications. As a general trend, fracture toughness is inversely proportional to the yield strength. In many metastable austenitic steels, fracture toughness increases as temperature falls below the critical temperature M_d, where deformation-induced martensite transformation intensifies [82][84]. However, the extent of transformation at a given strain may diminish at extremely low temperatures. At 4 K, fracture toughness in stable AISI 304 increases, while it decreases in the less stable AISI 304 L due to the brittle martensitic phase. Metallurgical factors (e.g., presence of interstitial elements, impurities, grain size, and microstructure) also influence fracture toughness. The chemical composition has the most significant impact [85].

3.2.3 List of materials

With their favorable strength-toughness combination and good fabricability, austenitic stainless steels have long been the preferred material for small-scale cryogenic storage vessels. These vessels typically have double walls and use carbon steel or aluminum alloy for the outer shells to reduce cost and weight. For large-scale LNG storage tanks, 9 %$_{wt}$ nickel ferritic steels are often chosen due to their higher strength and lower cost compared to austenitic stainless steels. Recently, 7 %$_{wt}$ nickel steel and high-manganese steel have been approved for LNG storage [61].

Since materials are commonly used in various product forms, are processed through different methods, and undergo various heat treatments, it is essential to evaluate their mechanical properties in the final microstructural condition. It is also crucial to assess the impact of impurities, inclusions, grain size, the effect of phase transformations, and the presence of residual stresses.

Table 6 lists the austenitic, austenitic-martensitic, and ferritic stainless steels potentially suitable for cryogenic storage tanks, indicating their nominal chemical composition.

Table 6: Chemical composition of austenitic, austenitic-martensitic, and ferritic stainless steels for cryogenic applications (adapted from [61]*)*

Steel grade	Nominal composition %$_{wt}$							
	C	Si	Mn	Cr	Ni	Mo	Others	Fe
Austenitic stainless steels								

AISI 201	0.15	1.00	5.50-7.50	16.00-18.00	3.50-5.50	-	N: 0.25	Balance
AISI 202	0.15	1.00	7.50-10.00	17.00-19.00	4.00-6.00	-	N: 0.25	Balance
AISI 301	0.15	1.00	2.00	16.00-18.00	6.00-8.00	-	-	Balance
AISI 302	0.15	1.00	2.00	17.00-19.00	9.00-10.00	-	-	Balance
AISI 304	0.08	1.00	2.00	18.00-20.00	8.00-10.50	-	-	Balance
AISI 304 L	0.03	1.00	2.00	18.00-20.00	8.00-12.00	-	-	Balance
AISI 304 LN	0.03	1.00	2.00	18.00-20.00	8.00-10.50	-	N: 0.10-0.16	Balance
AISI 310	0.25	1.50	1.50	24.00-26.00	19.00-22.00	-	N: 0.03	Balance
AISI 316	0.08	1.00	2.00	16.00-18.00	10.00-14.00	2.00-3.00	-	Balance
AISI 316 L	0.03	1.00	2.00	16.00-18.00	10.00-14.00	2.00-3.00	-	Balance
AISI 316 LN	0.03	1.00	2.00	16.00-18.00	10.00-14.00	2.00-3.00	N: 0.10-0.16	Balance
AISI 316 Ti	0.10	1.00	2.00	16.00-18.00	11.00-14.00	2.00-3.00	Ti: 5C-0.60	Balance
AISI 321	0.08	1.00	2.00	17.00-19.00	10.00-12.00	-	Ti: 5C-0.60	Balance
AISI 347	0.08	0.75	1.50	17.00-19.00	9.00-13.00	-	Nb: 10C N: 0.03	Balance
AISI 374 N	0.08	0.75	1.50	17.00-19.00	9.00-12.00	-	Nb: 10C N: 0.20	Balance
20Cr-6.5Mn-6Ni	0.07	0.50	6.00-7.00	19.50-21.50	5.50-6.50	-	-	Balance
23Ni-11Cr-3Ti-Mo	0.10	0.60	0.60	10.00-12.50	21.00-25.00	1.00-1.60	Ti: 2.60-3.20 B: 0.02 Al: 0.80	Balance
12Cr21	0.09-0.14	0.80	0.80	20.00-22.00	4.80-5.80	-	Ti: 0.25-0.50 Al: 0.08	Balance
12X18H10T	0.07-0.12	2.00	0.80	17.00-19.00	9.00-11.00	-	Ti: 5C-0.80	Balance
18Cr-12Ni-4Si-Mn-Ti	0.12-0.17	3.80-4.50	0.50-1.00	17.00-19.00	11.00-13.00	-	Ti: 0.40-0.70	Balance
Z2CND 17-13	0.05	-	-	16.50-17.50	11.00-12.00	2.50-3.00	-	Balance
17Cr-13.5Ni-3V-Ti	0.12	1.00	1.00	16.00-18.00	11.00-14.00	-	V: 2.50-4.00 Ti: 0.40-0.80	Balance
Austenitic-martensitic stainless steels								
17Cr-6.5Ni	0.09	0.80	0.90	16.00-18.00	6.00-7.00	-	-	Balance

17Cr-6.5Ni-Mo-Cu	0.05-0.09	0.80	0.80	15.50-17.50	5.00-8.00	0.30-0.60	-	Balance
Ferritic stainless steels								
ASTM A553 Type I	0.15	0.15-0.30	1.00	-	8.50-9.00	-	-	Balance
4Ni-Mn-Mo	0.14-0.20	0.17-0.37	0.25-0.55	1.35-1.65	4.00-4.40	0.30-0.40	-	Balance

3.2.4 Hydrogen effect on the mechanical properties of steels

Hydrogen embrittlement is a type of environmental degradation that reduces the mechanical properties of metallic materials through interactions with hydrogen atoms. Equipment exposed to hydrogen-rich atmospheres experiences the absorption and adsorption of hydrogen atoms. They dissociate on the metal surface, enter the lattice, diffuse through the bulk material, and accumulate in zones with elevated stress triaxiality [86]. This local concentration affects the material's resistance to residual or applied loads and can compromise its integrity. Hydrogen solubility tends to be lower in BCC metals (e.g., ferritic steels) than in FCC ones (e.g., austenitic stainless steels). This is due to the smaller size of the interstitial sites in BCC materials [87][88].

Tensile properties, fracture resistance, and fatigue crack growth rate must be evaluated under cryogenic conditions and high-purity hydrogen exposure to assess the performance and structural integrity of LH_2 handling equipment [89].

Hydrogen-induced damage commonly appears as a loss of ductility [90]. It can be quantified through tensile tests by comparing the reduction in cross-sectional area at fracture in hydrogen-containing and reference environments. This difference is typically expressed in terms of embrittlement index (EI), defined as per Eq. 3 [91]:

$$EI = \frac{RA_{ref} - RA_{H_2}}{RA_{ref}} \cdot 100 = \frac{\left[(A_i - A_f)/A_i\right]_{ref} - \left[(A_i - A_f)/A_i\right]_{H_2}}{\left[(A_i - A_f)/A_i\right]_{ref}} \cdot 100 \quad (3)$$

where RA_{ref} and RA_{H2} represent the reduced area at fracture in air or another inert gas and a hydrogen atmosphere, while A_i and A_f indicate the cross-section before and after the test. The higher the embrittlement index, the more significant the loss of ductility in the material. Although hydrogen embrittlement significantly impacts elongation and reduction of area at fracture, elastic properties, yield strength, and ultimate tensile strength remain largely unaffected [92][93].

Geometrical imperfections, notches, and other stress concentrator effects can significantly increase the severity of hydrogen embrittlement. This is due to a high-triaxial stress region ahead of the notch and a high-strain zone at the notch root. In these areas, more hydrogen atoms tend to accumulate, thus generating concentration peaks and, consequently, spots of localized embrittlement [94]. Similarly to smooth specimens, notched specimens typically show considerable losses in reduced area at fracture with minimal modifications in YS and UTS [89]. Table 7 summarizes the HE susceptibility of various austenitic stainless steels. Slow strain rate tensile tests were conducted at 24 °C in a 69 MPa hydrogen environment.

Table 7: HE susceptibility of austenitic stainless steels (adapted from [95]*)*

HE susceptibility	Notes	EI	Austenitic steels
Negligible	Suitable for high-pressure hydrogen environments	0.00 – 0.03	A286, 216, 316, 22-13-5
Small	Potentially usable in hydrogen environments under specific temperature and pressure conditions	0.04 – 0.10	309S, 310, 347, 18-3-Mn
Medium-high	Potentially usable in hydrogen environment at low pressure, after assessing fracture properties and fatigue performance	0.11 – 0.30	Tenelon, A302B, 304L, 304N, 305, 308L, 321, 21-6-9 + 0.1N, 21-6-9 + 0.3N
High	Not recommended for hydrogen service	0.31 – 0.50	18-2-12, 18-18 Plus, 18-2-Mn
Extreme	Not usable if hydrogen is present, even in limited amounts	0.51 – 1.00	CG-27

The evaluation of fracture and fatigue performance is also crucial to completely assess the hydrogen-metal compatibility [96]–[99]. In fact, fracture resistance can be significantly reduced when a material is exposed to pressurized H_2. Weld zones are particularly affected and could create brittle spots in otherwise ductile steels. Hydrogen exposure reduces the critical stress required to initiate a crack but also decreases the material's resistance to further crack propagation [74].

In addition, hydrogen can adversely affect a metal's resistance to FCGR when subjected to cyclic loads induced by pressurization and depressurization cycles (e.g., when the vessel is filled and emptied) [100]. Minor geometrical defects, particularly in WZs and HAZs, act as stress concentrators and are preferential crack initiation sites. Unfortunately, such minor flaws are very difficult to avoid, even in equipment never used in hydrogen environments [101]. Several testing campaigns highlighted that, when a non-pre-cracked component operates in the high-cycle fatigue domain, its fatigue life is almost unaffected by the operating environment (even at elevated hydrogen purity and pressure) [102]. However, in the low-cycle fatigue domain, the exposure to hydrogen environments tends to accelerate the FCGR by one or two orders of magnitude, depending on the stress intensity range [103]. The stress intensity threshold (ΔK_{th}), i.e., the stress-intensity range below which crack do not propagate under cyclic loading, depends on the strength and microstructure of the material, but it generally ranges between 10 and 15 $MPa \cdot m^{-1/2}$ [104], [105]. This value is reduced in hydrogen environments, typically by 10-25 %. The higher the hydrogen partial pressure, the more significant the reduction in ΔK_{th} will be [106][107]. However, this parameter is also influenced by several material characteristics and properties, loading parameters, and environmental factors.

3.2.5 Factors influencing hydrogen embrittlement

Hydrogen embrittlement results from the complex interplay of multiple factors. A primary aspect is the nature of the hydrogen environment, which includes parameters like pressure, temperature, hydrogen purity, and form (either atomic or molecular). The second key factor is the material: the chemical composition, grain shape, size, orientation, presence of heterogeneities, phase stability, yield, ultimate tensile strength, and surface conditions can remarkably affect the susceptibility to HE. The third factor is the stress field, i.e., the type of loading (either monotonic or cyclic), residual stresses, strain rate, load frequency, and amplitude [74]. While the individual effects of these factors have been investigated, their combination still needs to be fully understood [108]. Figure 17 provides a schematic representation of the interdependence of environmental, material, and mechanical factors on the HE susceptibility of engineering materials.

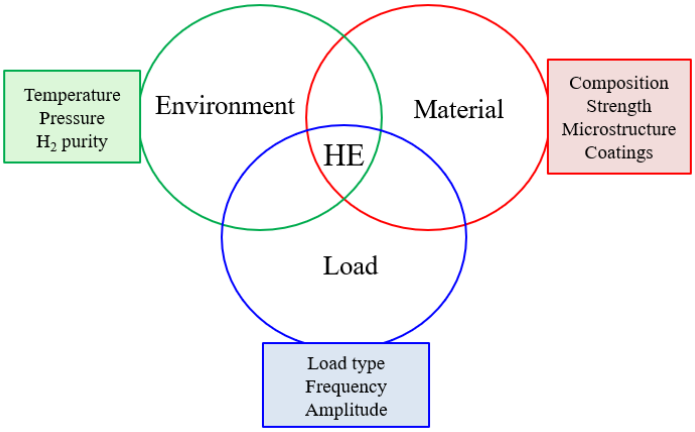

Figure 17: Factor influencing the severity of hydrogen embrittlement [74]

The operating temperature affects the kinetics of surface reactions as well as hydrogen solubility, diffusivity, and trapping. Therefore, the magnitude of hydrogen-induced degradation of the mechanical properties should be evaluated under realistic temperature conditions. In the case of LH_2 handling and storage equipment, tests at cryogenic temperatures are necessary to assess the hydrogen effect on the system's reliability. San Marchi and Somerday [89] observed that austenitic stainless steels are most susceptible to hydrogen embrittlement at temperatures ranging from –70 and –20 °C. This is mainly due to strain-induced martensite transformation, which forms a highly susceptible microstructure at low temperatures and under mechanical load. Yang et al. [109] discovered that AISI 304 austenitic stainless steel, typically used for LH_2 storage tanks, manifests a decreased HE susceptibility as the temperature drops from 25 to –50 °C, then increases when the temperature falls below –50 °C. Notably, HE effects vanish at temperatures below –150 °C due to reduced hydrogen diffusion. Michler and Naumann [110] showed that increasing nickel content above 12.5 $\%_{wt}$ and achieving a homogenous microstructure can substantially minimize the temperature-dependent effects of HE in austenitic stainless steels. Additionally, Ogata [111] demonstrated that in austenitic stainless steels, HE is almost insensitive to temperature variations and does not become apparent until a specific level of deformation is reached. The influence of temperature on the HE susceptibility can be partially explained through the hydrogen trapping model, where H atoms are considered to diffuse and become trapped at vacancies or other microstructural features. At cryogenic temperatures, however, the hydrogen diffusion coefficient is too low,

and a sufficient accumulation at these sites is not possible, thus preventing a severe degradation of the mechanical properties [74].

In addition, the hydrogen partial pressure is a crucial factor affecting the severity of HE. As per Sievert's law, the hydrogen solubility in a crystal lattice increases proportionally to the square root of the hydrogen partial pressure. Therefore, the higher the pressure, the higher the hydrogen concentration within the material and, consequently, the higher the reduction in mechanical properties [112]. Nevertheless, the trap occupation is pressure-dependent only over a specific pressure range, above which it reaches saturation when H atoms occupy all available traps. The maximum hydrogen concentration within the metal lattice depends on the microstructure and yield strength [113]. Generally, the pressure dependency of hydrogen-induced degradation in fracture toughness is more remarkable for low-strength steels than for high-strength ones [114]. Fatigue performance declines as hydrogen pressure increases, influenced by the stress intensity range. At high ΔK, the fatigue crack growth rate is relatively unaffected by pressure changes, whereas at low ΔK, it can become ten times higher as hydrogen pressure rises from 0.02 to 100 MPa [115].

Microstructural features, such as dislocations, non-metallic inclusions, and precipitates, affect hydrogen mobility within the crystal lattice [111]. These reversible traps are considered primary contributors to HE [116]. Generally, higher levels of cold work lead to a higher dislocation density, resulting in more reversible traps and, consequently, heightened susceptibility to hydrogen embrittlement [117]. Notably, steels of the same grade produced in different years or through varied manufacturing methods may exhibit distinct microstructures and mechanical properties due to better refinement and cleanliness [118]. Grain refinement introduces additional grain boundaries but creates more trapping sites; therefore, it has a twofold opposite effect on the material's susceptibility to hydrogen-induced degradation. Experimental evidence suggests that fine-grained microstructures are more resistant to HE than coarse-grained ones, even if other studies indicate a critical grain size that maximizes hydrogen diffusion [119]–[121]. Overall, the relationship between grain size and HE severity is a topic of ongoing debate.

Weld and heat-affected zones often exhibit the highest amount of microscopic and macroscopic defects. Residual stresses, different microstructures resulting from various heating and cooling processes, weld flaws, and geometric defects contribute to crack initiation and propagation in H_2 environments [122]. The welding technique has a remarkable influence on the severity of HE since the processes form different amounts of martensite or acicular ferrite in the HAZ [74]. Each weld type is characterized by distinct residual stresses and resulting microstructures and should be carefully selected when realizing equipment for LH_2 storage. Chemical composition also affects the material's susceptibility to hydrogen-induced damage. Various carbon equivalent formulas establish correlations between the material's susceptibility to HE and its alloying element content. They indicate the tendency to form martensite on cooling, a microstructure highly prone to hydrogen damage that can be typically found in weld zones [110][122].

The yield strength also plays a crucial role in the severity of HE. High-strength steels are generally recognized as having greater susceptibility to hydrogen-containing environments than low-strength ones [123]. This strength dependence is especially evident at lower H_2 pressures [114]. The low-strength austenitic steels (e.g., AISI 304 and AISI 316) typically used for LH_2 storage equipment demonstrate high resistance to crack growth propagation under monotonic loads [89].

In the case of cyclic loads, the frequency and stress ratio (i.e., the ratio between minimum and maximum stress intensity factor) play a critical role in fatigue performance. Since hydrogen embrittlement is a time-dependent phenomenon, FCGR generally increases as frequency decreases; lower frequencies provide longer exposure time per cycle, allowing more H atoms to absorb at the crack tip [89]. Although this frequency dependency of hydrogen-enhanced FCGR is commonly accepted, very few tests were conducted at frequencies lower than 0.1 Hz. Murakami et al. [124] investigated the fatigue performance of austenitic stainless steels in hydrogen environments and demonstrated that diffusible and non-diffusible hydrogen contributes to the acceleration in FCGR. Similarly, Matsunaga et al. [125] observed this frequency dependence in AISI 304 steel for both in-situ and ex-situ fatigue testing.

Table 8 provides a summary of the environmental, material, and mechanical parameters which influence the severity of HE, highlighting the actual conditions under which LH_2 storage equipment operates.

Table 8: Influencing factors for materials' susceptibility to HE (adapted from [74]*)*

Type	Factor	Greatest HE susceptibility	Notes
Environment	Hydrogen partial pressure	High hydrogen pressure	These conditions cannot be found in LH_2 storage tanks during normal operations, but are more likely for ancillary equipment handling gaseous hydrogen (e.g., tanks and pipes for boil-off gas)
	Temperature	Between –70 and –20 °C for austenitic steels	
	Hydrogen purity	High hydrogen purity	
Material	Microstructure	Untempered martensite	Welded areas can have an undesired martensitic microstructure; the welding process can minimize the formation of martensite on cooling
	Grain size	Coarse grains	
	Carbon equivalent	High carbon equivalent content	
	Strength	High strength	
	Welds and HAZs	Without post-weld heat treatments	
Load	Frequency	Low frequency	LH_2 storage equipment is cyclically filled and emptied and exposed to pressure fluctuations. Their frequency is extremely low, but also the amplitude is relatively limited (0.1 – 0.4 MPa)
	Amplitude	High stress amplitude	
	Monotonic load	High monotonic load	

4 Description of the thermal insulation systems

Thermal super-insulation systems are essential for storing and transporting liquid hydrogen and can be divided into two main categories: passive thermal insulation and active cooling insulation. Passive insulation is the most used approach and relies on high-performance materials, such as perlite, aerogel, spray-on foam insulation, glass microspheres, multi-layer insulation, and vacuum insulation panels, to minimize heat transfer and avoid the boil-off of the cryogenic fuel. These materials exhibit extremely high thermal resistance, representing an effective barrier for conductive, convective, and radiative heat transfer and maintaining the cryogenic environment required for LH_2 storage. In contrast, active cooling systems involve a cryogenic chiller, which uses energy to refrigerate the liquid hydrogen and achieve the target of zero boil-off. Active and passive insulation can be coupled with vapor-cooled shields, further reducing the heat transfer between the inside and outside of the tank. On the one hand, passive insulation is a simple and economical option for many applications, including large-scale storage tanks, but does not achieve zero boil-off. On the other hand, active cooling could eliminate boil-off, but the required additional equipment, is more complex, heavier, bulky, and expensive, and implies significant energy consumption [4]. This section presents the most common passive and active insulation systems, indicating their thermal and mechanical properties, potential safety issues, and aspects related to circularity and sustainability.

4.1 Perlite

Perlite is an amorphous volcanic rock that expands when rapidly heated to 900–1200 °C. It is widely used as an insulation material in cryogenic tanks, particularly within the evacuated annulus of double-walled tank systems. Expanded perlite (EP), shown in Figure 18, is used in construction, petrochemical, industrial, and chemical industries due to its excellent thermal insulation properties and lightweight nature [126], [127]. Perlite has been used as an insulation material in cryogenic applications since the 1960s, owing to its low thermal conductivity, low cost, and ease of handling. It is used as insulation in transport vessels for cryogenic fluids and in storage tanks for refrigerated gases, such as liquefied petroleum gas (LPG) and LNG [128], [129].

Figure 18: Expanded perlite powder [130]

4.1.1 Thermal properties

Perlite is a natural microporous material with thermal conductivity values ranging from 10^{-4} to 10^{-3} W/m·K, depending on the vacuum levels. It has a melting point of 1260 °C, indicating structural stability at high temperatures despite its worse insulation performance compared to alternatives like glass microspheres [131].

The thermal conductivity of perlite varies significantly with absolute pressure (P), thus affecting its performance as an insulator:

- **High vacuum ($P < 10^{-3}$ Pa)** – Perlite achieves a low thermal conductivity of 0.95 mW/m·K, comparable to that of multi-layer insulation at the same pressure, making it effective under ultralow-pressure conditions.
- **Moderate vacuum (10^{-3} Pa < P < 10^{-1} Pa)** – As pressure increases, perlite's thermal conductivity rises to 1 mW/m·K, showing a minor decrease in insulation effectiveness.
- **Ambient pressure ($P = 10^{5}$ Pa)** – At ambient pressures, perlite's thermal conductivity rises substantially to 44 mW/m·K, indicating a sharp reduction in insulation performance under non-evacuated conditions [11].

Perlite faces a reduction in insulation performance over time due to settling and compaction. These aspects are particularly critical in applications subjected to vibrations (such as shipping vessels) or thermal cycling. Settling occurs as perlite particles shift or compress, reducing the effective insulation thickness and forming voids that lead to higher thermal conductivity and increased heat transfer. This is especially problematic in cryogenic storage tanks that require long-term thermal stability [132]. Thermal cycling, i.e., the repetitive cooling and heating cycles in cryogenic applications, cause the expansion and contraction of the tank wall. This phenomenon affects perlite insulation since it leads to particle shift and compaction. Perlite tends to compact more at the tank bottom, forming gaps that constitute thermal bridges, which can significantly reduce perlite's insulation capability over time, making it less effective in maintaining cryogenic temperatures under repeated thermal cycling [132].

Perlite is a viable insulation material for cryogenic applications, particularly under high vacuum conditions. Despite its higher thermal conductivity compared to other opacified siliceous powders, perlite remains widely used due to its cost-effectiveness, ease of drying and handling [128]. However, its performance is compromised by factors such as vacuum degradation, settling, and compaction from thermal cycling and vibration. Given these limitations, perlite may be best suited for stationary cryogenic applications with stable vacuum conditions, while alternatives like glass bubbles may be preferable in mobile or long-term cryogenic storages.

4.1.2 Mechanical properties

Expanded perlite particles are hollow and porous, resulting in low bulk density (ranging from 32 to 150 kg/m³). This property, along with its low thermal conductivity, makes perlite an attractive material for a wide range of applications, including lightweight building materials, cryogenic insulation systems, and fillers in polymer composites [127], [133]. The mechanical strength of perlite is a crucial factor in determining its suitability for different applications. Key mechanical properties of perlite include also compressive strength and impact resistance [126], [134]. Perlite has relatively low compressive strength due to its porous structure and

thin-walled bubbles. This property depends on factors like density, particle size, and expansion conditions. Whereby perlite with a higher density usually exhibits a higher compressive strength [126], [134]. In addition, adding perlite to polymer composites can improve their impact resistance. This is because perlite particles can absorb energy during impact, thus preventing crack propagation through the polymer matrix [126]. Several studies report the incorporation of perlite, both raw and expanded, into polymeric composites to improve their mechanical, thermal, and rheological properties [135]–[139].

It is important to note that the mechanical properties of perlite can vary depending on the source and expansion process. Factors such as the chemical composition of raw perlite, temperature, and heating rate during expansion can influence the structure and morphology of the resulting expanded perlite, thus affecting its mechanical properties. Therefore, a complete characterization of perlite is essential to understand its mechanical behavior and optimize its performance. One challenge in using perlite for cryogenic insulation is its moisture content, as moisture can significantly increase evacuation time and reduce insulation efficiency. Therefore, it is essential to use dry perlite or take steps to dry perlite before using it in cryogenic applications.

Despite the extensive use of perlite across various industries, there are still some gaps in the research on its mechanical properties. The known sources do not directly address the effect of temperature on specific mechanical properties, such as tensile strength, flexural strength, or impact resistance. Moreover, data are usually available for perlite-containing materials (e.g., polymeric composites) but not for raw perlite. To fully understand how temperature affects the mechanical performance of perlite, more research is needed. This is particularly true in the analysis of microstructure, investigating how it changes at different temperatures and how these changes correlate with mechanical properties. Additional research would fill existing knowledge gaps and allow for a more efficient and safer application of perlite under various temperature conditions [127], [133], [134].

Some mechanical properties of perlite and perlite composites are shown in Figure 19: (a) Tensile curves of perlite composites (b) Tensile curves of expended perlite composites (c) Young's modulus, (d) Tensile strength and (e) Strain at yield as a function of perlite content [135]Figure 19.

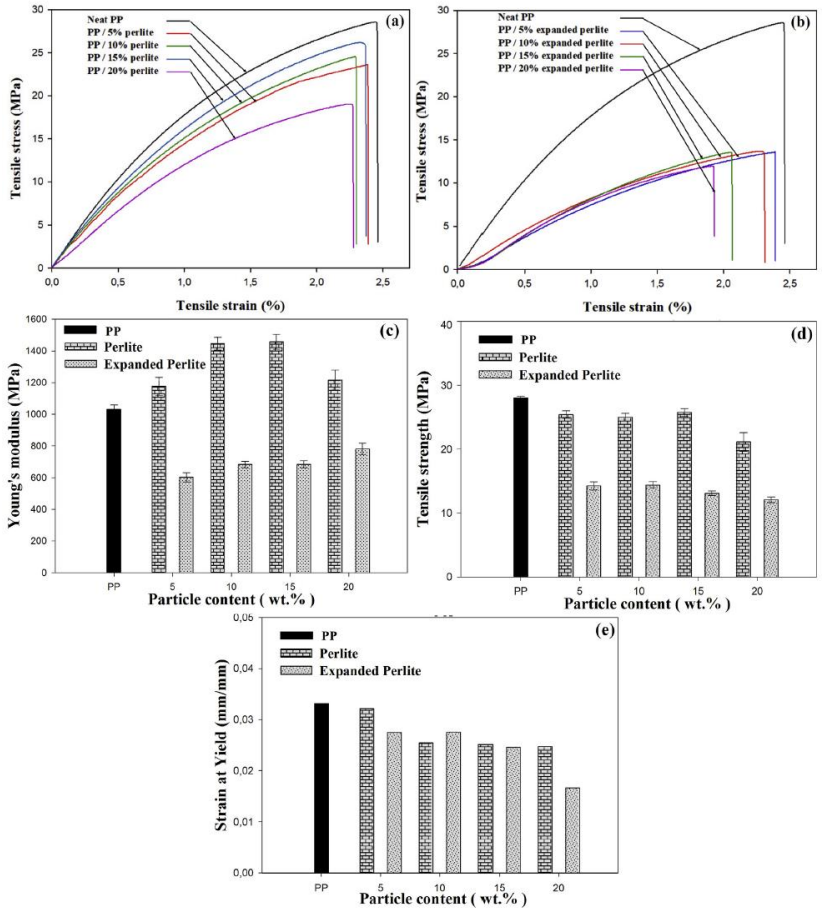

Figure 19: (a) Tensile curves of perlite composites (b) Tensile curves of expended perlite composites (c) Young's modulus, (d) Tensile strength and (e) Strain at yield as a function of perlite content [135]

Figure 20 shows the tensile properties of ethylene-propylene composite materials (EPM) containing different amounts of perlite.

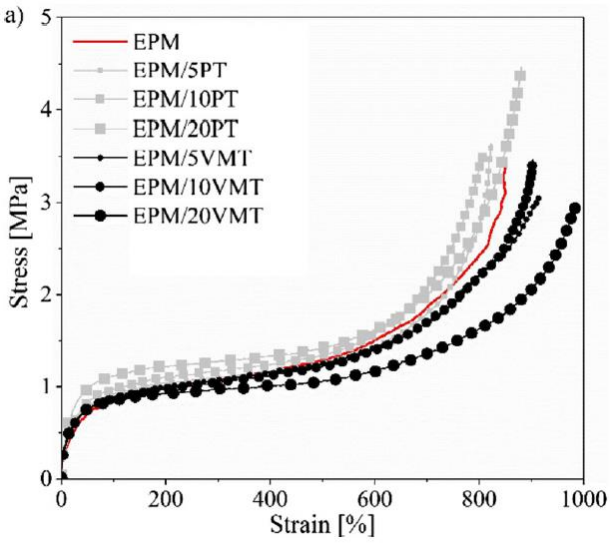

Figure 20: Tensile test curves of the studied EPM composites [140]

4.1.3 Safety issues

When evaluating the safety aspects of insulation materials, several key factors must be considered, including fire resistance, impact resilience, and protection against external threats.

In terms of fire resistance, Kusiorowski et al. [141] demonstrated that expanded perlite composites perform well under cellulosic fire conditions. In this kind of fire, the temperature of the system grows slowly, reaching 900 °C approximately after an hour, while a temperature of 500 °C may be reached after 5 minutes. When heated, perlite grains expand due to the rapid phase transition (from water to steam) within the perlite structure. The phase change reduces the material's density, which is influenced by the water content trapped within the perlite rock. Additionally, they report that large-scale tests confirm the fire-resistance qualities of the developed perlite boards. The best performing boards in terms of insulation performance and fire-resistance, are achieved in boards bound with a binder containing minimal alkaline substances, characterized by the lowest thermal conductivity.

For perlite used in bulk-fill insulation systems, testing under simulated fire scenarios measured a much lower specific heat flux through perlite insulation compared to MLI systems [142]. However, under high heat exposure, the perlite near the heat source may be degraded, thus turning into light yellow [142]. Despite this visible deterioration of the material, it remains resilient and appears promising even when it is fully engulfed by external fires.

Regarding external threats, earthquakes and other natural hazards must be considered. Shigapov et al. [143] suggest that perlite insulation has minimal effect on the oscillation of a filled tank during seismic events, although it significantly affects wall oscillation in empty tanks. These findings imply that earthquakes may have little impact on the structural integrity of perlite insulation. Nonetheless, vibrations could potentially cause perlite compression, altering its thermal properties [9].

4.1.4 Circularity and sustainability

Perlite is a sustainable option for a range of applications due to its relatively low environmental impact. It has remarkable sustainability credentials and a low environmental impact across various metrics. The carbon footprint of expanded perlite is around 0.18–0.21 kg_{CO2eq}/kg. This makes it superior to other insulating materials like foam glass or fossil-based materials.

Nevertheless, perlite poses some environmental concerns. Its mining disrupts ecosystems and habitats. The high-temperature heating process, which expands perlite is energy-intensive and contributes to greenhouse gas emissions. Furthermore, perlite is a non-renewable resource. Despite the enormous global reserves, continued mining depletes this limited resource.

The end-of-life treatment of different materials can be diverse and significantly influence the total life cycle impact of an insulation material. Various forms of waste treatment may account for additional impacts, while recyclability of a material may reduce its impact [144]. Pure perlite has a strong circularity and sustainability potential due to its multitude of applications ranging from horticulture [145] through construction industry [146] up to water treatment [147], while perlite composites may pose more limited usability as a recycled material (i.e. polymer-based

composites). Perlite is reusable if it is free of biological contamination. In the event of biological contamination, perlite must be sterilized through heat or chemicals before reuse

Global warming potential (GWP) expresses the material's relative contribution to greenhouse gas emissions (GHG). GWP is calculated at the manufacture, use, and end-of-life stages as the sum of GHG emissions multiplied by their respective GWP impact factors [148]. Expanded perlite presents superior GWP when compared on a mass-to-mass basis to similar alternatives such as mineral wool, expanded polystyrene (EPS), fiberglass, extruded polystyrene (XPS), and polyurethane foam. It accounts for only 0.52 kg_{CO2eq} compared to polystyrene, with 2.70 kg_{CO2eq}. As shown in Figure 21, when compared on a volume basis, perlite comes in third place, after fiberglass and EPS, with 60.1 kg_{CO2eq}/m^3.

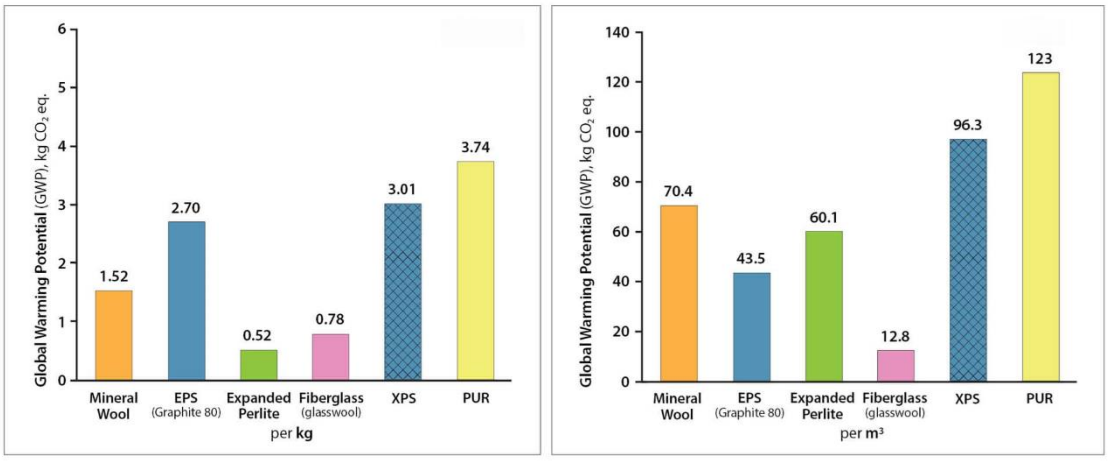

Figure 21: Global warming potential of expanded perlite and other building insulation materials calculated a) on a mass basis and b) on a volume basis [144]

4.2 Aerogel

Aerogels exhibit excellent thermal insulation performance at low temperatures, making them suitable for a variety of applications [7], [149], [150]. Aerogel blankets consist of a nano-porous silica aerogel embedded within a fiber matrix, creating a highly effective insulation system that remains efficient across a wide range of pressures. These properties make aerogel blankets suitable for applications where structural durability and thermal stability are critical [151]. As an example, Figure 22 shows a high-performance aerogel insulation for building applications.

Figure 22: High-performance aerogel-based produced by Aspen Aerogels Inc. [152]

4.2.1 Thermal properties

Aerogel beads have demonstrated superior performance compared to traditional insulation materials, such as perlite powder and MLI, in cryogenic environments. Opacified aerogels, such as those with carbon black incorporation, have shown even lower thermal conductivity in high-vacuum conditions [150], [153]. Aerogels have been proposed as insulation for various space applications, including cryogenic umbilical connections, storage dewars, and cryogenic transfer lines [153]. Moreover, the enhanced thermal insulation properties of aerogels make them promising for LNG storage systems [154].

Cryogel is an aerogel-based material valued for its extremely low thermal conductivity and designed for cryogenic service. Cryogel blankets incorporate silica aerogel particles within a fiber matrix, which helps to stabilize the insulation structure and improve its resilience. This composite structure creates multiple air pockets within the material, thus reducing conduction and convection. Typical values of thermal conductivity range from 1 to 10 mW/m·K [11].

Cryogel blankets exhibit low thermal conductivity in high-vacuum environments, with values as low as 1.5 mW/m·K (i.e., comparable to high-density perlite). However, as pressure increases, Cryogel's thermal conductivity also rises, reaching approximately 12.3 mW/m·K at atmospheric pressure. The increase in thermal conductivity with pressure is primarily due to enhanced heat transfer through gas conduction and convection in less-evacuated environments.

- **High vacuum ($P < 10^{-3}$ Pa)** – Thermal conductivity is approximately 1.5 mW/m·K, ideal for minimal heat leakage in cryogenic storage.
- **Soft vacuum ($10 \text{ Pa} < P < 10^{3}$ Pa)** – Heat transfer becomes complex as multiple mechanisms (i.e., conduction through the solid phase, radiation, conduction through the gas phase, and convection) contribute to the total heat flow.
- **Ambient pressure ($P = 10^{5}$ Pa)** – Thermal conductivity increases to around 12.3 mW/m·K, limiting the effectiveness of the insulator under non-vacuum conditions [151].

The fiber matrix within the Cryogel blanket influences its thermal properties by providing better thermal stability and improving the resistance to mechanical stresses. Nevertheless, the fiber matrix itself has a higher thermal conductivity (30.6 mW/m·K at ambient temperature) than the

Cryogel composite (19.1 mW/m·K), as it lacks the same insulating properties of the aerogel particles. However, this matrix adds resilience against physical stress, making aerogel blankets more durable than pure aerogel powders, which are susceptible to settling and compaction.

There are alternative forms of aerogels exhibiting different characteristics than the conventional blankets:

- **Aerogel powders** – Offer similar thermal conductivity under vacuum conditions as perlite but have a higher risk of settling in mobile applications. Their low weight and high compressive strength make them viable for stationary applications, though high production costs limit their use in large-scale storage systems.
- **Aerogel-fiberglass composite blankets** – These materials provide effective insulation even at lower vacuum levels, though they are less efficient than MLI under high vacuum conditions. They can be a suitable choice where MLI is impractical [155].

Lisowski et al. [155] conducted research in the performance of two aerogel materials at different pressures and temperature conditions. Under consideration was the abovementioned Cryogel and a material called Cryolite. The results are visualized in Figure 23.

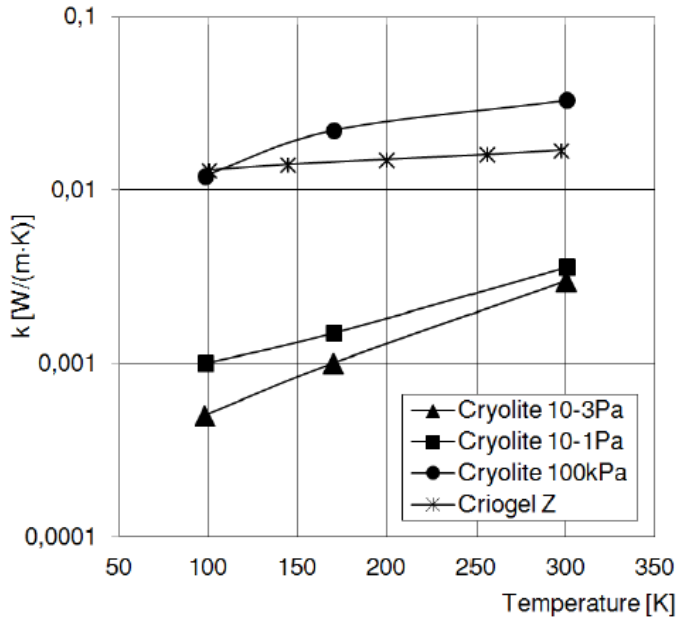

Figure 23: Thermal conductivity of Cryogel and Cryolite at different temperatures [155]

Cryolite's thermal conductivity increases with temperature, with the highest values at ambient pressure. The lowest values are observed at an absolute pressure of 10^{-3} Pa. In contrast, Cryogel Z's thermal conductivity remains approximately equal to 10 mW/m·K, almost unaffected by temperature variations. The thermal conductivity of this material was not tested at different pressures; therefore, no general conclusions can be drawn regarding the pressure dependency.

Aerogel blanket insulation, with its low thermal conductivity, is an effective choice for cryogenic applications requiring long-term thermal stability. While its performance varies with vacuum

levels, it remains efficient at high vacuum and acceptable under soft vacuum, being potentially suitable for a range of cryogenic storage and transport applications.

4.2.2 Mechanical properties

Aerogels are known for their low density, high surface area, and low thermal conductivity. Despite their remarkable properties, the intrinsic mechanical fragility of aerogels has been a significant obstacle to their widespread use for cryogenic applications [156], [157]. The mechanical properties of aerogels, such as compressive strength, elastic modulus, and toughness, are strongly influenced by their microstructure, including density, pore size, and the interconnectivity of the framework structure [158]–[160]. In particular, the low density and high porosity, hallmark features of aerogels, contribute to their fragile nature [159], [161]. Conventional particle-based aerogels tend to exhibit brittle behavior under load, limiting their capacity to withstand significant mechanical stresses [159].

Various strategies have been explored to improve the mechanical properties of aerogels, including:

- **Polymer reinforcement –** Incorporating polymers into the aerogel matrix can significantly enhance strength and flexibility [162]–[164].
- **Microstructure modification –** Adjusting processing parameters during aerogel synthesis can lead to a more robust microstructure with better interconnectivity, resulting in improved mechanical properties [158], [165].
- **Use of 1D or 2D building blocks –** Utilizing nanowires, nanofibers, or nanosheets as building blocks instead of particles allows for more efficient bending deformation, enhancing the aerogel's strength and elasticity [159].
- **Thermal treatment –** Carbonization or pyrolysis in an inert atmosphere can increase the mechanical stability of the aerogel, especially at high temperatures [165], [166].

Despite advances in the improvement of aerogels mechanical properties, there are still challenges, such as their inherent fragility and limited durability. Further improving the mechanical strength and toughness of aerogels remains a focus area for research. In addition, evaluating the long-term performance of aerogels in cryogenic environments, particularly under cyclic mechanical and thermal stresses, is essential to ensure their reliability.

In summary, research on aerogels exhibited significant progress in enhancing their robustness in terms of mechanical properties. However, fragility remains a concern that requires further investigation including the development of new reinforcement strategies which can offer promising pathways for developing high-performance aerogels with improved mechanical properties [167]–[169].

Figure 24 shows the compressive modulus versus density of various aerogels, produced through different processes.

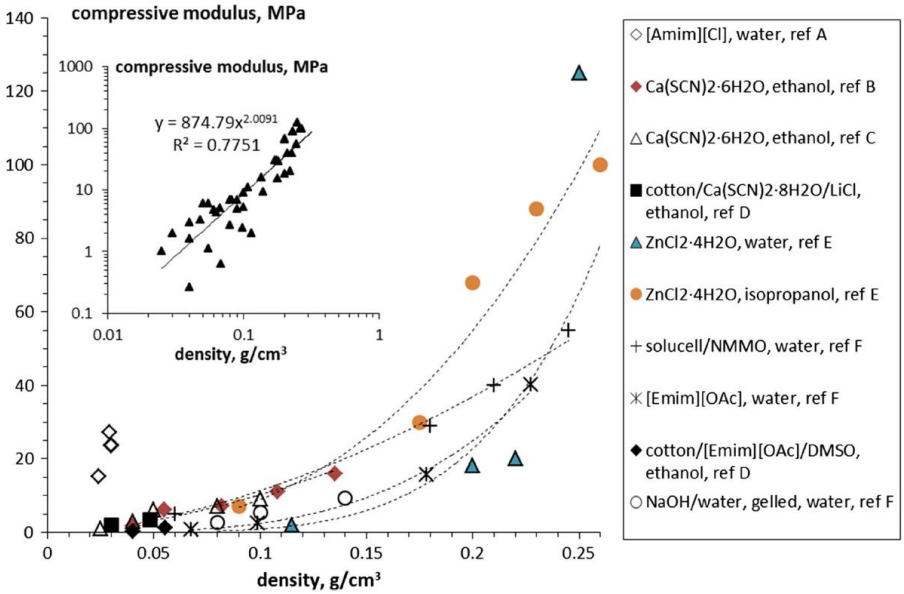

Figure 24: Compressive modulus versus aerogel density for various cellulose origins dissolved in different solvents and coagulated in different non-solvents. Dashed lines indicate power-law fits [170]

A typical stress-strain curve of silica aerogel-polyester composite is shown in Figure 25.

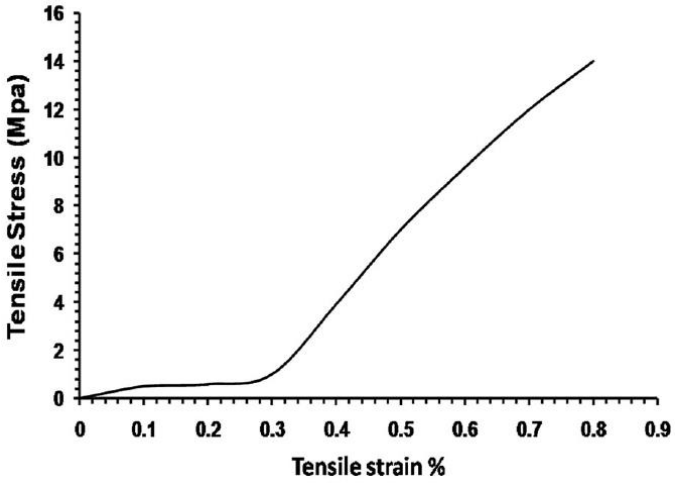

Figure 25: Stress–strain curve for silica aerogel-polyester composite [171]

Table 9 summarizes the mechanical and thermal parameters for a silica aerogel produced through different methods.

Table 9: Comparison of key mechanical and thermal parameters of SiC aerogels prepared using three different building blocks [159]

Building blocks	Preparation methods	Strength [MPa]	Recoverable strain [%]	Thermal conductivity [W/m·K]	Maximum tolerable temperature in air [°C]
0D	Sol-gel method	1.32	< 3	0.049	–
0D	Preceramic polymer pyrolysis method	1.6	< 10	–	1500
		10	–	–	1200
		16	< 10	–	1600
1D	Chemical vapor deposition	0.02	0.6	0.029	1000
		0.025	0.6	0.035	1100
		0.0306	0.5	–	1100
		0.0206	0.7	0.026	1000
		5.7	0.2	0.121	1100
		1.255	0.4	0.0393	1200
		0.026	0.8	0.0284	1200
2D	Carbon thermal reduction	–	–	0.03	1000
		0.47	0.04	–	–
		2	0.9	–	–
		0.03	0.6	0.025	1000
		3.79	0.1	0.046	1100
2D	Ice crystal-induced self-assembly of nanofibers or nanowires	≈ 0.052	0.6	0.019	1200
		9.8	< 5	0.02	800
		0.017	0.8	0.024	1200
		0.11	< 10	0.03	750
		≈ 0.035	< 20	0.161 (at 600 °C)	–
		0.82	0.3	0.1597 (at 600 °C)	–
		0.073	< 20	0.063 (at 100 °C)	1000
2D	Sacrificial template	≈ 8	0.8	0.014	1200
		0.0014	0.6	0.019	1100
		≈ 0.016	0.95	–	–
		0.02	0.6	0.026	–

4.2.3 Safety issues

Aerogel KF-PVA-BGP comprises a tubular structure of hollow kapok fibers with a polyvinyl alcohol binder and a biguanide phosphonate flame-retardant crosslinker. This insulation material exhibits strong potential for emerging applications due to its exceptional fire safety and flame-retardant properties [172].

Similarly, silica-based aerogel porous boards demonstrate excellent fire safety performance. According to Liu et al. [173], this insulation system significantly reduces combustion intensity and limits heat release during burning. From this perspective, aerogel insulation systems stand out as a safe choice, characterized by excellent fire resistance. However, further research is necessary to assess the safety of aerogel insulation under conditions of vibration and accidental scenarios, such as impacts of external objects (e.g., missiles and debris), exposure to ambient air due to cracking, and other undesired events.

4.2.4 Circularity and sustainability

Sustainability and circularity of the aerogels strongly depends on their production method. The sustainability and circularity of aerogels strongly depend on their production methods. The most significant environmental impacts and energy demands originate from the drying processes and the raw materials and solvents used across various stages of production, including gelation, aging, and drying [174]. Additionally, examining the final products and production processes of aerogels, it can be concluded that they are better than polyurethane-based materials in terms of net energy, greenhouse gas emissions, and development of less solid waste [175].

Environmental impacts associated with aerogels differs, with global warming potentials ranging from 4.40 kg_{CO2eq} to 6,970 kg_{CO2eq}, acidification potentials from 0.034 kg_{SO2eq} to 930 kg_{SO2eq}, and eutrophication potentials from 0.003 $kg_{PO4-3eq}$ to 2.56 kg $_{PO4-3eq}$. These variations are due to differences in precursors, solvents, production techniques, drying techniques, and application areas (Figure 26, Figure 27 and Figure 28) [174].

Figure 26: Global warming potentials of different aerogels [174]

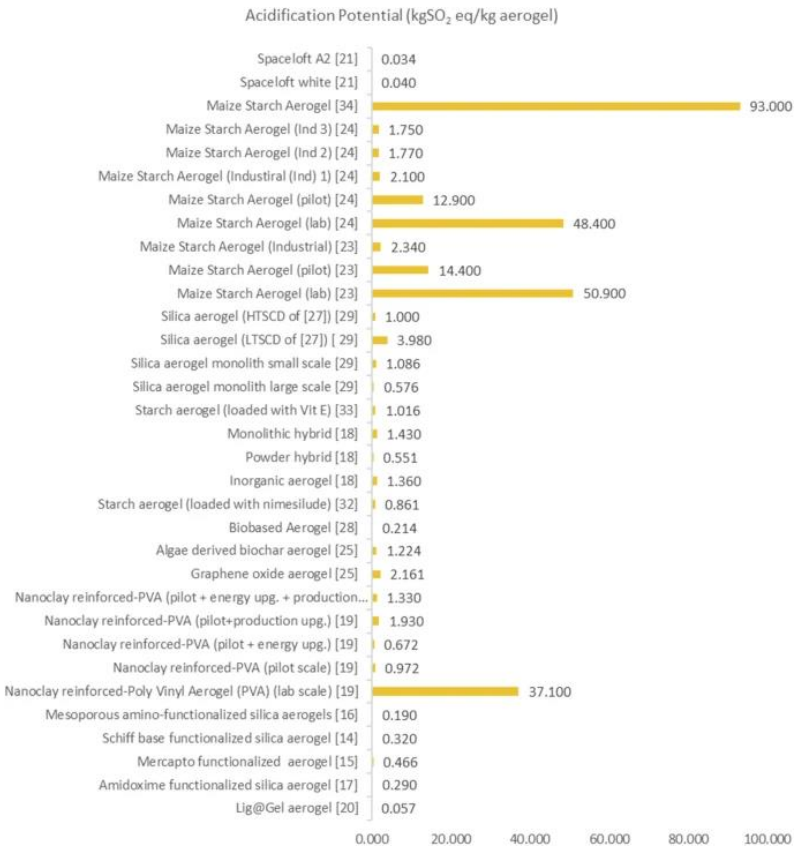

Figure 27: Acidification potentials of aerogels [174]

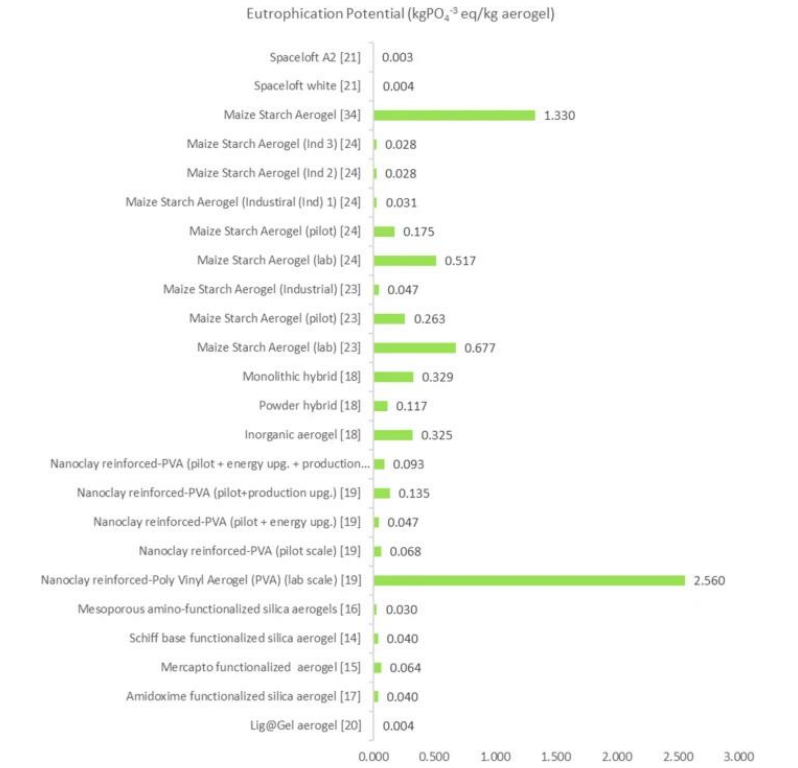

Figure 28: Eutrophication potentials of aerogels [174]

Aside from this, the life-cycle consideration cannot overlook the environmental impact resulting from the production of protective masks, which are primarily made of glass microfiber, melt-blown glass fiber, polypropylene (PP), or polyethylene terephthalate (PET). This is because their production involves high energy consumption, high costs and elevated emissions of pollutants, significantly limiting their wide range of sustainable applications.

Additionally, the environmental toxicity impacts of accidental or spontaneous aeroparticle dispersion should be considered along with any potential toxic effects brought on by the chemicals' release, which may result in ecosystem deterioration and a decline in biodiversity. Acute or long-term impacts on human health can result from these chemicals' ability to seep into the soil, harm aquatic life and important soil symbionts, and indirectly reach agro- and animal products and the food chain [176].

Aerogel waste management presents significant uncertainty, due to the complexity of its composite structure. There is a lack of information regarding their disposal with the only exception being silica-based aerogels that are deemed non-toxic and disposed of as sand [174], adopting chemical, physical or thermal strategies [177]. To reduce the dispersion of aeroparticles into the environment and the exposure of workers to the particles, aerogel materials should be stored in a waste container or plastic bags that are labeled as hazardous waste before disposal [178]. Aerogel wastes end up in landfills or incinerators, which can lead to the release of volatile compounds in the atmosphere over time, as well as to the deposit of and significant accumulation of dust which can affect the performance and safety of disposal plants, with direct and adverse environmental and human health impacts. These remarks should also be extended to bio-based aerogels, which are generally considered environmentally friendly and non-harmful because when they are disposed of in landfills. They are subjected to breakage, thus emitting dust which negatively affects the environment and human health. Furthermore, considering aerogels can potentially contain additives [177], industrial waste landfills should be advised on the right waste procedures to be considered.

4.3 Spray-on foam insulation

Spray-on foam insulation (SOFI) is a type of insulation material applied as a liquid that expands into a foam upon application. SOFI has been tested across a range of pressures and temperatures to assess its insulation effectiveness under various conditions [179]. Rigid polyurethane foams (PU) are widely used as thermal insulation materials in cryogenic applications. They provide effective thermal insulation and structural support in LNG tanks. Their ability to withstand thermal stresses induced by cryogenic cooling and resist crack propagation is crucial to ensuring the long-term integrity of these tanks [180]. PU and polyisocyanurate (PIR) foams have been employed as external thermal insulation on space launch vehicles, such as the Space Shuttle. In these applications, the foams must meet strict performance requirements, including low density, high strength, low thermal conductivity, and resistance to thermal shocks and vibrations [181]. PU foams are also used in various other cryogenic applications, such as insulation for cryogenic pipelines, cryogenic fluid storage containers, and scientific equipment. In each case, foam selection and application methods depend on requirements tailored for the specific applications [180]. In general, spray polyurethane has simpler processing and lower cost compared to other application methods

[182], [183]. Figure 29 shows the schematic of a spray-on foam insulation system for cryogenic applications.

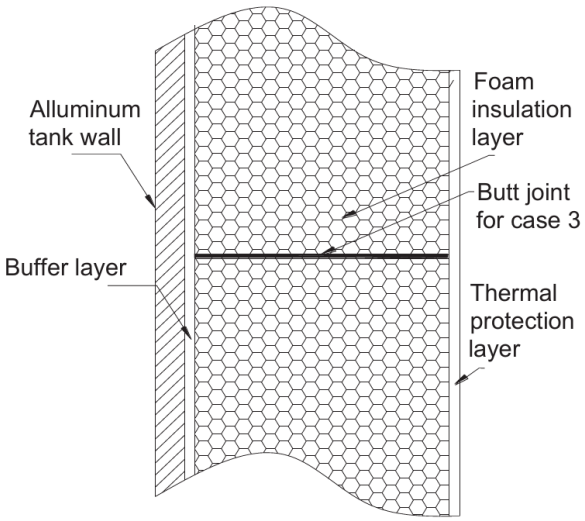

Figure 29: Schematic of a cryogenic foam insulation system [184]

4.3.1 Thermal properties

The thermal performance of SOFI is primarily assessed by its apparent thermal conductivity, which varies with pressure and temperature. Testing by Fesmire et al. [179] measured SOFI's thermal conductivity under conditions ranging from high vacuum to ambient pressure and across temperature from **–**200 to 20 °C. The results are summarized as follows:

- **High vacuum ($P < 10^{-3}$ Pa) –** SOFI achieves its lowest thermal conductivity of approximately 7.5 mW/m·K, making it effective in minimizing heat transfer.
- **Soft vacuum ($10 \text{ Pa} < P < 10^{3}$ Pa) –** Soft vacuum conditions introduce various heat transfer modes, which increase the overall heat flux.
- **Ambient pressure ($P = 10^{5}$ Pa) –** SOFI's thermal conductivity increases to around 21 mW/m·K, as gas conduction and convection begin to influence heat transfer more significantly.

SOFI's insulation performance tends to degrade over time due to environmental exposure. After 24 months, SOFI manifests an increase in thermal conductivity from approximately 20 to 29 mW/m·K, indicating a reduction in insulation effectiveness. This degradation highlights the need for routine assessment and potential replacement in applications where SOFI is exposed to harsh environmental conditions (e.g., maritime environments) [179].

In cryogenic conditions, SOFI absorbs moisture from the surrounding atmosphere, a process known as cryogenic moisture uptake. During cold propellant loading, a large amount of moisture can accumulate within the SOFI due to temperature gradients. For example, non-aged samples of the SOFI material NCFI 24-124 absorbed about 30% of their weight in water during a standard cryogenic cycle, indicating potential impacts on thermal performance and durability in humid environments [179].

There are two main types of thermal insulation foams:

- **Closed-cell foams** – Closed-cell foams (e.g., Polyurethane-A and Polyisocyanurate-A) exhibit thermal conductivity as low as 18 mW/m·K. Polyisocyanurate-A is the most effective insulation material. These foams are generally preferred for cryogenic applications due to their superior insulating properties and structural stability.
- **Open-cell foams**: Open-cell foams (e.g., Polyurethane-C and Polyurethane-D) have higher thermal conductivity and are less dense, making them less effective insulators but potentially beneficial in applications where lighter materials are required.
- **Typical foams**: Typical foams, such as rigid polyurethane or polystyrene, generally exhibit higher thermal conductivity (35–55 mW/m·K) and may be less suitable for mobile cryogenic tanks due to their lower thermal performance, rigidity, and flammability [185].

Table 10 summarizes the thermal conductivities and densities of various foams used in cryogenic applications. The variations in thermal conductivity over a narrow temperature range are shown in Figure 30 [185].

Table 10: Thermal conductivity and density (measured at ambient pressure) of various foams with closed-cell and open-cell structures

Material	**Thermal Conductivity (mW/m·K)**	**Density (kg/m³)**
Polyurethane-A (Closed Cell)	23	28.9
Polyurethane-B (Closed Cell)	25	35.0
Polyurethane-C (Open Cell)	38	6.83
Polyurethane-D (Open Cell)	33	17.2
Polyisocyanurate-A (Closed Cell)	18	32.0
Polyisocyanurate-B (Closed Cell)	24	32.0

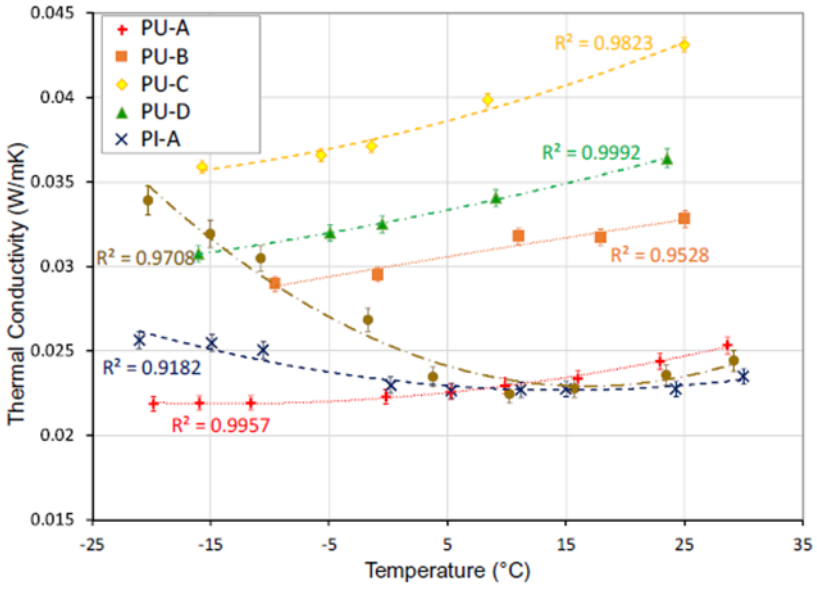

Figure 30: Thermal conductivities of various foams as a function of temperature [185]

SOFI remains an effective insulation material for cryogenic applications under high-vacuum conditions. However, its performance is subject to degradation from environmental exposure and cryogenic moisture uptake. Closed-cell materials, particularly polyisocyanurate foams, offer lower thermal conductivity and improved insulation efficiency. The choice of foam insulation depends on application-specific requirements, with considerations for structural stability, thermal cycling, and long-term environmental resilience.

4.3.2 Mechanical properties

Spray polyurethane foams (SPF) are prized for their distinctive mechanical properties, which make them suitable for diverse applications from building to cryogenic insulation. Their cellular structure, comprising a solid polymer matrix with gas-filled cells, provides exceptional compressive strength, impact resistance, and rigidity while maintaining low density [182], [183].

The mechanical properties of foams are primarily influenced by factors such as density, cell structure (size, shape, and distribution), polymer matrix composition, and temperature. As foam density increases, its compressive strength, tensile strength, and Young's modulus also increases. This is due to the greater amount of solid material present in denser foams, which guarantee a higher resistance to deformation.

Along with density, the size, shape, and distribution of cells within the foam play crucial roles in determining its mechanical properties. Foams with smaller, more uniform cells generally exhibit greater strength and stiffness than those with larger, irregular cells. In fact, smaller, uniform cells distribute stress more effectively across the foam structure.

The nature of the polymer matrix, including its chemical composition, molecular weight, and degree of cross-linking, significantly influences the foam's mechanical properties. For instance,

polyurethane foams derived from polyester polyols tend to be stronger and stiffer than those derived from polyether polyols, due to the stronger ester bonds in the polyester matrix [182], [186].

Finally, the temperature has a profound effect on the mechanical properties of foams. Generally, as temperature decreases, foams become stiffer and more brittle, with increased strength and Young's modulus but reduced ductility. This behavior is attributed to the reduced mobility of polymer chains at lower temperatures, leading to restricted deformation and higher susceptibility to fracture [180], [182].

Despite the great potential and flexibility of this material, using spray polyurethane foam in cryogenic environments presents specific challenges. First, PU foams may become brittle at cryogenic temperatures, leading to cracking and delamination. Selecting the right foam formulation, including the type of polyol and blowing agent, is essential to improve resilience at low temperatures [180], [182], [183]. Second, the foam adhesion to the substrate, typically aluminum or austenitic stainless steel, is critical for insulation performance in cryogenic conditions. Foam formulation and surface preparation play important roles in ensuring adequate adhesion. Replacing diethylene glycol with bio-based polyols, while beneficial for sustainability, may reduce adhesion [180], [183]. Finally, the so-called "cryopumping effect" occurs when air condenses within foam cells during cryogenic cooling. This condensed air can expand during reheating, causing stress and damage to the foam. Using closed-cell foams and applying foam properly to minimize defects can help mitigate the cryopumping effect [183].

Figure 31 shows the compressive strength of various PU foams as a function of temperature (ranging from –60 to 120 °C).

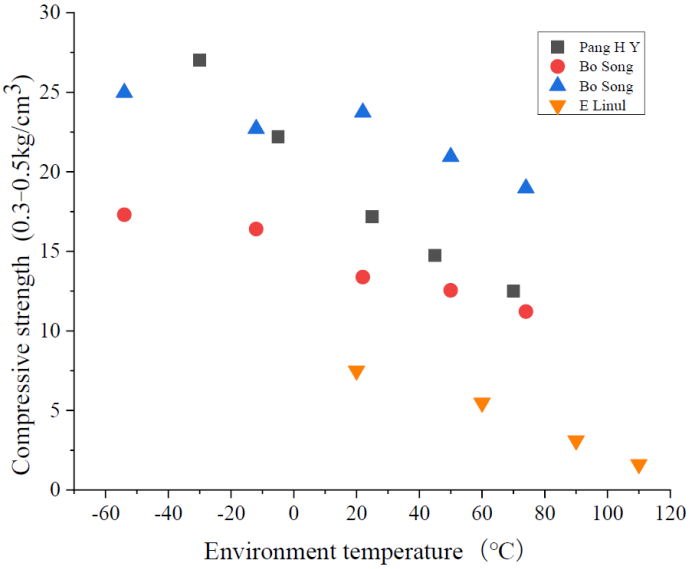

Figure 31: Compressive strength of various polyurethane foams at different temperatures [182]

Figure 32 depicts the density and compressive strength of different polyurethane composites with various weight fractions of TiO_2 and TiO_2-ZnO fillers.

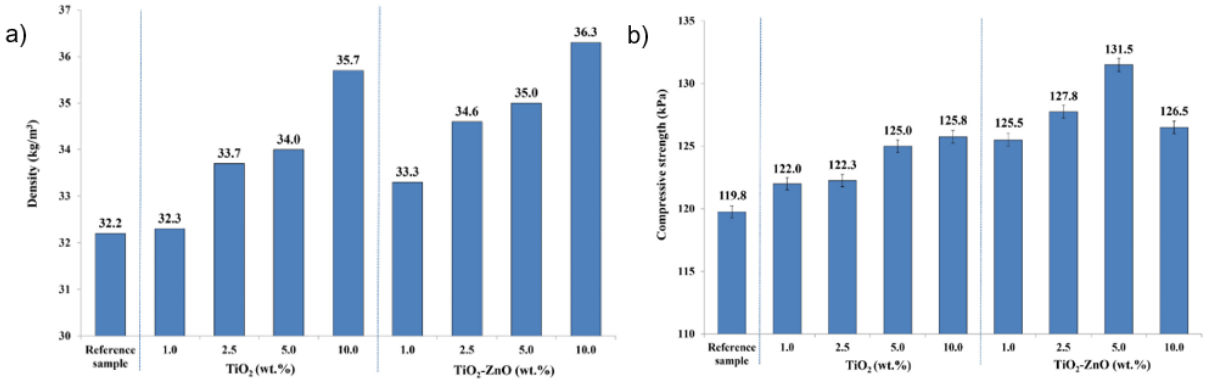

Figure 32: Density and compressive strength of polyurethane composites with TiO_2 and TiO_2–ZnO fillers [187]

4.3.3 Safety issues

It is well established that polyurethane foam board and polystyrene (PS) board are highly flammable. In fact, Liu et al. [173] indicate that these materials remain flammable even when flame retardants are incorporated into the foam boards. In contrast, Hirschler [188] suggests that the addition of fire retardants and the use of barriers or co-extrusion with fire-resistant foams (e.g., polychloroprene or polyisocyanurate foams) can significantly improve the fire resistance of polyurethane foams.

Additionally, Schuerer et al. [189] point out that spray-on foam insulation does not adhere well to metal fuel tanks, potentially causing issues for mobile applications. This lack of adhesion could also pose challenges in the transport of liquid hydrogen tanks, where vibrations may weaken the tank-insulation interface. Such degradation may increase liquid hydrogen evaporation, requiring additional venting. Another concern raised by Schuerer et al. [189] is the presence of weak spots in SOFI, attributed to inconsistencies in PU foam mixing, which can compromise the structural integrity of the insulation system.

In terms of crashworthiness, Paulino and Teixeira-Dias [190] note that PU foam is not the most effective cellular material. Nonetheless, PU foam has demonstrated better performance than aluminium foam, particularly in impact energy absorption. However, the performance difference is minimal, suggesting that overall system safety should consider the material composition of tank walls and support structures.

From an environmental standpoint, Rescigno [191] emphasizes that the utilization of SOFI systems requires additional maintenance of pressure relief devices compared to MLI systems. In fact, SOFIs are particularly sensitive to changes in environmental conditions. Nonetheless, the degradation resulting from environmental factors and operating conditions, such as vibration and humidity, is predictable, thus making these materials relatively stable.

4.3.4 Circularity and sustainability

Spray on foam insulation presents significant challenges from the circularity and sustainability point of view. The evaluation of its environmental impact is complex. While it can reduce carbon

footprint through improved thermal efficiency and durability, the manufacturing process and disposal issues raise concerns. Its production involves chemicals and energy-intensive processes, which are not ideal.

An issue associated with spray-on foam is related to the chemicals used as blowing agents (such as HFC-245fa, HFC-365mfc, and HCFC-141b), which have an extremely high GWP. It is suggested to use closed-cell foams which have significantly lower global warming potential [192]. The second approach was proposed by Chemours Company [193], [194] and lies in replacing the conventional blowing agent for PU foam, i.e., hydrofluorocarbon (HFC), with hydrofluoroolefin (HFO) (GWP < 2). This substitution allowed to reduce the GWP of the spray-on foam insulation by over 99 % compared to the conventional HFC blowing agent.

Wildnauer et al. [195] analyzed different open and closed cell spray-on polyurethane foam systems commonly used for building applications and summarized in Table 11.

Table 11: Spray-on foam products for building applications [195]

Product	Blowing Agent			Relevant Standards		
	HFC	HFO	Reactive	ASTM	CAN/ULC	ICC
Open cell			X	WK30150 (under development)	S712.1	ICC 1100; ICC-ES AC377
Closed cell	X	X		C1029 Type I and II	S705.1	ICC 1100; ICC-ES AC377
2-component, low pressure (2K-LP)	X	X				ICC-1100; ICC-ES AC377
Roofing	X	X		C1029 Type III and IV; D7245		

With respect to recyclability and disposal, SOFI poses some challenges. Even though chemical recycling is technically possible, from the environmental standpoint, it is not a viable option due to the use of harsh chemical in the process. According to research conducted by the chemical company BASF, only around 1 % of spray foam insulation is currently recycled. This low rate stems from technical difficulties and a lack of widespread recycling infrastructure [196]. It has been reported that the removal of SOFI layer after its end of life (around 75 years) is problematic [195]. The waste management of SOFI poses yet another environmental challenge. Most SOFI ends up in landfills due to recycling difficulties. Moreover, SOFI incineration emits atmospheric contaminants like HCB dioxins and fine particles. While challenges persist, ongoing research and development offer hope for more sustainable solutions [196].

4.4 Glass microspheres

Glass bubbles, also known as glass microspheres, are small, hollow spheres made from glass. These microspheres typically have diameters ranging from a few microns to several millimeters. Glass bubbles are often used as a bulk-fill powder in cryogenic applications, providing effective insulation even when exposed to variable mechanical stresses. Along with the low thermal conductivity and high resistance to compaction, their structure makes them particularly suitable for environments requiring stable, long-term insulation performance. Figure 33 shows a charge of glass bubbles obtained from a 96 % SiO_2 gel and magnified through an optimal microscope.

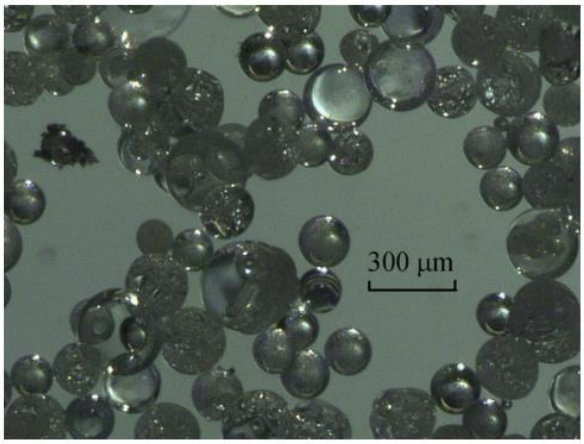

Figure 33: Optical micrograph of hollow glass microspheres produced from high silica gel particles [197]

4.4.1 Thermal properties

Glass microspheres consist of heat-resistant materials with high melting temperatures, ranging from 1400 to 1600 °C. This high melting point makes them well-suited for applications requiring structural stability and resilience to extreme temperatures. The geometry and surface of glass microspheres is well-defined compared to the porous perlites. Therefore, microspheres of similar size as perlites have a comparatively smaller surface. A larger surface area tends to lead to more outgassing, which is essential for the long-time performance or service intervals [198]. The density of glass microspheres ranges between 65 and 350 kg/m³ and varies with the size and morphology of the spheres. The density of the microspheres used in the LH_2 storage at the Kennedy Space Center is around 65 kg/m³ and provides a lightweight and effective insulation solution [132].

The thermal conductivity of glass bubbles is exceptionally low in high-vacuum conditions, which is essential for minimizing heat transfer in cryogenic storage:

- **High vacuum (P < 0.13 Pa) –** Under high vacuum, glass microspheres achieve minimal thermal conductivity, as low as 0.9 mW/m·K, performing well in cryogenic environments.
- **Moderate vacuum (0.13 Pa < P < 13.3 Pa) –** Glass microspheres continue to provide stable insulation with low thermal conductivity (typically 1.5 mW/m·K) at moderate vacuum levels, showing lower heat conduction compared to alternative materials like perlite and aerogel.

Fesmire et al. [11] performed test to compare the thermal performance of perlite powder and glass microspheres under varying pressure conditions. Figure 34 visualizes these results.

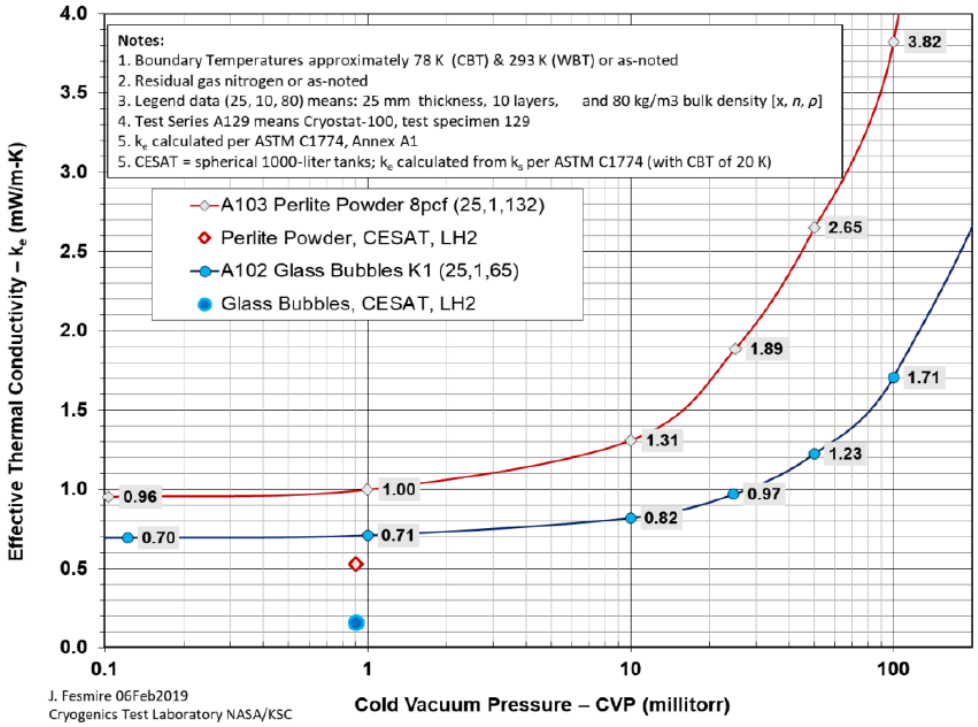

Figure 34: Comparison of the thermal performance of perlite powder and glass microspheres as a function of the vacuum level [11]

Glass microspheres exhibit excellent resilience against settling and compaction, even in environments with frequent movement or vibrations. Road transport tests, simulating real-world vibration, showed that glass bubbles retained their insulation properties with minimal performance degradation. This compaction resistance is crucial for cryogenic tanks that may experience vibrations over their lifespan, ensuring consistent insulation effectiveness without significant loss of performance due to settling [132].

In applications involving repeated thermal cycling (cooling and warming), glass microspheres maintain their thermal performance. Unlike materials prone to compacting under thermal cycling, glass bubbles remain largely unchanged, avoiding the formation of gaps or thermal bridges that could increase heat transfer [132]. They have lower thermal conductivity than perlite under similar conditions and maintain structural stability over time, making them highly suitable for cryogenic insulation where both low heat transfer and mechanical resilience are required [155].

To summarize, glass microspheres provide a highly promising insulation material for cryogenic storage applications. Their stability under high-vacuum, resistance to compaction, and resilience through thermal cycling make them a valuable choice for applications requiring consistent and durable insulation over time. Their low thermal conductivity and high melting point further enhance their suitability in high-demand environments.

4.4.2 Mechanical properties

Glass microspheres, whether solid, hollow, or porous, exhibit a range of mechanical properties that make them valuable for cryogenic applications. Key properties such as mechanical

strength, hardness, density, and brittleness play a crucial role in determining their suitability for specific uses [168], [199]. The morphological classification of glass microspheres is crucial for understanding their mechanical properties, as different internal structures result in distinct properties. The main categories of glass microspheres are:

- **Solid glass microspheres (SGMs) –** These microspheres are characterized by a solid internal structure, without any cavities or pores [168].
- **Hollow glass microspheres (HGMs) –** HGMs are distinguished by their hollow structure, with an internal cavity filled with air or another gas. This feature gives them low density and high compressive strength [168], [200].
- **Porous glass microspheres (PGMs) –** PGMs have a porous structure with interconnected pores. This porosity can be classified into macropores ($d > 50$ nm), mesopores (50 nm $< d < 2$ nm), and micropores ($d < 2$ nm) [168].
- **Hollow glass microspheres with porous walls (PWHGMs) –** These microspheres combine the characteristics of HGMs and PGMs, possessing a hollow structure with porous internal walls [168].

The mechanical properties of glass microspheres are influenced by factors such as glass composition, microsphere size, thermal treatments applied, and porosity. Different glass compositions yield different mechanical properties, as demonstrated by the higher breakage resistance of alumino-borosilicate glass microspheres (SG7) compared to yttrium-aluminosilicate glass (YAS) [169].

In addition, the size of the microspheres affects their mechanical properties, possibly due to thermal differences during the flame spheroidization process. Larger microspheres may exhibit increased fragility due to internal stresses resulting from the faster cooling of the outer surface compared to the internal volume [169].

Thermal treatments, and particularly annealing processes, can influence the mechanical properties of glass microspheres. Finally, the porosity of glass microspheres impacts their mechanical properties [168], [169]. HGMs have a lower density than SGMs, and therefore a comparatively lower load-bearing capability.

Using HGMs in cryogenic applications requires attention to factors such as:

- **Mechanical strength –** HGMs need to withstand the extreme temperature and pressure conditions typical of cryogenic environments. Selecting HGMs with adequate mechanical strength is crucial to ensure the integrity of the insulation system [167], [169].
- **Compatibility with other materials –** The compatibility of HGMs with other structural materials of the cryogenic tank, such as adhesives and coatings, should be considered to ensure the expected mechanical performance [167], [169].

In conclusion, hollow glass microspheres show significant potential for cryogenic applications, especially in liquid hydrogen storage, primarily due to their low thermal conductivity, which minimizes evaporation. Additionally, their low weight contributes to reducing the overall mass of the storage system. However, cryogenic applications require careful analysis of the mechanical properties of HGMs. Compressive strength is crucial to withstand the pressures inside cryogenic tanks, and this property improves with increased HGM density. Another critical

factor is mechanical strength at low temperatures. HGMs must endure the extreme temperatures of the cryogenic environment without fracturing or losing integrity. Studies show that annealing can enhance the strength of glass microspheres, reducing internal defects and relieving residual stresses generated in the spheroidization process. Glass composition also impacts mechanical properties. Alumino-borosilicate glass microspheres have demonstrated higher breakage resistance compared to yttrium-aluminosilicate glass. Additionally, coatings like carbon black or titanium dioxide can be applied to increase the strength and opacity of HGMs [167]–[169].

The mechanical properties of hollow glass microspheres with different particle sizes are collected in Table 12.

Table 12: Summary of mechanical and elastic properties of different HGMs after sintering at 600 °C [167]

HGM size (μm)	Yield strength (MPa)	Young's modulus (MPa)
5-30	0.96	21.1
50-90	18.13	216.8
90-125	5.69	43.7

Figure 35 shows the probability of failure of SG7 glass microspheres and YAS glass microspheres with an average diameter of 75 μm as a function of stress.

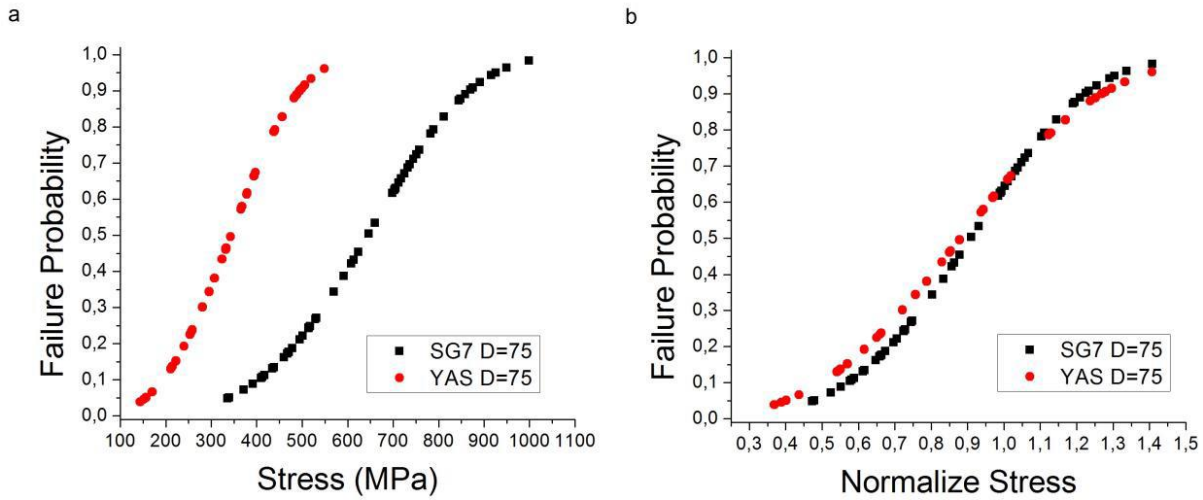

Figure 35: (a) Probability of failure at different stress values for 75 μm SG7 glass microspheres and 75 μm YAS glass microspheres, both without annealing process; (b) Probability of failure at different stresses normalized with the scale parameter of each set of 75 μm microspheres [169]

4.4.3 Safety issues

Among bulk insulation materials, microspheres exhibit superior performance in resisting degradation under fire conditions. As noted by Eberwein et al. [142], the heat flow through a double-walled system enclosing glass microspheres remains almost unaffected during fire scenarios, resulting in a lower pressure increase within the tank. Additionally, hollow glass microspheres have significantly lower fire risks compared to thermoplastic polyurethane. In

fact, they produce less smoke and toxic gas emissions and release less heat when burned [201]. Furthermore, studies show that glass bubbles and aerogel particles exhibit minimal compression under vibration [9],[21]. Therefore, insulation systems containing glass microspheres emerge as the inherently safest option, considering the available literature (which is still relatively limited).

4.4.4 Circularity and sustainability

Even though the research efforts in the area of glass bubbles bulk-fill material as cryogenic insulation system dates back to 1970 [203] a limited amount of information on the subject of LCA has been published. According to Delogu et al. [204], one can assume that, similarly to the other glasses, the main environmental impact comes from the production stages due to the heating process at 1400 °C. Their study used LCA processes and conditions for borosilicate glass as a substitution for HGMs for the automotive application. As shown in Figure 36, there are several different methods of fabrication of glass microspheres, including the flame synthesis process, liquid droplet method, dried gel process, and electrical arc plasma. Each of them may have a different environmental footprint [168].

Schlanbusch et al. [205] presented a new approach integrating the LCA in the design of hollow silica nanospheres (HSN) for thermal insulation applications. They showed that the environmental impact of the production of HNS can be considered at the planning stage, thus determining the most environmentally friendly choices. In his study, they concluded that the chemicals' indirect emissions and embodied energy must be considered to reduce the environmental impact of the production. Due to the indirect impact of ethanol and tetraethyl orthosilicate, the silica coating process was the most energy and emission-intensive step. Direct energy consumption and CO_2 emissions from the combustion of the template were less important, and the fabrication of the template was found to be comparatively insignificant. Additionally, ethanol consumption should be minimized to improve the environmental impact since it is accountable for most emissions due to the large final demand for ethanol.

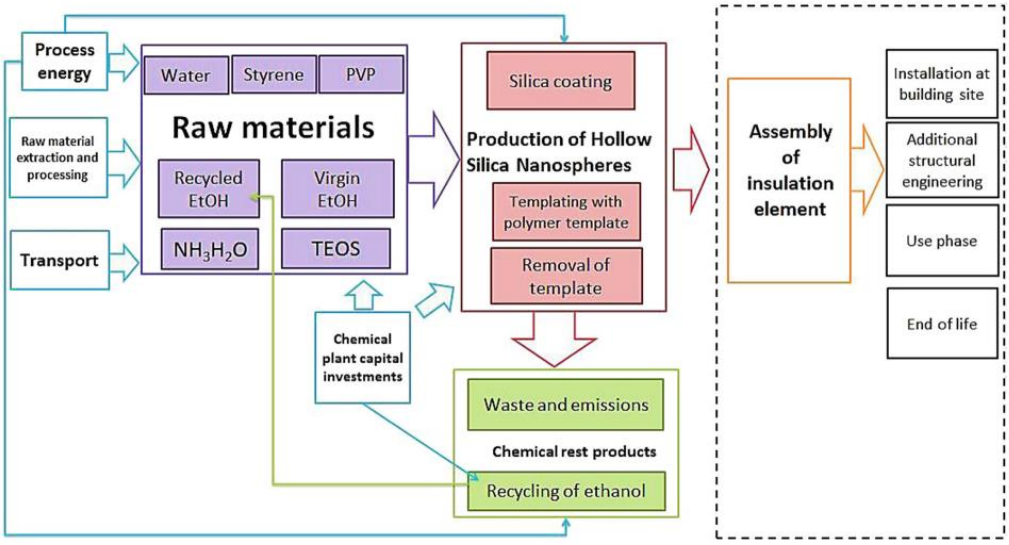

Figure 36: Illustration of the system model and system boundaries [168]

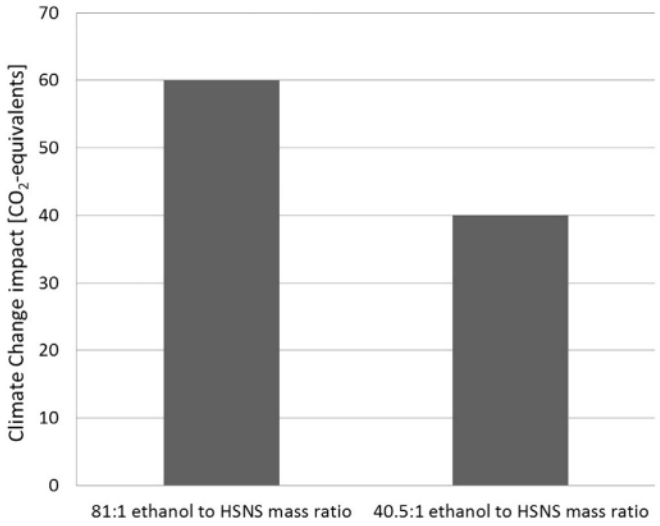

Figure 37: Climate change impact for two scenarios of hollow silica nanosphere production [205]

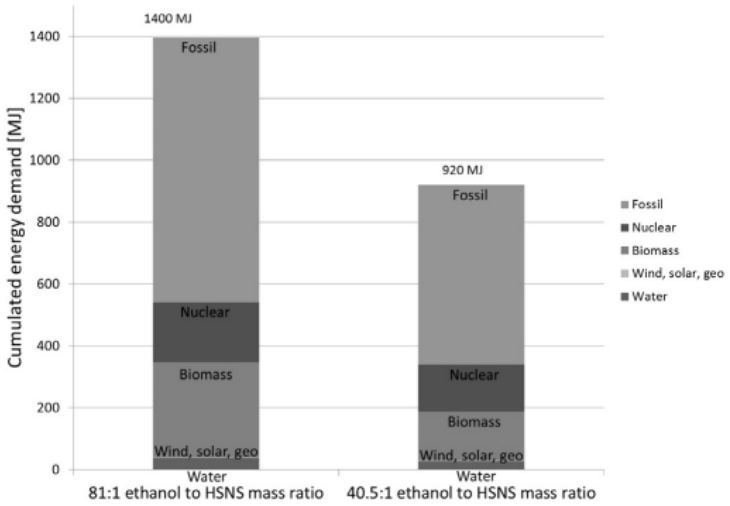

Figure 38: Cumulated energy demand for two scenarios of hollow silica nanosphere production [205]

Hollow glass bubbles are a low-density material. Therefore, they can reduce the weight and volume of the insulation, thus lowering fuel consumption for transportation and providing energy and cost-saving benefits. According to 3M, their 3M™ K1 Microspheres have a density of 0.125 g/cc (whereas perlite has a density of 0.15 g/cc).

At the end of their life, loose HGMs (without added binders) can be ground or crushed and reused as a substrate for glass production or as additives (e.g., filler in the construction or composite industries) [206].

4.5 Multi-layer insulation

Multi-layer insulation (MLI) systems are designed to provide minimal thermal conductivity in cryogenic environments by using layers of highly reflecting material separated by low conductive and highly transmissive spacers. MLI systems are highly effective for reducing heat transfer and are frequently used in applications requiring extreme thermal insulation and where the space is strongly limited [207]. In fact, MLI is a crucial component in spacecraft and cryogenic systems. Figure 39 shows an example of an MLI system and a schematic with several layers of spacer and reflective material.

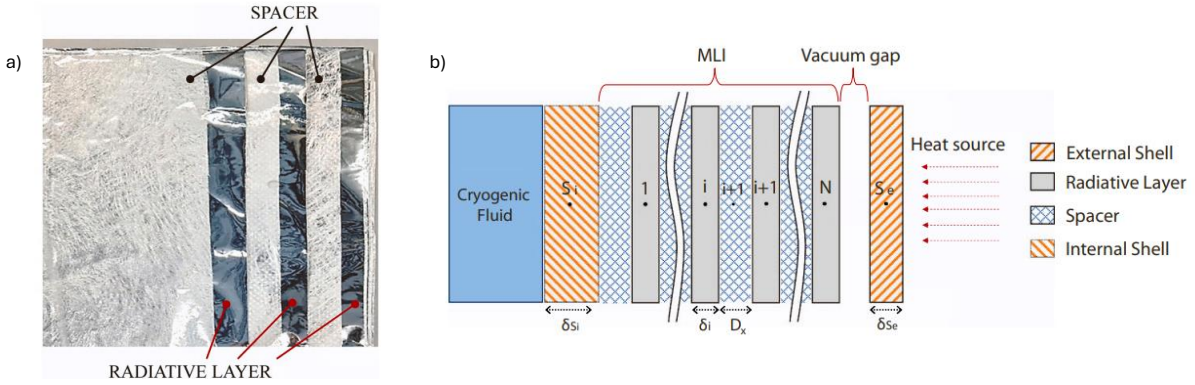

Figure 39: a) Multi-layer insulation with alternated spacers and radiative layers and b) Schematic of MLI system with N layers between the internal and external shells (adapted from [207]*)*

4.5.1 Thermal properties

MLI varies in composition, with typically aluminized polyester foil or pure aluminum foils as reflective layers, and polyester fleeces or glass fibers as spacer. The different materials offer different melting temperatures and insulation properties, as reported in Table 13. Polyester-based MLI offers a better thermal insulation compared to the aluminum and glass fleece-based MLIs. Nevertheless, the last one can withstand higher temperatures, making it suitable for environments with potential thermal exposure.

Table 13: Thermal conductivity and melting temperature of polyester and fiberglass MLI [131]

Insulation material	**Thermal conductivity (W/m·K)**	**Melting temperature (°C)**
Vacuum + polyester-based MLI	10^{-6} to 10^{-5}	140–400
Vacuum + aluminum and glass fleece-based MLI	10^{-6} to 10^{-5}	1000–1400 (660 for Aluminum)

MLI achieves the lowest thermal conductivity among the insulation materials currently available, when it is used in high-vacuum conditions. MLI performance is highly sensitive to pressure, with significant variations as vacuum levels change:

- **High vacuum ($P < 10^{-3}$ Pa) –** MLI exhibits extremely low thermal conductivity, i.e., 0.028 mW/m·K. This performance is ideal for applications requiring extremely low heat transfer and minimal space occupation.
- **Moderate vacuum (10^{-3} Pa < P < 10^{-1} Pa) –** At slightly higher pressures, MLI's thermal conductivity increases to around 0.072 mW/m·K, reflecting a significant reduction in insulation effectiveness.
- **Ambient pressure ($P = 10^{5}$ Pa) –** At ambient pressure, MLI's thermal conductivity rises sharply to approximately 35 mW/m·K, significantly reducing its effectiveness in non-vacuumed environments [155].

Therefore, MLI's effectiveness is highly dependent on maintaining high vacuum levels, as well as on the structural integrity of its layers. Mechanical compression and edge effects can compromise the vacuum conditions, thus increasing the thermal conductivity and allowing for higher heat transfer. Proper placement and handling are essential for optimal performance, particularly in applications where MLI may be exposed to external stresses [155].

In some configurations, MLI is used in conjunction with other insulation materials, such as aerogel or fiberglass blankets to enhance the insulation efficiency. The combination of materials can improve the performance depending on the placement (e.g., on the warm or cold side), thus making MLI suitable for various environmental conditions and configurations [155].

In conclusion, MLI offers exceptional insulation performance in high-vacuum conditions, with thermal conductivities as low as 0.028 mW/m·K. However, its effectiveness decreases as vacuum conditions degrade, and it is sensitive to mechanical stress. MLI's insulation capability can be enhanced when combined with materials like aerogel or fiberglass blankets, making it a versatile option for a range of high-demand cryogenic applications.

4.5.2 Mechanical properties

Mechanical properties of MLI systems depend on the number of layers. Studies have shown that increasing the number of layers enhances strength, impact resistance, and fatigue life [208]. However, the available literature lacks research on the mechanical properties of these materials, despite acknowledging their impact on MLI's overall thermal performance [6], [209]–[211].

The literature identifies compression of MLI as a critical factor that can significantly degrade its thermal performance. Compression increases heat transfer by conduction, as it reduces the space between layers, intensifying contact between them. Layer density, spacer material type, and the magnitude of the compressive load directly influence the degree of compression [210]–[213].

Additionally, the layer density, defined as the number of layers per unit thickness, plays a fundamental role in balancing thermal performance and mechanical robustness. Higher density can enhance thermal performance in high-vacuum conditions and makes MLI more resistant to compression. Conversely, lower density reduces thermal conductivity but leaves the insulation more vulnerable to compressive loads. Finding the optimal density requires careful analysis of operating conditions and anticipated mechanical loads [211], [213].

The spacer material used in MLI also affects both thermal performance and mechanical resistance. Meshes, such as those made from polyester and silk, provide better thermal performance compared to materials like fiberglass foils. However, the compressive strength of the spacer material is a critical factor. While thermally efficient, meshes can deform under load, compromising insulation effectiveness over time [212], [213].

Despite the recognized importance of mechanical properties for MLI performance, available sources usually focus on thermal properties and do not provide specific data on mechanical properties. Information on tensile strength, compression, and flexural properties of various types of MLI, under different conditions and spacer materials, is essential for designing efficient and reliable systems. The lack of specific data on the mechanical properties of MLIs highlights the need for further research in this area.

4.5.3 Safety issues

For MLI systems, it is well known that the system's degradation depends on the materials used and the potential causes and effects of vacuum loss. Eberwein et al. [142] investigated three types of MLI: one utilizing polyester layers and two others with pure aluminum layers separated by glass fibers. The MLI with polyester layers exhibited significant damage when exposed to external heat sources due to polyester's lower thermal degradation temperature compared MLI based on aluminum and glass fibers. Additionally, pyrolysis products were released during testing, which increased the heat flow in fire scenarios, resulting in higher peak heat flow and higher vacuum loss. Similar findings by Camplese et al. [207] suggest that polyester-based MLI systems for cryogenic applications are particularly vulnerable to degradation in realistic fire scenarios. The simulations show that the polyester-based MLI can maintain its thermal properties only for a few minutes. This behavior is highlighted in Figure 40, where heat flux and temperature values are illustrated over time for different types of MLI.

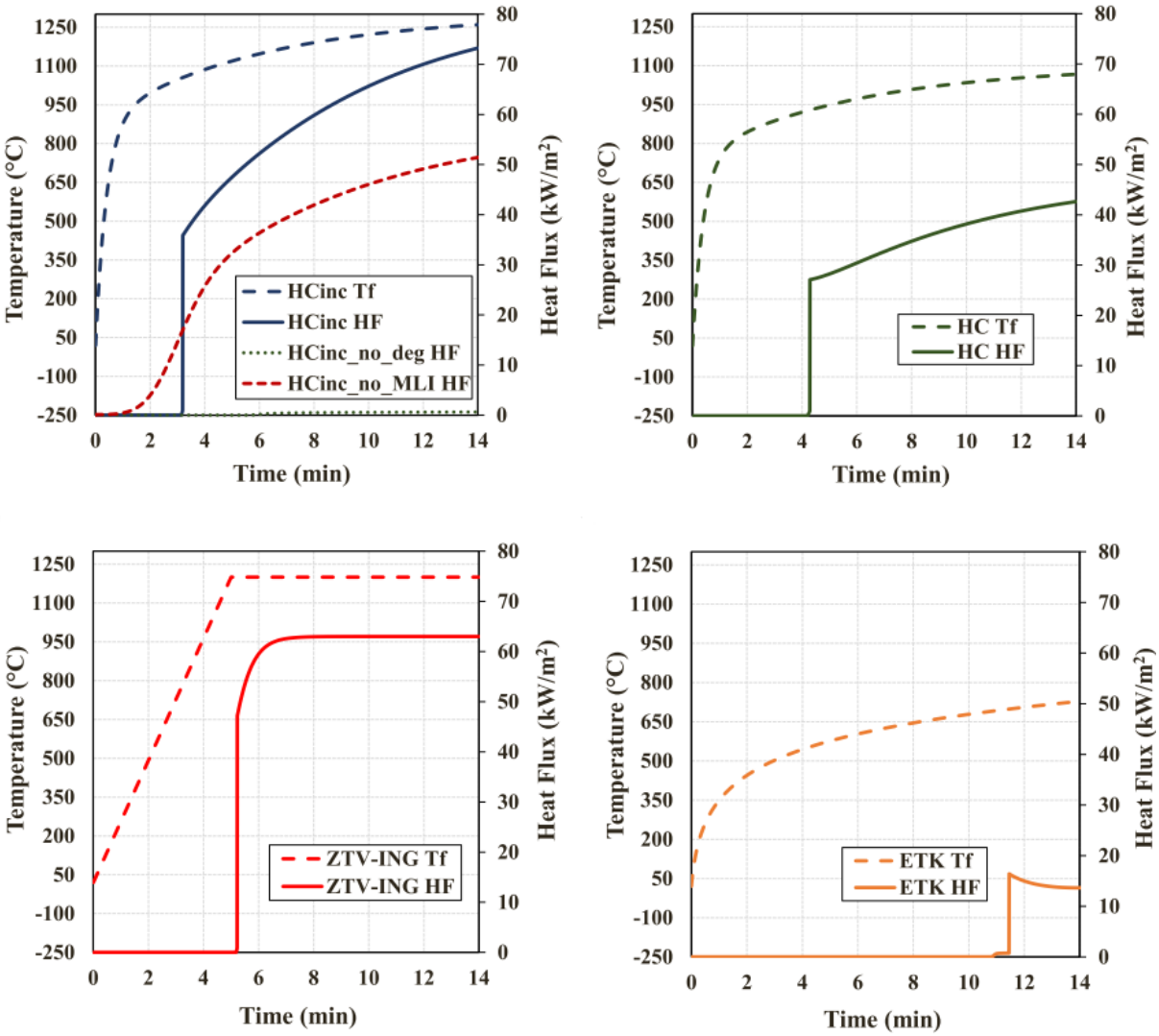

Figure 40: Heat flux from the fire through the inner shell (solid lines) calculated by a model and assumed fire temperatures (dashed lines) over time, compared for different standard fires on polyester-based MLI [207]

Nevertheless, the authors noticed that, if one MLI layer resists, the tank is well insulated during fire exposure. An important factor in this context could be the deterioration of the vacuum. This increases the heat flow between layers and inner tank, thus protecting the innermost layers [214]. Conversely, the aluminum-based MLI samples with glass fibers spacers exhibited only limited damage under similar operating conditions. Additionally, an MLI made of aluminum foils, fiberglass papers, and Dacron showed a time to failure for liquid hydrogen tanks below 11 minutes considering the worst-case fire scenarios [215]. Consequently, the existing literature indicates that polyester-based MLI systems have unsatisfactory performances under external fire conditions.

Regarding liquid hydrogen evaporation, MLI systems provide superior performance by extending the service life of pressure relief devices and thermodynamic ventilation system (TVS) during the normal tank's operations by up to 90 % [12]. This estimation does not consider undesired events such as external fires and severe mechanical vibrations. Additionally, it was highlighted that MLI systems significantly reduce thermal stratification and thermal gradients within cryogenic tanks. Since thermal cycling is a primary factor affecting tank's degradation

and failure at constant operating pressure, MLI usage may increase the operating life of the LH_2 storage equipment. However, the author also demonstrated that when the MLI loses its vacuum, the evaporation rate within the tank might exceed that of SOFI, accelerating the degradation of cryogenic valves and TVS components. Thus, the causes of vacuum loss in MLI systems require further investigation.

4.5.4 Circularity and sustainability

Since MLI is a composite material, the sustainability and circularity depend on its constituents. Swanstrom et al. [216] compared environmental balances of three different insulations systems, namely MLI, evacuated glass fibers, and conventional polyurethane foam. These systems are referred to as Insulation Concept 1, Insulation Concept 2, and Insulation Concept 3. Table 14 summarizes the amount of structural materials used to manufacture the tank, considering these three options.

Table 14: Materials used to manufacture the tank (in kg) [216]

Insulation concept 1	
Stainless steel, total	140.6
Tombak metal or stainless steel	0.323
Polyester foil, 6 μm thickness	0.877
Tissue, 55 μm thickness, knit woven from monofilament polyester yarn (spacer)	0.530
Al 99.999% target, effective mass	0.114
Zeolite or other getter used during manufacture phase	0.090
Ethanol for cleaning of the tank	1
Rubber material for wheels	2
Permanent total mass (empty tank)	144.5
Insulation concept 2	
Stainless steel, total	99.7
Tombak metal or stainless steel	0.242
Glass fibers	47.8
Fe_3O_4-powder, mean grain diameter below 0.1 mm (opacifier)	7.17
Zeolite or other getter used during manufacture phase	0.299
Ethanol for cleaning of the tank	1
Polymer material for wheels	2
Permanent total mass (empty tank)	157.2
Insulation concept 3	
Stainless steel	73.6
Tombak metal or stainless steel	0.323
PU-foam	255.4
Fiber reinforced PU envelope (mantle)	9.14
Adhesive tape	0.761
Adhesive	0.2
Ethanol for cleaning of the inner container	1
Polymer material for wheels	2
Permanent total mass (empty tank)	341.4

Swanson et al. assumed that the tank was insulated with 30 highly reflecting radiation shields (6 µm Mylar foils metalized with 40 nm Al on both sides), with spacers in between, wrapped around the inner container and the bellows over their lengths and on upper and lower front sides of the tank. The complete overlap of the foils was assumed at the top and bottom of the tank. A layer of knit woven from monofilament polyester yarn of 55 µm was used as a spacer

material. Getter material was used to maintain the vacuum (below 10^{-2} Pa). Re-evacuation and exchange of the getter material were assumed every five years of operation. The width of the insulation space was 20 mm. The inner and outer containers, neck, bellows, and mechanical supports of the tank yielded a material consumption of 140.9 kg stainless steel.

The GWP values obtained for these three insulation concepts reflect the sum over the manufacture, use, and end-of-life phases. As shown in Figure 41 and Figure 42, the total GWP values, taken over the tanks' lifetime (i.e., 20 years), amounted to 2,922, 29,640, and 57,820 kg_{CO2eq} of which "true" CO_2 emissions constitute 97 %, 96 %, and 96 %, respectively. Notably, MLI presents the lowest GWP [216].

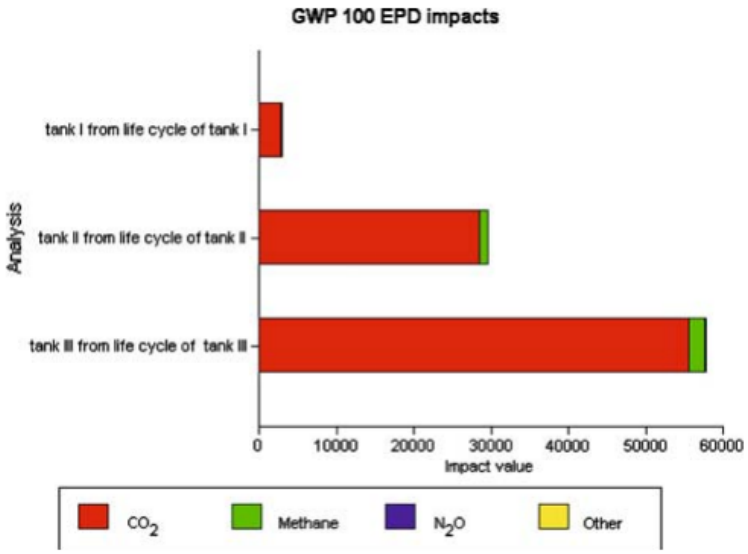

Figure 41: GWP of the three insulation concepts, indicating the main contributing pollutants (in kg_{CO2eq}) [216]

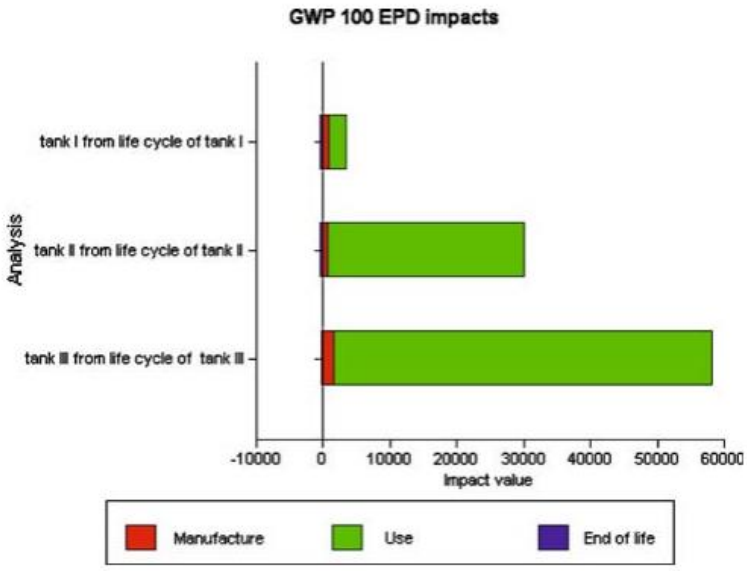

Figure 42 GWP of the three insulation concepts, indicating the different phases of the lifecycle (in kg_{CO2eq}) [216]

4.6 Vacuum-insulation panels

Vacuum insulation panels comprise a rigid, highly porous core material encased in a gas-tight barrier envelope, which is evacuated and sealed. Typical core materials are polyurethane, aerogel, fumed silica, and glass fiber, while the envelope is commonly made of aluminum or metalized multi-layer. Moreover, getters are added to absorb residual gases or vapor within the sealed envelope. This structure minimizes conductive, convective, and radiative heat transfer, and offers extremely low thermal conductivities depending on the core materials and vacuum level. Although most literature focuses on building applications, the vacuum insulation principle is highly relevant for cryogenic applications too. Figure 43 illustrates the cross-section of a vacuum-insulation panel, showing the external cover layer, the multiplayer envelope (composed of protective, barrier, and sealing layers), the microporous core material, and the getter.

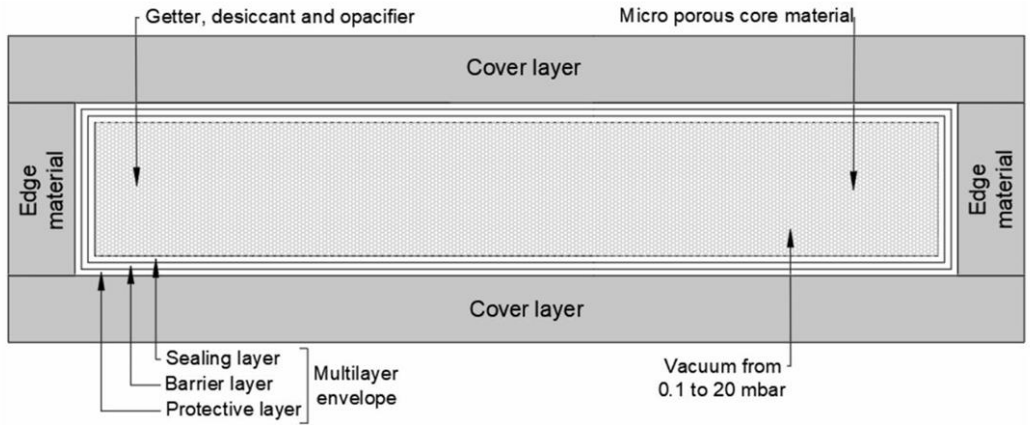

Figure 43: Schematic of a vacuum-insulation panel [217]

4.6.1 Thermal properties

Vacuum insulation panels are primarily composed of fumed silica, a material chosen for its exceptionally low thermal conductivity (around 4 mW/m·K under vacuum conditions). Figure 44 shows the insulation performance of fumed silica as a function of pressure compared to glass fibers, polyurethane and polystyrene foams.

However, the thermal performance of VIPs is influenced by several factors, including internal pressure and moisture content. As the internal pressure increases, the thermal conductivity of the core material also rises. Similarly, the presence of moisture can significantly degrade the thermal performance, with an observed increase of 0.5 mW/m·K per mass percent of water in fumed silica [218].

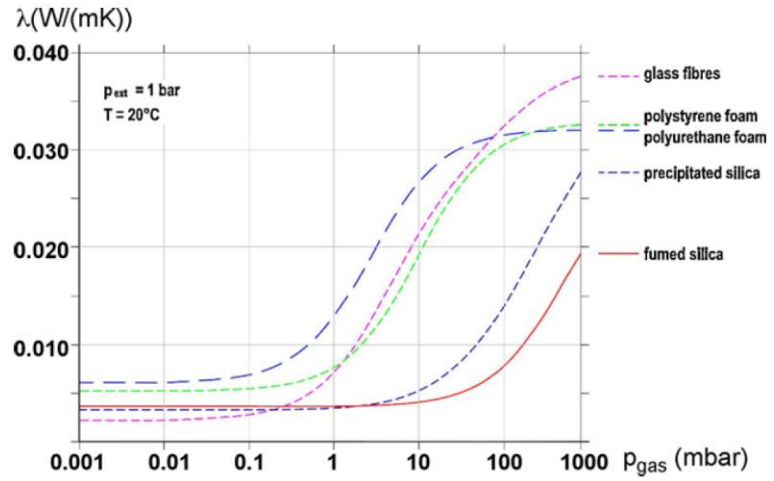

Figure 44: Thermal conductivity of fumed silica compared with other insulation materials as a function of pressure [218]

VIPs employ various mechanisms to minimize heat transfer. Radiative heat transfer is reduced by incorporating opacifiers like silicon carbide powder, which make the core material opaque to infrared radiation. The solid conduction within the core is minimized due to the high porosity and small pore size of fumed silica. Additionally, the gaseous thermal conductivity is significantly reduced under vacuum conditions, thanks to the Knudsen effect, where gas molecules collide more frequently with pore walls than with each other [218]. As shown in Figure 45, the gaseous thermal conductivity depends on the size of the pores along with the vacuum level. The smaller the size of the pores, the lower the thermal conductivity.

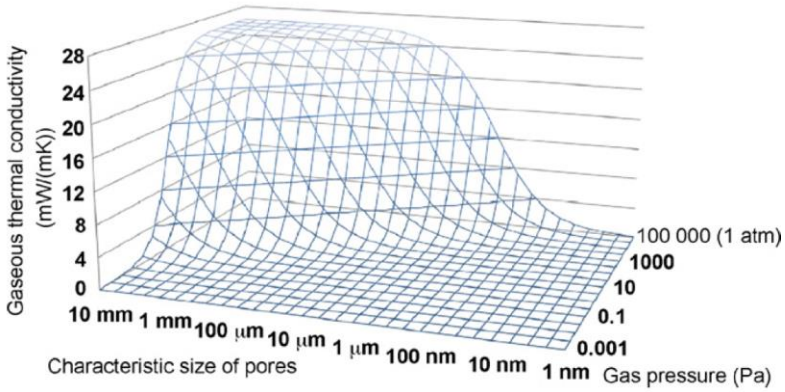

Figure 45: Thermal conductivity of the air as a function of pore size and gas pressure at room temperature [218]

Thermal bridging is another critical aspect of VIP performance. The envelope of VIPs, often made from multi-layered films with aluminum, can contribute to thermal bridging. The linear thermal transmittance of the envelope varies based on the material and thickness of the layers. Thermal bridging at the panel edges is particularly significant, as it can increase the effective thermal conductivity of the panel beyond the center-of-panel value [218]. If the difference in thermal conductivity between the evacuated core and the envelope materials is more significant, edge effects can additionally reduce the overall thermal performance of VIPs [219].

As shown in Figure 46, any increases in internal pressure and moisture content lead to higher thermal conductivity. To mitigate this, getters and desiccants are often added to the core material to absorb gases and moisture, thereby prolonging the panels' service life [218].

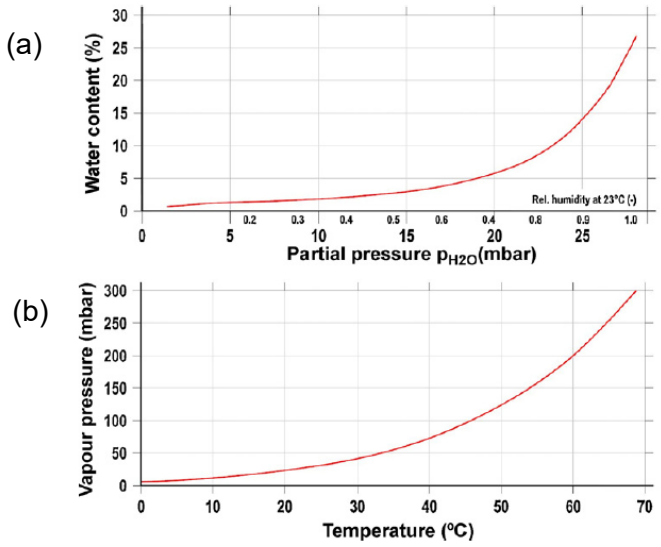

Figure 46: (a) The partial pressure of vapor (p_{H2O}) as a function of the water content in fumed silica and (b) the partial pressure of vapor as a function of temperature [218]

As a result of this degradation, the effective thermal conductivity of fumed silica VIPs ranges from 7 to 9 mW/m·K in a time span of approximately 25 years [219].

Improvements in VIP technology focus on enhancing the thermal performance of the core material and the envelope. In fact, developing core materials with even lower thermal conductivity and better resistance to moisture can significantly improve VIP performance. Innovations in envelope materials that offer superior gas and moisture barrier properties can reduce thermal bridging and extend the service life of VIPs [218].

In summary, while VIPs offer significant advantages in thermal insulation due to their low thermal conductivity, their performance is influenced by internal pressure, moisture content, and thermal bridging. Continuous advancements in materials and construction techniques are essential to maximize their effectiveness.

4.6.2 Mechanical properties

The mechanical properties of VIPs depend on their core material composition and filler ratios, with compressive strength and deformation modules varying accordingly. Factors influencing VIP performance include material properties, design, and operating conditions [220], [221]. The mechanical properties of VIPs are primarily influenced by the core material characteristics and the compaction during manufacturing. In particular, the compression strength is crucial to ensure that the VIP maintains its structure and thermal performance under load. Tensile strength refers to the VIP's ability to resist deformation under stress. The type of material used in the core can significantly affect tensile strength. Finally, the dimensional stability ensures that the VIP maintains its dimensions at different temperature and humidity conditions. The

choice of barrier material and the sealing process influence the VIP's dimensional stability [219], [222], [223].

Since VIPs are composite insulation systems, rather than real materials, the mechanical properties of the different constituting parts should be considered separately:

- **Envelope material –** For cryogenic applications, the typical polymer film envelopes used in building VIPs may not be suitable due to fragility at low temperatures. Metal envelopes, such as stainless steel, are more suitable for cryogenic applications, as they offer better mechanical resistance and reduced gas permeability at extremely low temperatures.
- **Core material –** Core materials must have low thermal conductivity at cryogenic temperatures. Glass microspheres, pyrogenic silica, and expanded perlite are promising core materials for cryogenic VIPs. Core material opacity is also critical, as thermal radiation becomes a relevant heat transfer mode at low temperatures. Adding opacifiers, such as carbon black or silicon carbide, can help minimize radiative heat transfer.
- **Vacuum generation and maintenance –** Maintaining a high vacuum level is essential for the long-term performance of cryogenic VIPs. Using getters to absorb residual gases and minimize vacuum degradation over time may be crucial [220], [224].

Although VIPs show promising potential for cryogenic applications, further research is needed. Detailed analyses of the mechanical behavior of VIPs at cryogenic temperatures is crucial. This includes investigating compression strength, tensile strength, and impact resistance at low temperatures [225], [226]. Developing envelopes with low gas permeability is essential to ensure long-term vacuum performance [225], [226]. Finally, research on core materials with improved thermal conductivity and good mechanical properties at cryogenic temperatures is crucial [225], [226].

To sum up, VIPs show great potential for LH_2 insulation systems due to their low thermal conductivity and modularity. Nevertheless, challenges remain regarding the mechanical properties and long-term durability of VIPs at cryogenic temperatures. Additional research focused on enhancing the mechanical properties of VIPs and developing robust envelope and core materials for cryogenic applications [220], [225], [226].

As an example, Figure 47 depicts the stress-strain curves of various natural fibers under compression.

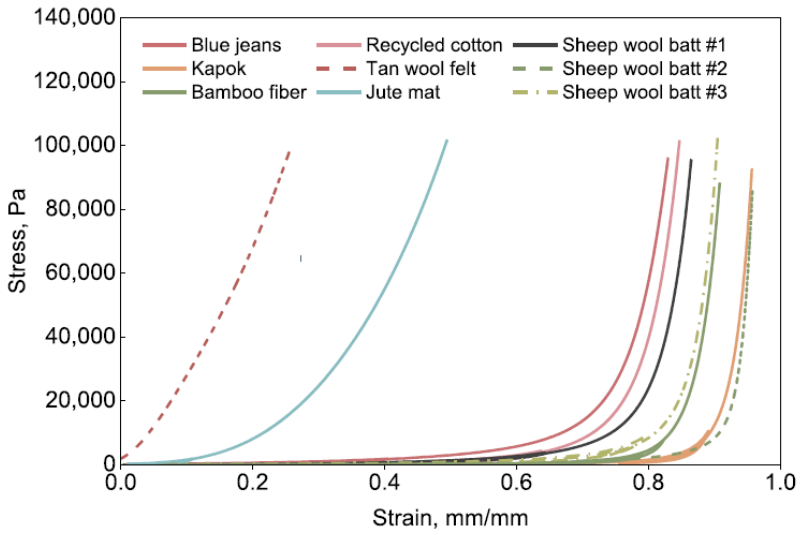

Figure 47: Stress–strain curves of natural fiber under compression [227]

Figure 48 shows the strength-elongation curve of a typical envelope material.

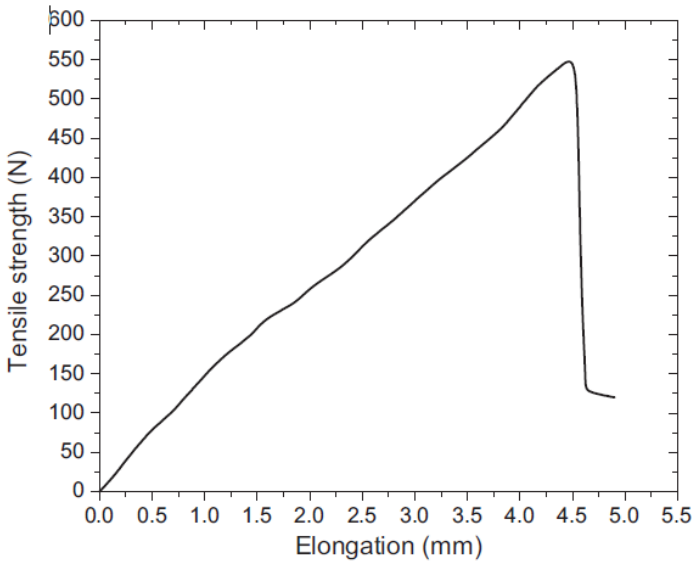

Figure 48: Strength–elongation curve of laminated aluminum foil [228]

4.6.3 Safety issues

When evaluating vacuum insulation panels, system safety largely depends on the material selection, correct material interfaces, and the potential consequences of vacuum loss. Various insulation panels with laminated aluminum foil reinforced with fiberglass cloth are applicable to large scale storage tanks for cryogenic substances since they provide enhanced fire protection [228]. However, the safety of vacuum insulation panels can be further strengthened when integrated into high-insulation fire doors (HIFDs). HIFDs are a type of door designed to provide high-level protection against the spread of fire and heat between different areas of a building. Thus, these doors not only prevent the spread of flames but also limit heat transfer. To optimize insulation performance, VIPs, ceramic boards, graphite covering tapes (GCTs), and glass wool are commonly used within HIFDs [229]. In testing, HIFD systems exhibited

strong fire resistance, airtightness, and condensation control. In particular, GCTs notably enhance fire resistance and airtightness, meeting the standard safety requirements and performing well at temperatures down to –20 °C.

Therefore, material selection is crucial for ensuring fire safety and resilience under real operating conditions. However, as for MLI, limited information exists on vacuum loss scenarios, the impact of vibrations on the structural integrity of these systems, or the effect of interface compatibility issues between the various materials composing VIPs.

4.6.4 Circularity and sustainability

Dovjak et al. [230] analyzed 15 different insulation materials, namely glass wool (GW), low- (LdSW) and high-density stone wool (HdSW), foamed glass (FG), expanded polystyrene (EPS), expanded polystyrene with infrared reflectors (EPSir-r), extruded polystyrene (XPS), polyurethane (PU), polyisocyanurate (PIR) and phenolic boards (PHE), low- (LdSW) and high-density wood fiber boards (HdWF), cellulose fiber (CF), straw bales (SB), and vacuum insulation panels (VIP) made of a fumed silica core and a vapor-resistant barrier foil. Figure 49 compares the global warming potential of these materials; Figure 50 shows the acidification potential, Figure 51 the ozone depletion potential, and Figure 52 the eutrophication potential. The authors reported that VIPs are the most impactful insulation material in almost all the categories. The extraction and production processes of the core materials are the major contributors to the environmental burden of VIPs. In the case of cores made of fumed silica, the extraction and production processes account for more than 90 % of the overall environmental impact. Conversely, all organic-natural insulations have a net negative impact in terms of GWP due to the CO_2 sequestration in wood and straw.

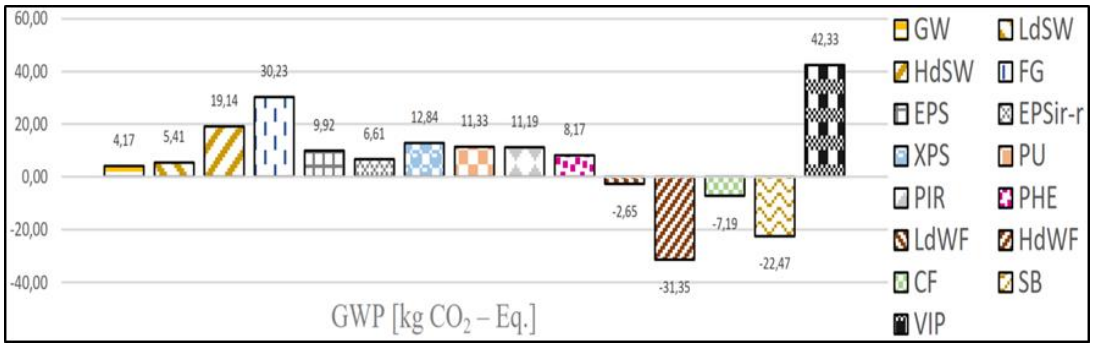

Figure 49: GWP of different insulation materials [230]

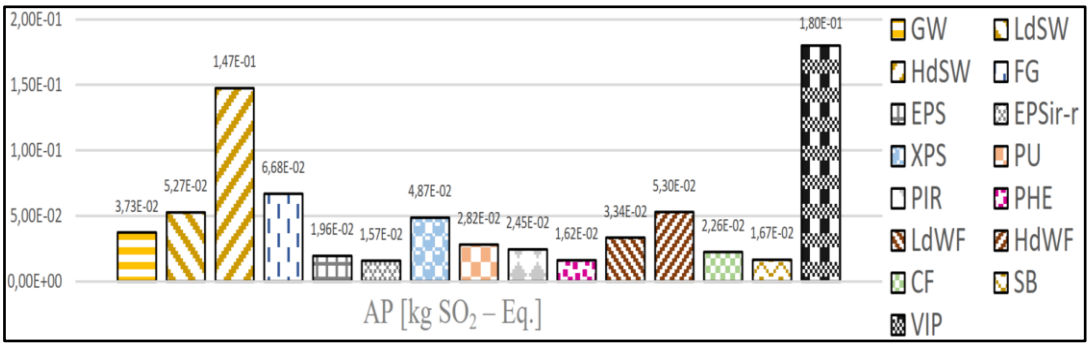

Figure 50: AP of different insulation materials [230]

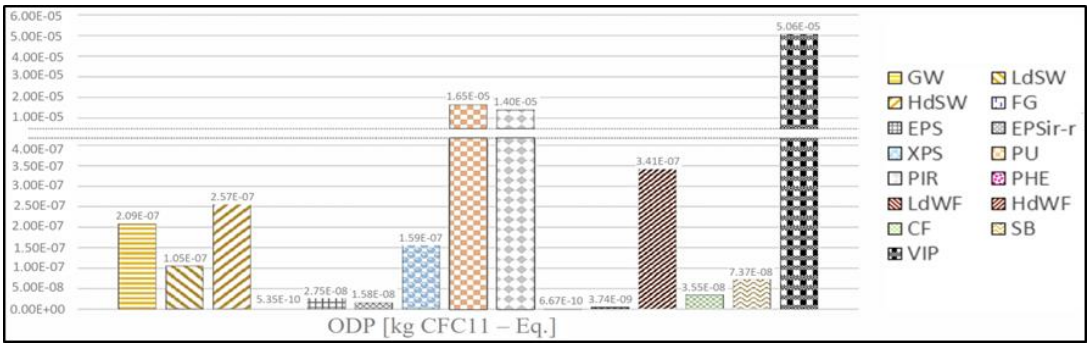

Figure 51: ODP of different insulation materials [230]

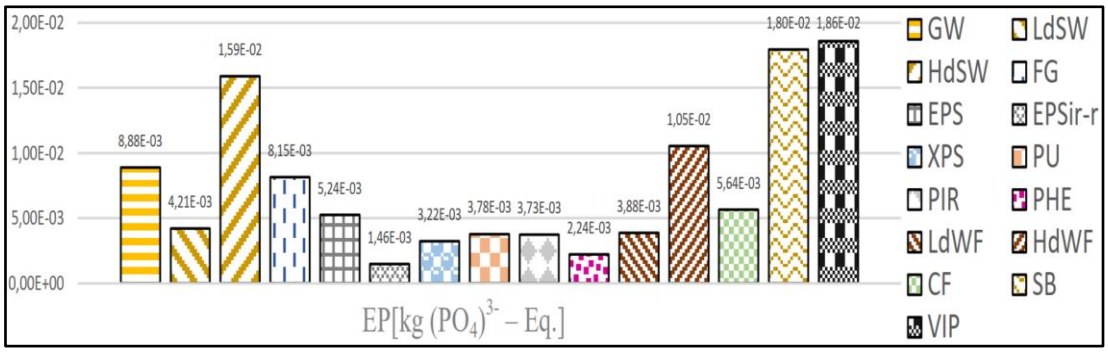

Figure 52: EP of different insulation materials [230]

Core materials are the key contributors to the environmental impact of VIPs. Resalati et al. [231] presented the “cradle-to-gate” lifecycle assessment of different core materials, highlighting their environmental impact. The results referred to pyrogenic silica, glass fiber, expanded polystyrene, aerogel, hybrid sawdust (30 $\%_{wt}$), and pyrogenic silica (55 $\%_{wt}$) are shown in Figure 53 and Figure 54. Pyrogenic silica presented the highest impact in seven of the selected impact categories, while expanded polystyrene had the lowest impact in eight. Expanded polystyrene was reported to have an environmental impact 20 % lower than the maximum in all the categories except for the photochemical ozone creation potential category. This category showed the highest impact due to the emissions of non-methane volatile organic compounds. The hybrid core presented the second-highest impact in six of the nine selected impact categories. Regarding the ODP impact category, the core material with the highest impact was aerogel, followed by glass fiber. The relatively lower values for the expanded polystyrene can be associated with the lower density of the material used (three to seven times lower than the other materials).

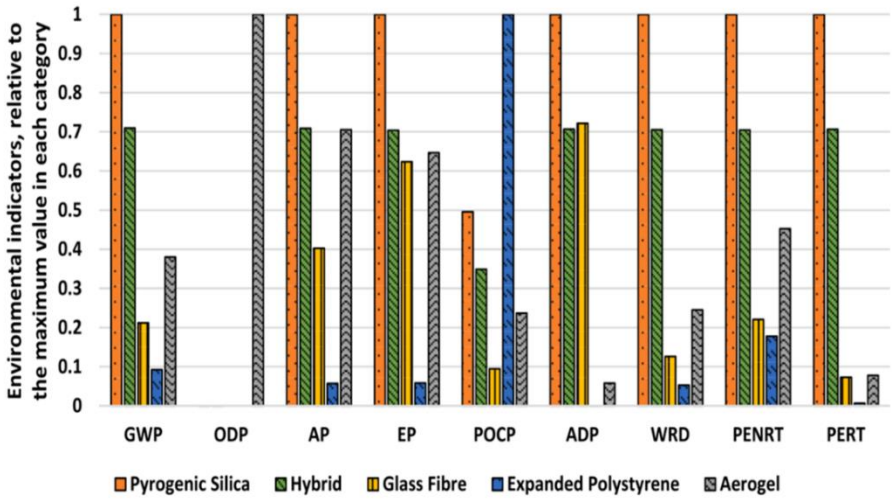

Figure 53: Lifecycle assessment for different VIP core materials [231]

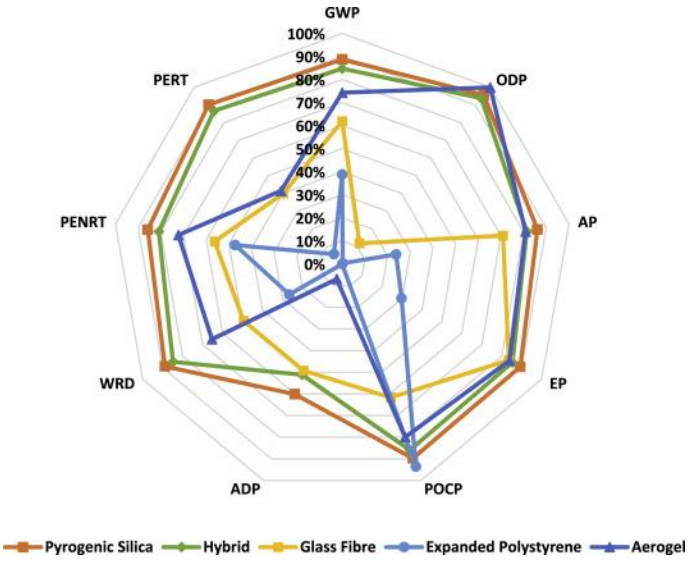

Figure 54: Contribution of the core material to the overall environmental impact of VIPs [231]

4.7 Vapor cooled shields

As effective as the insulation material can be, it can only reduce the heat transfer between the LH_2 storage tank and the surrounding environment. Therefore, heat leakages are inevitable and lead to a continuous boil-off. The hydrogen vapor must be vented once the tank reaches the maximum allowable pressure. Almost all the heat entering the cryogenic storage tank is converted into latent heat and removed from the system after venting. The temperature of the boil-off gas vapor is slightly higher than the hydrogen saturation temperature at the storage pressure. The sensible heat of hydrogen from the saturation temperature (i.e., -253 °C) to room temperature is approximately 3.5 MJ/kg, i.e., nine times higher than that of natural gas [2]. As a result, a limited mass of hydrogen gas can release a significant amount of cooling energy. Hence, it is possible to use this sensible heat in a vapor-cooled shield (VCS) around the tank to limit further boil-off. The higher the ratio of sensible to latent heat, the higher the effectiveness of the VCS. Since hydrogen has high sensible and low latent heat, this

technological solution can be highly beneficial for large-scale storage systems, especially compared to other cryogens. Notably, the higher the storage pressure, the higher the sensible-to-latent heat ratio. Therefore, VCSs are particularly promising for tanks with relatively high operating pressure, although this is unfeasible for large-scale systems [4]. Figure 55 illustrates a schematic of a tank equipped with a vapor-cooled shield.

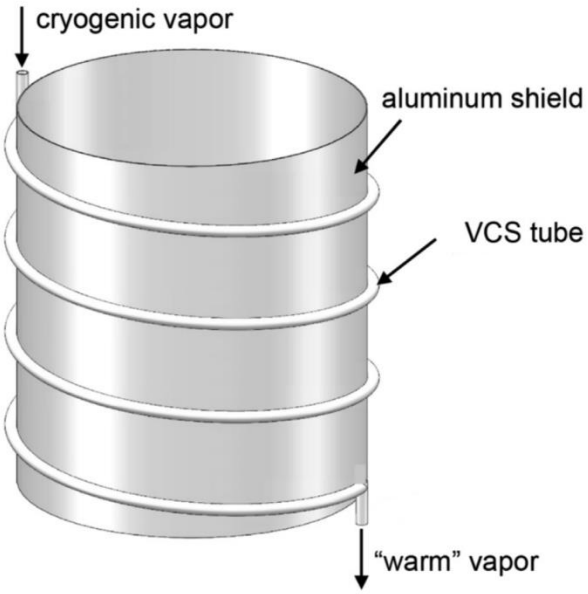

Figure 55: Schematic of a vapor-cooled shield [232]

Vapor-cooled shields can be integrated with various insulation systems. A combination of evacuated perlite powder and VCSs was proposed to improve the insulation performance of LH_2 storage tanks. Scott [233] developed a computational model based on the principles of conservation of mass and energy and theorized the advantages of using the sensible heat of hydrogen vapor to minimize further boil-off. The results showed that a 61 % reduction in the daily boil-off rate could be obtained by positioning the VCS between the inner and the outer walls (approximately 35 % from the outer jacket). Other studies focused on the optimal positioning of the vapor-cooled shields. For instance, Cunnington [234] developed a model based on the second law of thermodynamics and applied it to an integrated MLI-VCS insulation system. This study optimized the system's design, varying the location and number of shields, and the temperature of the boil-off gas. This study highlighted how two shield units can significantly improve the insulation performance. Another study proved how three VCS layers guarantee the maximum heat flux reduction in real-world applications. The benefit of such a complex system is more significant when the temperature difference between the outer and inner walls is high [235].

Nast et al. [236] applied VCSs to long-term LH_2 storage systems for aerospace applications and proved how a single vapor-cooled shield could halve the boil-off rate. Kim and Kang [237] compared three integrated insulation systems: fully-filled MLI with serial-type double VCSs, fully-filled MLI with parallel-type double VCSs, and partially-filled MLI with single VCS. The simulation results indicated that the optimal locations of the serial-type VCSs were at 30 % and 60 % of the distance between the inner and outer walls. In addition, the serial-type double VCSs outperformed the parallel-type double VCSs by 16 %, thus achieving the highest boil-off rate reduction. Babac et al. [238] extended the previous model for serial-type double VCSs to

include 2D conduction and convection, accounting for the temperature dependence of heat capacity and thermal conductivity and the heat transfer through the tank base. A 20 % discrepancy in heat leakage predictions was observed when considering temperature-dependent hydrogen properties. In particular, the accurate evaluation of the hydrogen thermal conductivity significantly impacted the results. A better insulation performance was achieved for larger VCS diameters. Moreover, the comparison between single and double VCSs indicated no substantial difference in performance attributed to replacing MLI material with hydrogen gas (with high thermal conductivity) in the double VCS configuration.

Liu et al. [239] studied the heat transfer for an MLI-VCS insulation and concluded that VCS offers notable benefits for substances with a high sensible-to-latent heat ratio. Heat conduction was the only heat transfer mechanism across the composite MLI-VCS insulation. Radiative heat transfer, solid conduction, and residual gas convection were neglected, thus providing an inaccurate temperature distribution inside the insulation system.

More sophisticated thermodynamic models were developed to account for multiple heat transfer modes and realistically estimate the heat transfer in insulation systems based on the integration of variable density multi-layer insulation (VDMLI) or spray-on foam insulation with VCSs. Jiang et al. [240] developed a model for foam-VCS-VDMLI that could consider multiple heat transfer modes. Gas conduction and forced convection were considered in the VCS, conduction in the foam, and radiation and conduction in the VDMLI. The optimal thermal insulation performance, corresponding to a heat leakage reduction of 60 %, was obtained by positioning the VCS at the midpoint of the VDMLI's thickness. Subsequent research [232] proposed and validated with experimental data a transient model to predict the thermal behavior of an MLI-VCS system. The study also investigated the transient temperature profile and heat flux variation through the MLI and VCS. The system performance was benchmarked with conventional multi-layer insulation, highlighting the crucial benefits of this LH_2 storage solution. Figure 56 shows a schematic of the combination of MLI and VCS in a liquid hydrogen storage tank.

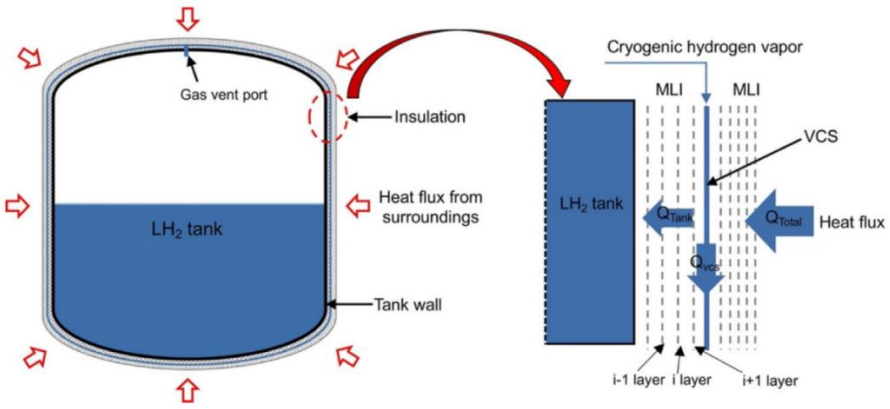

Figure 56: Integrated insulation system for LH_2 storage tank based on MLI and VCS [232]

Zheng et al. [241] optimized two different insulation systems for LH_2 storage tanks: a single VCS with MLI and a double VCS with MLI. It was proven that the single VCS should be positioned at 50 % of the insulation thickness, while the double VCSs at 30 % and 60 %. The highest heat reductions were 50 % and 59 % for the single and double VCSs. Further addition of VCS layers increased the system's complexity without improving the insulation performance. In the case of loss of vacuum, when the pressure between the walls reaches 10 Pa, the VCS

can guarantee a heat leakage reduction of 46 % and 54 % for single and double VCS compared to a conventional MLI system. In addition, it was found that the optimal position of the VCSs is approximately 30 % of the insulation thickness in VDMLI and 50 % of the insulation thickness in MLI. Therefore, the VCS should be significantly closer to the cold wall in VDMLI systems. These configurations could reduce the heat flux by 66 % and 58 % for the two insulation systems [242]. Finally, Zheng et al. [243] proposed a novel insulation system combining hollow glass microspheres with VCS. This solution was designed for large-scale and long-term LH_2 storage systems, taking advantage of the low thermal conductivity, ease of installation and maintenance of HGMs. Similarly to the VDMLI, in the case of HGMs insulation, the optimal positioning of the VCS was approximately 30 % from the cold wall. The heat flux reduction was 57 %, 65 %, and 68 % for single, double, and triple vapor-cooled shields, respectively.

Beyond the computational models, only a few prototypes of small-scale LH_2 tanks equipped with VCSs were built and tested. Liggett [244] designed a tank insulation system comprising 30 layers of MLI and two copper VCSs, using boil-off gas and an optional para-to-ortho converter. The latter component exploited the endothermic nature of the para-to-ortho hydrogen conversion to further remove heat from the system. The test results showed a significantly lower boil-off reduction compared to the simulations. Considering the best configuration for a single VCS, the 35 % reduction from the experiments significantly deviated from the predicted 66 %. Considering double VCSs and para-to-ortho converter, the boil-off rate was reduced by 26 %, while the computational model predicted a 78 % reduction. Therefore, further experimental studies should be conducted to investigate the potential of VCSs for large-scale LH_2 storage tanks.

4.8 Active cooling systems

Passive thermal protection can minimize the heat transfer between the LH_2 and the surrounding environment, but active cooling techniques must be implemented to achieve zero boil-off. Currently, research on active cooling systems focuses on aerospace applications and is only adopted for small-scale liquid hydrogen storages. This is due to the inherent difficulties of handling the boil-off gas in space environments. European and American space agencies conducted extensive research on zero boil-off technologies for cryogenic propellants, indicating four technical solutions:

- Condensers embedded inside the tank
- Cryogenic heat pipes and heat exchangers
- Spray bars and circulating pumps
- Broad area cooling shields with circulating gas pumps

Figure 57 shows a schematic of these techniques for achieving zero-boil off in LH_2 tanks for aerospace applications.

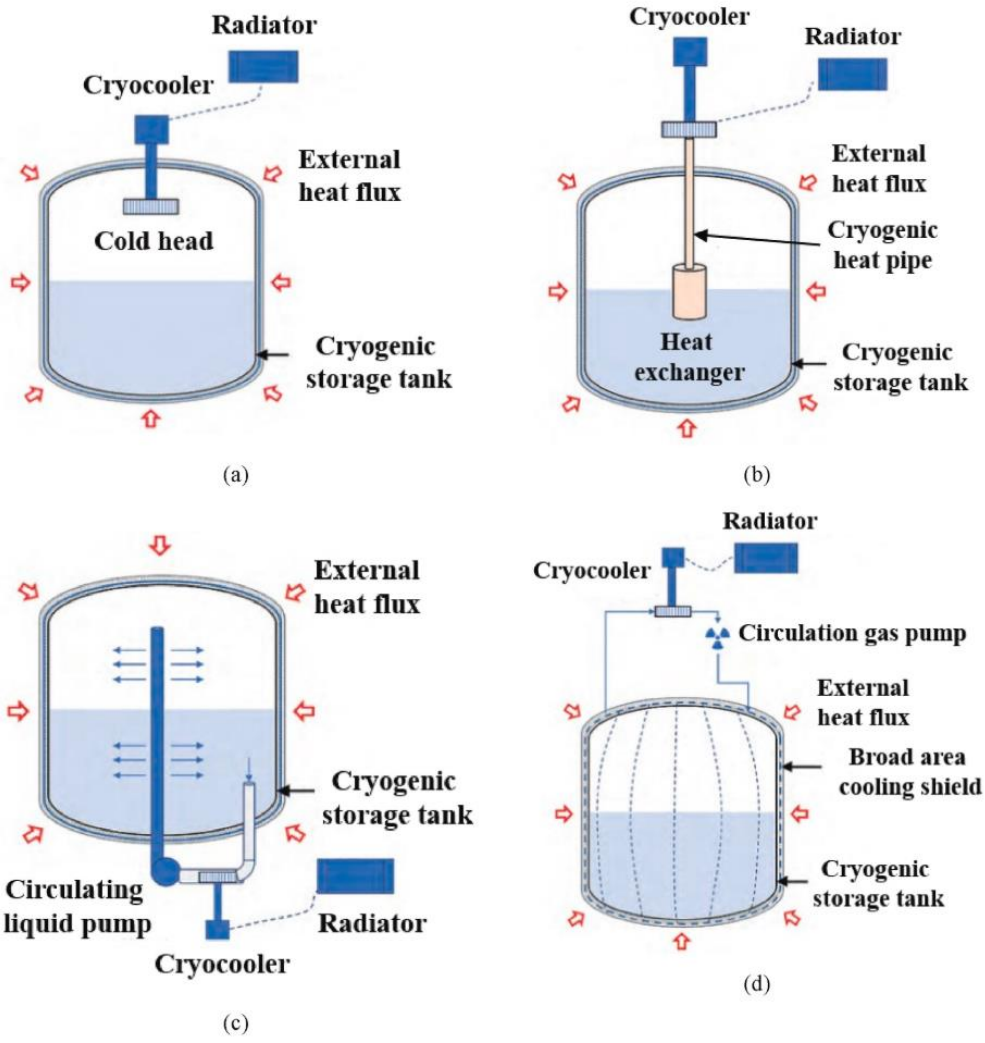

Figure 57: Schematic of zero boil-off systems for cryogenic fuels: (a) condenser embedded inside tank, (b) cryogenic heat pipe and heat exchanger, (c) spray bar and circulating pump, (d) broad area cooling shield and circulating gas pump [4]

The first approach is based on a cryocooler integrated with the storage tank. Nevertheless, this approach introduces parasitic heat leakages that limit the benefits of the active cooling system. As a result, the refrigerator must be kept as far as possible from the storage systems [245]. The NASA Ames Research Center proposed to decouple the cryocooler and the tank by introducing a heat exchanger with pressurized helium [246]. This approach ensures that the cooling capacity generated by the refrigerator is efficiently transferred to the cryogen. An alternative method is based on a circulating pump that sucks LH_2 from the tank, cools it below the saturation temperature through a cryocooler, and injects it into the tank through spray bars. Nevertheless, among these four methods, the broad area cooling shield with a circulating gas pump is the only potentially suitable for large-scale tanks. This method, known as distributed cooling, combines active heat removal with cooled shields in the insulation material. It guarantees minimal parasitic heat leakage, low power consumption, and limited thermal stratification within the storage tank [247].

5 Description and design of the ancillary components for LH_2 storage tanks

The safe and efficient storage of liquid hydrogen requires integrating various ancillary components that allow the handling and transferring of the cryogenic fuel and ensure system integrity under operations. Critical elements of an LH_2 storage system include cryopumps, valves, pressure relief devices, pipes, and flexible hoses, each playing a crucial role in maintaining the appropriate conditions for LH_2 containment and transfer. Cryopumps are essential for transferring liquid hydrogen from supply systems to storage tanks and from storage tanks to delivery terminals. Valves control the flow of LH_2, allowing for both manual and automated regulation of the dispensing processes. Pressure relief devices are designed to safeguard the system from pressure buildups, typically by venting excess hydrogen vapor in a controlled manner, thus preventing any losses of containment. Flexible hoses and pipes facilitate the transfer of liquid hydrogen between various components. These equipment items are crucial for the overall performance of an LH_2 storage system, contributing to operational efficiency and compliance with safety standards.

5.1 Cryopumps

Liquid hydrogen pumps are critical devices for moving and transferring liquid hydrogen by increasing the fluid pressure, while maintaining its extremely low temperatures. These components are crucial to facilitate efficient storage and delivery. By leveraging the unique properties of LH_2, such as its high density compared to gaseous hydrogen, these pumps significantly reduce energy consumption while streamlining hydrogen infrastructure. Cryogenic pumps typically operate immersed in LH_2, maintaining temperatures around –253 °C [248].

Piston-driven pumps are a type of reciprocating pump that achieves multi-stage compression. In the first stage, the pump raises the fluid pressure to around 6 bar, moving the hydrogen out of near-saturation conditions and preventing cavitation. The second stage further increases pressure to target levels, as high as 875 bar. One of the most notable features of piston-driven liquid hydrogen pumps is their exceptional energy efficiency. They require significantly less electricity for compression than typical compressors for gaseous hydrogen, consuming approximately 1.1 kWh/kg_{LH2} compared to the 3 kWh/ kg_{H2} of the diaphragm compressors. This efficiency stems from the higher density of LH_2, which reduces the work required to achieve high pressures.

As an example, Linde developed a piston pump which offers a flow rate of 1.55 kg/min. These capabilities enable rapid refueling, with car tanks being filled in under three minutes and truck tanks in less than five minutes. From an operational perspective, liquid hydrogen pumps provide several advantages. They eliminate the need for intermediate high-pressure buffer storage systems, simplify station designs, and reduce infrastructure costs. They also allow continuous back-to-back refueling without downtime, making them ideal for high-demand hydrogen stations and large-scale applications. Despite their efficiency, piston-driven LH_2 pumps face challenges such as boil-off losses. Heat transfer through the pump's components can cause hydrogen evaporation, and losses during idle or warm-up periods contribute to inefficiencies. However, minimizing the distance between the pump and the storage tank, along with improved venting protocols and operational practices, can mitigate these losses.

Qiu et al. [249] focused on a reciprocating LH_2 pump designed to compress hydrogen from 4 to 876 bar, catering to high-pressure hydrogen refueling needs. The pump features a two-cylinder structure, with the first cylinder pre-compressing LH_2 to 6–8 bar and the second cylinder increasing the pressure to supercritical levels. It achieves a delivery rate of 50–70 kg/h and operates efficiently at a design frequency of 2 Hz, maintaining an isentropic efficiency of 97.30 % and a volumetric efficiency of 90.76 %. The suction valve, with a spring stiffness of 130 N/m and maximum displacement of 10 mm, and the discharge valve, with a stiffness of 500 N/m and displacement of 2.5 mm, ensure a stable flow and an efficient compression. Figure 58 shows the structure of a reciprocating liquid hydrogen pump, highlighting the most critical parts, such as the flow passage, the inlet of the first cylinder, the suction valve, and the discharge valve.

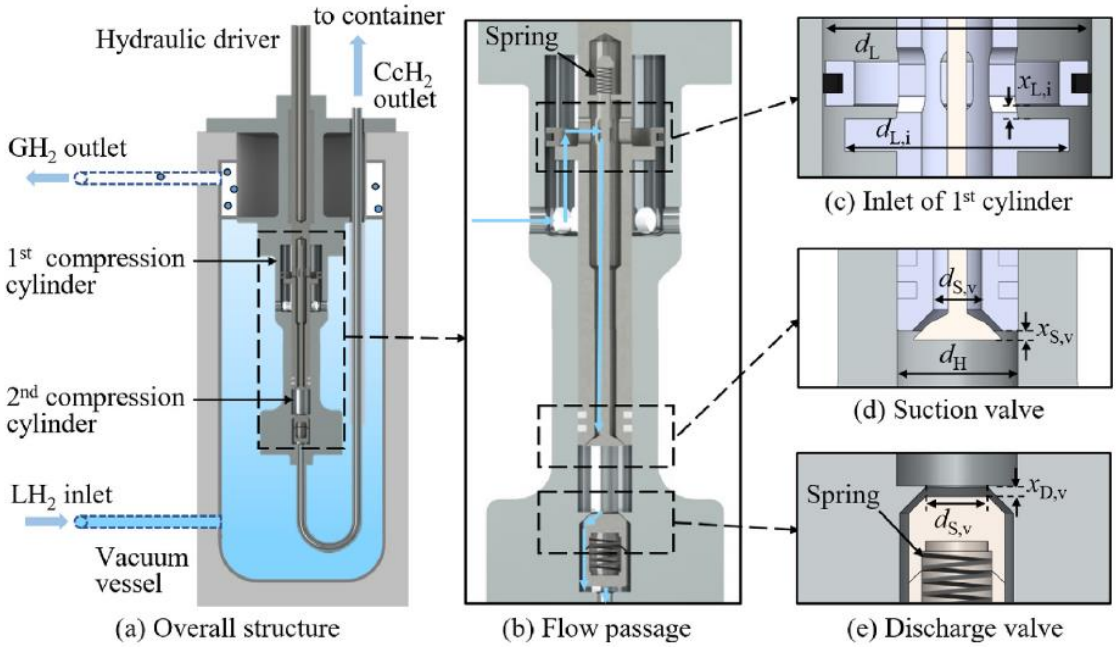

Figure 58: Structure of reciprocating LH_2 pump: (a) overall structure of the pump, (b) flow passage inside the pump, (c) inlet of the first cylinder, (d) suction valve, and (e) discharge valve [249]

Nevertheless, key challenges include managing cavitation, which can be mitigated by maintaining at least 2 °C subcooling and optimizing valve dynamics. Although the thermal losses are minimized, the boil-off rate of approximately 0.012 kg/day remains a factor. Moreover, the pump commonly shows high efficiency at elevated pressures but reduced volumetric efficiency due to clearance volume effects. This pump exemplifies advanced engineering for reliable, high-performance LH_2 compression, critical to hydrogen refueling stations and larger-scale systems [249].

The international standard ISO 24490 [250] focuses on the fabrication, testing, and installation of cryogenic pumps. It applies to centrifugal and reciprocating pumps, emphasizing robust design principles and rigorous testing protocols to ensure they can withstand the mechanical and thermal stresses associated with cryogenic applications.

5.2 Valves and pressure relief devices

In cryogenic systems, valves are particularly critical due to the unique challenges posed by low temperatures and pressure increases within the tank. Valves are essential components ensuring the system reliability and safety, guaranteeing both flow control and pressure relief. Various valves are integrated with LH_2 tanks or directly connected to their ancillary components. Table 15 summarizes the main valves used for liquid hydrogen handling, their construction type, and the internal operating elements.

Table 15: Valves used in hydrogen applications [251]

	On/off	***Flow control***	***Non-return***	***Safety function***
Valve type	Ball valve Butterfly valve Wedge gate valve	Globe valve Needle valve Control Valve Orbit ball valve	Swing check valve Dual plate check valve Piston check valve Axial check valve	Pressure safety valve Pressure relief valve
Construction type	Bolted body pieces Body and bonnet Welded body and bonnet	Bolted body pieces Body and bonnet Welded body and bonnet	One-piece design	Bolted body and bonnet
Internal operating element	Ball Disk Wedge	V-shape ball Disk	Ball Disk	Disk

Safety valves are designed to release excess boil-off gas from the tank to avoid overpressurization. They are generally divided into two primary categories: pressure relief valves (PRVs) and pressure safety valves (PSVs). While these terms are sometimes used as synonyms, there are notable differences between the two [252]. Pressure relief valves protect the pressurized system (i.e., cryogenic tanks, hydrogen gas tanks, piping, etc.) against overpressurization that could lead to bursts and leakages. There are many types of pressure relief valves, including spring-activated relief valves, pilot-operated relief valves, and temperature-activated relief valves. In addition, burst disks, eutectic plugs, and other devices can reduce the internal pressure of a storage tank [253].

A safety valve is engineered to open quickly and completely when a set pressure threshold is reached. It is predominantly used in gas systems where overpressurization could lead to operational hazards. This type of valve operates by fully opening if the gas pressure increases above a predefined value and remains open until the pressure drops significantly below the set point, ensuring all excess gas is vented. Safety valves are essential for guaranteeing that a pressure vessel's maximum allowable working pressure (MAWP) is never exceeded [252]. In contrast, pressure relief valves open gradually and proportionally to the increase in pressure beyond their set limit [252]. Relief valves typically have a pressure tolerance of ±3 % of the designated set point or ±0.1 bar (0.01 MPa), depending on which value is higher [254].

Meissner et al. [255] highlighted the valves commonly used as pressure relief devices in cryogenic systems for hydrogen supply, indicating also the relative standards. The pressure relief unit includes resealable safety valves (categories A and B) and burst discs, each serving distinct roles:

- **Resealable safety valves of category A –** This valve is employed for continuously venting small amounts of boil-off gas, maintaining consistent pressure management for hydrogen storage tanks. While the valve adheres to ISO 21013-1 [256], it is worth noting that this component should be classified as a relief valve rather than a safety valve.
- **Resealable safety valves of category B –** Designed as an emergency relief mechanism, this valve addresses high rates of hydrogen evaporation, preventing the overpressurization of cryogenic storage tanks. Its resealable feature allows repeated use after activation, ensuring system resilience. The valve complies with ISO 21013- 1 [256].
- **Burst discs –** The burst disc acts as a standby redundancy to the resealable safety valve and serves as a secondary safety measure. Its integration with the system ensures compliance with ISO 21013-2 [257].

Any supply systems for liquid hydrogen (i.e., pipes connected to the inlet and outlet of the tank) include the following key components:

- **Check valves –** This valve is installed to prevent the uncontrolled flow of liquid and gaseous hydrogen within the supply system. It ensures system safety and correct operations by permitting flow in only one direction, thereby avoiding backflow. The design and functional requirements of this valve adhere to ISO 21011 [258].
- **Automatic valves –** This component is critical for accurately controlling LH_2 mass flow to and from the storage tank, enabling high flexibility during normal and abnormal operations. The valve complies with the standard ISO 21011 [258].

When testing during the production phase, valves classified as Category A and Category B must endure 2’000 and 100 opening-closing cycles, respectively. However, ISO 21011 does not specify the condition tests for the check and automatic valves. Nevertheless, factors such as ice formation, vibration, thermal cycles, low-temperature embrittlement, and hydrogen embrittlement must be considered while testing such equipment.

Figure 59 illustrates a schematic of a loading line for LH_2 storage tanks, equipped with various types of valves.

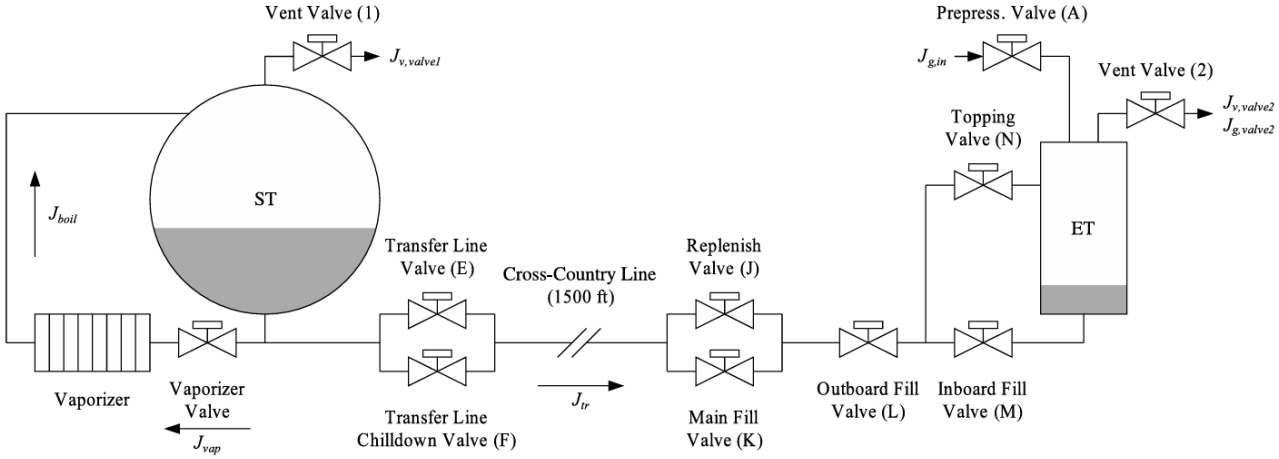

Figure 59: Process flow diagram of a LH_2 loading line for a storage tank [259]

A lip seal, typically constructed from Teflon® combined with a metallic spring, is designed for cryogenic applications. It can operate effectively at temperatures as low as –253 °C, making it suitable for liquid hydrogen systems [252], [260]. Polytetrafluoroethylene (PTFE) has a minimum operational temperature of approximately –46 °C. Nevertheless, reinforcing PTFE with materials such as graphite or fiberglass significantly enhances its performance at extremely low temperatures, reducing the minimum operational temperature to –150 °C [261]–[265]. This extended range makes reinforced PTFE suitable for applications requiring enhanced mechanical stability and chemical resistance in cryogenic environments, such as liquid hydrogen equipment. It is widely adopted for the soft seats of ball and butterfly valves. Polychlorotrifluoroethylene (PCTFE) can be used for the same purposes in cryogenic environments [251].

By way of illustration, Figure 60 represents the technical drawing of a wedge gate valve, highlighting the main parts and the typical materials.

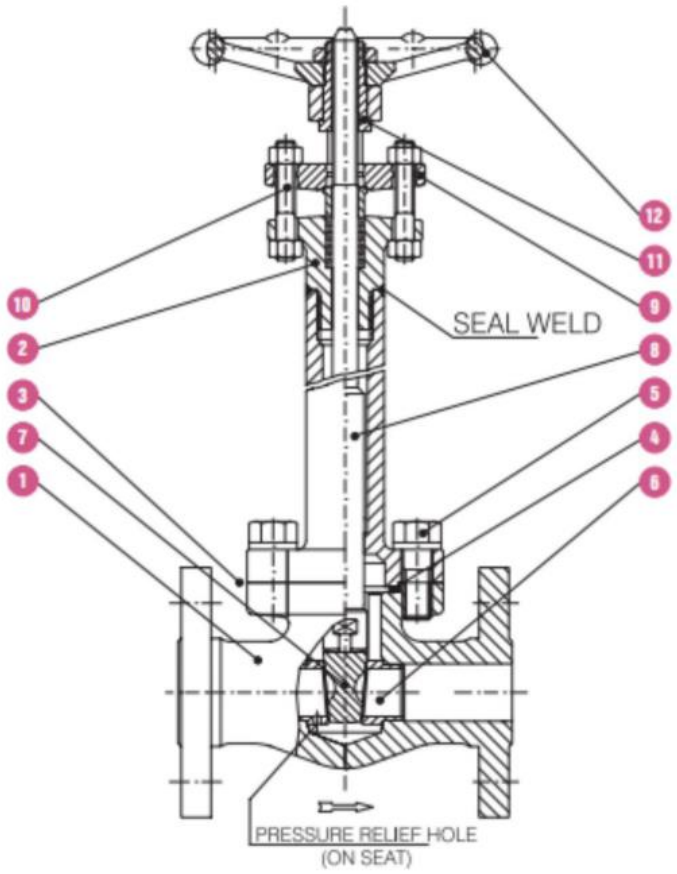

Figure 60: Technical drawing of a wedge gate valve for cryogenic service [251]

ID	Valve part	Material
1	Body	Stainless steel AISI 316
2	Bonnet	Stainless steel AISI 316
3	Body and bonnet joint	-
4	Gasket	Graphite / graphite + Stainless steel AISI 316 / Stainless steel AISI 316
5	Body and bonnet bolting (bolt and nut)	Stainless steel AISI 316
6	Seat	Stainless steel AISI 316
7	Wedge	Stainless steel AISI 316
8	Stem	Stainless steel AISI 316
9	Gland and flange	Stainless steel AISI 316
10	Gland bolt and nut	Low alloy steel with hot dip galvanized / Stainless steel AISI 316
11	Yoke sleeve	Carbon steel / Stainless steel AISI 316
12	Handwheel	Carbon steel / Stainless steel AISI 316

Considering the application involving exposure to flammable substances, it is essential to design and evaluate valves for their ability to withstand fires. First, a valve should be able to seal effectively even after the soft seat has melted due to exposure to extremely high temperatures. Second, the materials used for the valve's soft components must be fire-resistant. Graphite is a common choice. Lastly, electrical continuity is crucial and can be obtained by incorporating antistatic devices or springs into the valve [262], [266].

Maintenance of pressure relief devices typically requires inspecting and resetting the relief pressure, as well as replacing components like soft materials, seats, and other parts prone to wear. This equipment is susceptible to several failure modes, including failure to open, premature opening, inability to reseat after activation, leakage past the valve seat, and mechanical failure. The component breakdown determines a total loss of pressure in the system. In the event of a leak, a pressure drop triggers an alarm, which subsequently causes the system to shut down [253]. Pressure relief devices operating in industrial environments are exposed to various stress factors, including fluctuations in environmental and mechanical conditions. Factors that frequently contribute to failures include cyclic pressure and temperature changes, corrosion, buildup of deposits, material creep, design flaws, vibration, improper handling, inadequate maintenance, process upsets, and manufacturing defects [253].

Typical maintenance tasks for valves involve replacing components such as o-rings, seat seals, and metallic bellows. It may also include replacing parts of the control unit, such as the actuator's diaphragm and compressed air gasket, as well as the solenoid valves for the positioner. In fact, pressure safety valves can block after opening until the internal pressure is equal to the ambient pressure. This phenomenon determines large losses of fuel.

Additionally, maintaining the cleanliness of the valve parts and ensuring very low humidity are crucial for successful maintenance [267]. The main maintenance strategies for the various parts of valves for cryogenic service are summarized as follows:

- **Seat seal –** The performance of the seat seal can degrade over time due to the buildup of particles on its surface. Therefore, preventive maintenance should be adjusted based on the cleanliness of the plant (such as the quality of supply gas and the overall frequency of maintenance). A general recommendation is to replace the seals every five to seven years.
- **Bellow –** Whenever the seals are being replaced, the valve inserts with bellows should also be removed. This is an ideal opportunity to inspect the bellows for any potential damage. Misaligned or deformed bellows can lead to excessive wear on the stem-centering elements, potentially damaging the flow plug's surface. Additionally, stems that stick or move unevenly are more prone to failure from fatigue than properly aligned, well-guided stems.
- **Static seal –** Like the seat seal, the static seal should be addressed by removing the valve stem. This operation is generally performed during seat seal replacement, typically every five to seven years, considering the loss of elasticity in the elastomeric material due to aging.
- **Pneumatic actuators –** Pneumatic actuators can be maintained by replacing the diaphragm and air gaskets that connect the air chamber to the stem. It is recommended to perform preventive maintenance on actuators every 15-20 years, though this interval may need to be shortened to five to seven years for valves exposed to particularly severe operating conditions.
- **Solenoid valves, positioners, and air regulation units –** Malfunctions of components controlling the air pressure circuit are inherently difficult to predict. However, these components are located outside the valve housing and are easily replaceable unless the valve operates in areas with restricted access. Leaks in internal or external connections can be identified using a detection spray and repaired by replacing the faulty components.

5.3 Pipes

Transporting cryogenic fluids poses unique challenges due to their low boiling temperatures and the need to minimize product loss from vaporization. The scientific literature has explored various aspects of cryogenic transport in pipelines, ranging from heat transfer modeling to structural analysis of vacuum-insulated piping systems [131], [268], [269]. Liquid hydrogen, with a boiling point of -253 °C at ambient pressure, requires extremely effective thermal insulation during transport to minimize boil-off. Several studies emphasized the importance of high-performance insulation materials, such as multi-layer vacuum insulation (MLVI), to keep the LH_2 temperature within acceptable limits [131], [268], [269].

Numerical models are often used to predict the onset of nucleate boiling and its impact on flow characteristics. Nucleate boiling is a heat transfer process that occurs when a liquid is heated above its boiling point on a solid surface, forming vapor bubbles at specific surface sites called nucleation sites. These sites are typically microscopic cavities or surface imperfections that retain vapor or gas, providing a starting point for bubble formation [131], [268].

Various insulation materials have been investigated for cryogenic pipes, each with advantages and disadvantages regarding thermal performance, cost, and ease of installation. Vacuum insulation, combined with different internal filling materials, has proven effective in reducing heat transfer. The multi-layer Mylar mesh combined with vacuum insulation has shown superior thermal performance among filling materials. Other commonly used materials include perlite powder, fiberglass, polyurethane foam, and aerogels [131], [268]. Figure 61 shows the schematic of a multi-layer vacuum-insulated pipe for LH_2 transport. A double-walled configuration allows to keep high-vacuum conditions to minimize conductive, convective, and radiative heat transfer. Inner and outer walls are connected through a complex system that minimizes conduction.

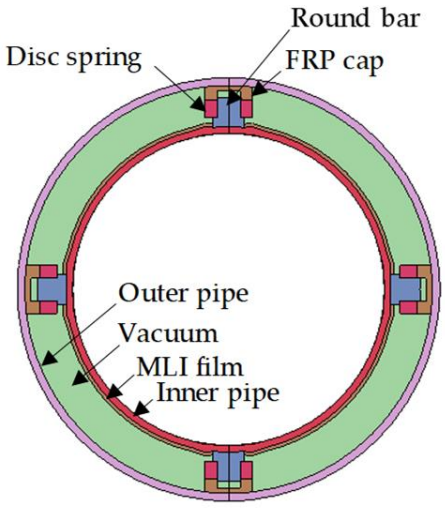

Figure 61: Cross-section of a multi-layer vacuum-insulated pipe [269]

Table 16 summarizes the geometrical characteristics of the MLVI pipe, distinguishing between the various layers of different structural and insulating materials.

Table 16: Geometrical properties of the multi-layer vacuum-insulated pipe [269]

Type	Thickness (mm)	Material
Inner pipe wall	3.44	Austenitic stainless steel
Insulation	1.82	Multi-layer insulation
Vacuum	19.43	-
Outer pipe wall	4.19	Austenitic stainless steel or carbon steel

5.4 Flexible hoses

Cryogenic hoses can be categorized according to the transported product and divided into two main types: corrugated metal hoses and cryogenic composite hoses. The first type of hoses are fully mature technology with low cost, high safety, and reliability. These advantages justify their widespread rollout. However, disadvantages include being heavier, having a large bending radius, and low flexibility, which makes alignment challenging during connections [270]. Conversely, cryogenic composite hoses are made of thermoplastic materials and metal reinforcing wires [270]–[272]. They were designed to address the challenges associated with corrugated metal hoses. As a result, composite hoses are lighter and have a smaller bending radius, thus facilitating pipe connections. However, due to the low-temperature brittleness of polymer materials and compatibility issues with certain products, their use is restricted in the transport of liquid hydrogen [270], [271].

Corrugated metal hoses are typically made of stainless steel, such as AISI 316 L, which exhibits good toughness at cryogenic temperature and is corrosion resistant. A typical design includes seven layers to ensure good structural performance and integrity of the flexible hose during unloading operations. The inner (or containment) layers consist of corrugated stainless steel separated by a polymer spacer. The space between the corrugated tubes is vacuumed to minimize conduction. The outer (or reinforcing) layers consist of high-strength carbon steel wires separated by polymer sleeves [270]–[272]. Figure 62 represents a floating-type reinforced metal corrugated hose and a suspended-type reinforced metal corrugated hose developed by Technip. Table 17 indicates the technical characteristics and performances of each layer.

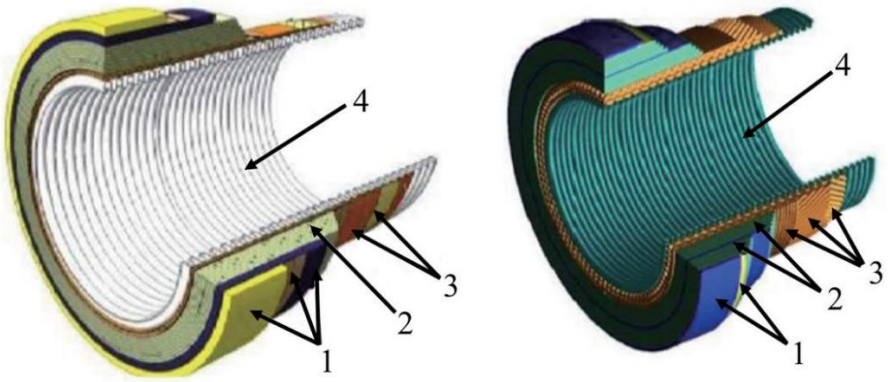

Figure 62: Floating-type (left) and suspended-type (right) configurations of reinforced metal corrugated hoses [270]

Table 17: Structure and features of reinforced metal corrugated hoses [270]

Number	Layer type	Characteristics
1	Outer protective layer	- It prevents corrosion of the hose walls and wear of critical materials coming from external environments. - The outer protective layers of the floating-type hoses are wound by thermoplastic elastic material. - The outer protective layers of the suspended-type hoses are wrapped by self-adhesive tape.
2	Insulation layer	- It reduces heat transfer, air condensation, and freezing on the outer wall. - It reduces the vaporization of the cryogenic product inside the hose. - The insulation layers of the floating-type hoses are wrapped by aerogel foam tape. - The insulation layers of the suspended-type hoses are wrapped by polyethylene foam tape.
3	Armored layer	- It is placed between the insulation layers and the metal inner tube, primarily bears axial loads, enhances the axial tensile strength of the hose. - It is wrapped by two layers of polyester fiber fabric. - The armored layer of the floating-type hose is additionally equipped with wear-resistant strips and flat steel strips. - The armored layer of the suspended-type is wrapped with nylon braided tape.
4	Metal inner tube	- It is a thin-walled corrugated tube made of AISI 316 L stainless steel. - It provides skeletal support and determines the inner diameter of the hoses. - It is capable to withstand the internal pressure of the hose in normal and abnormal conditions.

Cryogenic composite hoses are wound with multiple layers of polymer films and braided polymer fibers, tightened by internal and external helical metal wires to create a sealed tubular structure. The polymer film layers prevent leakage during product transport, the braided polymer layers increase axial and radial strength, and the internal and external helical metal wires provide skeletal support while enhancing the strength of the hoses [270], [272].

This technology is considered a promising alternative to metal hoses for liquid hydrogen transport. However, thermal insulation and hydrogen permeation remain critical challenges for composite hoses, leading to potential microcracks, fractures, and leaks [273]. To mitigate hydrogen permeation in composite hoses, NASA has developed a barrier membrane that prevents hydrogen penetration, ensuring the structural integrity of hoses and tanks [273]. Figure 63 shows the schematic of a composite hose for cryogenic service developed by Japan Meiji Company. The image indicates the inner and outer metal wires (1), the cryogenic-resistant fiber fabric layers (2), the cryogenic-resistant polymer film layers (3), and the impermeable film layers (4).

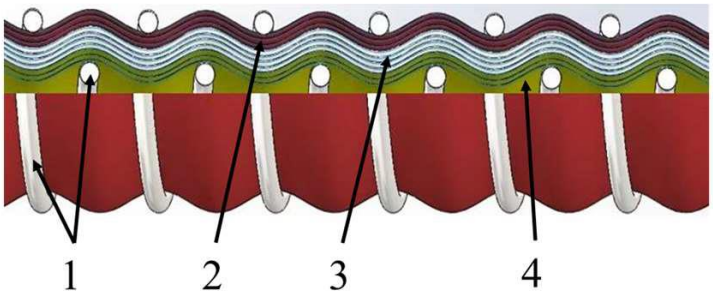

Figure 63: Schematic of cryogenic composite hoses by Japan Meiji Company [270]

Figure 64 represents a cryo-line composite hose, while Table 18 summarizes the technical characteristics and performances of the various layers.

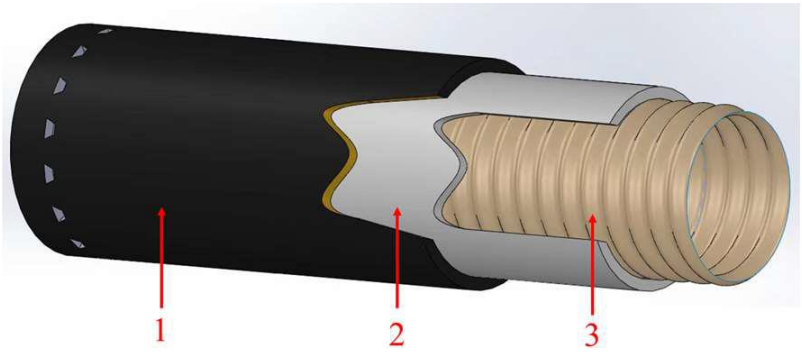

Figure 64: Schematic of cryo-line composite hose [270]

Table 18: Structure and features of cryo-line composite hose [270]

Number	Layer type	Characteristics
1	Outer protective layer	- It is based on the same technology used for bonded flexible hoses. - It protects the inner layers from corrosion and wear.
2	Insulation material + Leak monitoring system	- The material is designed to reduce heat loss within the structure and avoid ice formation on the outer cover of the cryogenic hoses. - The material has excellent properties over the entire temperature range. - The leak monitoring system based on optical fiber technology is included in the annular space to check the temperature within the structure and prevent any abnormal conditions.
3	Inner hose	- It is derived from the same technology used for reinforced metal corrugated hoses. - To achieve better sealing, the inner hose incorporates multiple films of polymeric material and woven fabric material.

6 Standards for LH_2 storage

Comprehensive and up-to-date regulations, engineering codes, and standards are crucial for any technical system's design, operation, inspection, and maintenance. A clear, rational, and internationally adopted regulatory framework can facilitate the widespread rollout of technologies with limited market penetration, such as hydrogen technologies. Ideally, these standards should define the minimal requirements for designing, installing, and assessing the fitness-for-service of LH_2 storage systems. In addition, they should indicate the best practices for operating, inspecting, and maintaining the components during their life and for decommissioning them if they do not comply with the minimal safety requirements or their performance is compromised. This section collects and analyses the most relevant international and European standards and recommended practices for liquid hydrogen storage, focusing on static and maritime applications. The technical committee ISO/TC 220 is responsible for standardizing insulated vessels for cryogenic service, including equipment design, definition of operational requirements, and development of guidelines for material selection, performance evaluations, and safety requirements. The CEN/TC 268 has the same responsibilities at a European level. In addition, the working group EIGA/WG-6 of the European Industrial Gases Association (EIGA) has the primary function of defining design criteria, material compatibility, operational and periodic inspection requirements for cryogenic storage vessels, developing industrial codes and guidelines, and reviewing incidents and accidents to propose ways to avoid re-occurrence.

Section 6.1 focuses on the standard for LH_2 storage tanks, while Section 6.2 is dedicated to the accessories for liquid hydrogen handling, such as valves, venting systems, flexible hoses, cryopumps, and safety devices. Section 6.3 delves into the material selection for cryogenic service, considering both structural and insulating materials. Section 6.4 presents the standards for large-scale storage tanks for refrigerated liquified gases. Finally, Section 6.5 is dedicated to vacuum insulation panels for building and industrial applications.

6.1 Standards for LH_2 storage tanks

The Compressed Gas Association developed its standard CGA H-3 [274] for cryogenic hydrogen storage, which indicates the minimum design and performance requirements for vacuum-insulated LH_2 tanks. It provides the tank design and manufacturing criteria and the technical details for the inner vessel, outer jacket, insulation system, and piping, specifying dimensions, shipping envelopes, and liquid withdrawal capacities. In addition, it indicates the requirements for cleaning, painting, testing, inspecting, and maintaining this equipment. These guidelines apply to vertical and horizontal tanks with a maximum allowable pressure of 12.1 bar and gross volume ranging from 3785 to 94600 liters. All transportable LH_2 containers are excluded. In addition, this standard does not include operation and installation requirements and emergency response procedures. CGA H-3 is going through the final stages of designation as an American National Standard (ANSI).

The code provided by the European Industrial Gases Association (EIGA 06/19 [275]) applies to the layout, design, and operation of liquid hydrogen tanks for fixed storage and transport by road, sea, and rail. EIGA 06/19 indicates the installation criteria, safety distances, testing, and commissioning procedures. In contrast, portable containers (e.g., pallet tanks and liquid cylinders) are excluded from the scope of this code. The document EIGA 114/09 [276] specifies

the procedure for putting into service, inspecting, requalifying, decommissioning, maintaining, and repairing static cryogenic vessels designed for a maximum pressure higher than 0.5 barg. EIGA 119/04 [277] addresses periodic inspection and testing of static vacuum-insulated cryogenic pressure vessels to store refrigerated liquefied gases. It is worth mentioning that national legislation for periodic inspection and testing varies considerably between European countries and has priority over the EIGA 119/04 guidelines. This aspect is addressed in EIGA PP 09/09 [278]. Since there is no mutual recognition of the periodic inspection performed in different countries, this document indicates the future actions to be considered at the European level. Finally, the document EIGA 151/15 [279] is more specific and provides guidelines for transportable or static cryogenic tanks, detailing the procedures to prevent their overpressurization during filling operations.

The standard ISO 13985 [280] of the International Organization for Standardization establishes the construction requirements for refillable LH_2 tanks permanently attached to land vehicles as well as the minimum safety requirements for loss of integrity, fires, and explosions. Although not specified, this standard applies to small-scale vacuum-insulated tanks and does not cover medium- and large-scale tankers and carriers for cryogenic fluids. These applications are specifically addressed by ISO 20421-1 [281], which indicates the requirements for the design, fabrication, inspection, and testing of vacuum-insulated cryogenic vessels capable of storing more than 450 liters of fluid. This document covers fixed, demountable, and portable tanks attached to generic means of transport. In addition, ISO 20421-2 [282] specifies the operational requirements for these transportable tanks and includes detailed procedures for putting them into service, filling, withdrawing, transporting, periodically inspecting, and maintaining. Emergency procedures in the case of abnormal operations are also addressed. These standards do not include general vehicle requirements and regulations for transporting these vessels by public road, rail, waterway, sea, and air. The European standards EN 13530-1 [283] and EN 13530-2 [284] specify the fundamental requirements, design and fabrication criteria, and inspection and testing procedures for transportable vacuum-insulated cryogenic vessels larger than 1000 liters and designed to operate above atmospheric pressure. This document covers fixed, demountable, and portable tanks attached to a road vehicle but is potentially applicable to other modes of transport. The standard EN 13530-3 [285] overlaps with ISO 20421-2 and covers the operational requirements for this equipment. The main difference between the ISO and EN standards is that the former applies to smaller tank sizes (tanks larger than 450 liters instead of 1000 liters) and various modes of transport. In addition, the European standards EN 14398-1 [286], EN 14398-2 [287], and EN 14398-3 [288] indicate the requirements for large transportable non-vacuum-insulated vessels for cryogenic applications. They cover the same tank sizes and fields of application of the standards for large transportable vacuum-insulated tanks.

The ISO standards 21029-1 [289] and 21029-2 [290] are specific for transportable vacuum-insulated cryogenic pressure vessels with a maximum volume of 1000 liters. The former indicates the design, fabrication, initial testing, and inspection requirements, while the latter specifies the operational requirements. It includes putting into service, filling, withdrawal, transport, maintenance, periodic inspection, and emergency procedures. Still, it does not include the specific regulations for transporting these vessels by public road, rail, waterway, sea, and air. In addition, open-top dewars and refillable transportable tanks are not considered in this document. The European standards EN 1251-1 [291], EN 1251-2 [292], and EN 1251-3 [293] apply to the same cryogenic service equipment designed for a maximum allowable pressure greater than atmospheric.

The standards ISO 21009-1 [294] and ISO 21009-2 [295] address static vacuum-insulated cryogenic vessels designed for a maximum allowable pressure of more than 0.5 bar. The former code indicates the design and fabrication requirements, inspection, and testing procedures, while the latter is dedicated to the operational and safety requirements. These standards also cover ancillary components permanently attached to static vessels. Nevertheless, additional requirements can apply for the installation of these vessels and are defined in specific regulations. The European standards for static vacuum-insulated cryogenic vessels are EN 13458-1 [296], EN 13458-2 [297], and EN 13458-3 [298]. The first two documents indicate the fundamental requirements, the design and fabrication criteria, and the inspection and testing procedures. Therefore, they perfectly overlap with ISO 21009-1. Similarly to ISO 21009-2, EN 13458-3 specifies the operational requirements of these cryogenic vessels, including the installation, start-up, filling, maintenance, and emergency procedures. In addition, static non-vacuum-insulated cryogenic vessels designed for a maximum allowable pressure greater than 0.5 bar have dedicated European standards (i.e., EN 14197-1 [299], EN 14197-2 [300], and EN 14197-3 [301]), which provide the same information and requirements of those for static vacuum-insulated vessels.

Table 19 collects the latest European and international standards for cryogenic storage tanks, specifying the scope and equipment type they cover.

Table 19: Standards for liquid hydrogen storage tanks

Standard	Year	Title	Scope	Equipment type
CGA H-3	2024	Standard for cryogenic hydrogen storage	Tank design criteria Performance requirements	Vacuum-insulated LH_2 storage tanks with maximum operating pressure lower than 12.1 bar, gross volume between 3785 and 94600 L, and for fixed storage
EIGA 06/19	2019	Safety in storage, handling and distribution of liquid hydrogen	Tank design criteria Operational requirements Procedures for testing and commissioning Minimum safety distances	Vacuum-insulated LH_2 tanks for fixed storage transport by road, sea, and rail
EIGA 114/09	2009	Operation of static cryogenic vessels	Procedures for putting into service, inspecting, requalifying, decommissioning, maintaining, and repairing Operational requirements	Static cryogenic vessels with maximum pressure higher than 0.5 barg
EIGA 119/04	2004	Periodic inspection of static cryogenic vessels	Procedures for periodic inspection and testing	Vacuum-insulated pressure tanks for fixed storage of refrigerated liquefied gases

EIGA 151/15	2015	Prevention of excessive pressure during filling of cryogenic vessels	Procedures for preventing overpressurization during filling operations	Vacuum-insulated pressure tanks for mobile and static storage of refrigerated liquefied gases
EIGA PP 09/09	2009	The PED – Periodic inspection and reassessment of static cryogenic vessels for use in the EU	Analysis of different national regulation in the EU countries regarding inspections Roadmap of regulatory actions to be undertaken	Vacuum-insulated pressure tanks for fixed storage of refrigerated liquefied gases
ISO 13985	2006	Liquid hydrogen – Land vehicle fuel tanks	Tank design criteria Testing methods Safety measures to prevent loss of life and property	Refillable LH_2 tanks permanently attached to land vehicles
ISO 20421-1	2019	Cryogenic vessels – Large transportable vacuum-insulated vessels – Part 1: Design, fabrication, inspection and testing	Tank design criteria Fabrication requirements Procedures for inspecting and testing	Transportable vacuum-insulated tanks with storage volume larger than 450 L
ISO 20421-2	2017	Cryogenic vessels – Large transportable vacuum-insulated vessels – Part 2: Operational requirements	Operational requirements Procedures for putting into service, filling, withdrawing, transporting, inspecting and maintaining Emergency procedures	Transportable vacuum-insulated tanks with storage volume larger than 450 L
ISO 21029-1	2019	Cryogenic vessels – Transportable vacuum-insulated vessels of not more than 1000 liters volume – Part 1: Design, fabrication, inspection and tests	Tank design criteria Fabrication requirements Procedures for inspecting and testing	Vacuum-insulated pressure vessels with storage volume lower than 1000 L
ISO 21029-2	2015	Cryogenic vessels – Transportable vacuum-insulated vessels of not more than 1000 liters volume – Part 2: Operational requirements	Operational requirements Procedures for putting into service, filling, withdrawing, transporting, inspecting and maintaining Emergency procedures	Vacuum-insulated pressure vessels with storage volume lower than 1000 L
ISO 21009-1	2022	Cryogenic vessels – Static vacuum-insulated vessels –	Tank design criteria	Fixed vacuum-insulated tanks with maximum

		Part 1: Desing, fabrication, inspection and tests	Fabrication requirements Procedures for inspecting and testing	operating pressure higher than 0.5 bar Ancillary components permanently attached to the tanks
ISO 21009-2	2015	Cryogenic vessels – Static vacuum-insulated vessels – Part 2: Operational requirements	Operational requirements Safety requirements	Fixed vacuum-insulated tanks with maximum operating pressure higher than 0.5 bar Ancillary components permanently attached to the tanks
EN 13530-1	2002	Cryogenic vessels – Large transportable vacuum insulated vessels – Part 1: Fundamental requirements	Fundamental requirements	Transportable vacuum-insulated tanks with storage volume larger than 1000 L
EN 13530-2	2002	Cryogenic vessels – Large transportable vacuum insulated vessels – Part 2: Design, fabrication, inspection and testing	Tank design criteria Fabrication requirements Procedures for inspecting and testing	Transportable vacuum-insulated tanks with storage volume larger than 1000 L
EN 13530-3	2002	Cryogenic vessels – Large transportable vacuum insulated vessels – Part 3: Operational requirements	Operational requirements Procedure for installing, putting into service, filling, and maintaining Emergency procedures	Transportable vacuum-insulated tanks with storage volume larger than 1000 L
EN 14398-1	2003	Cryogenic vessels – Large transportable non-vacuum insulated vessels – Part 1: Fundamental requirements	Fundamental requirements	Transportable non-vacuum-insulated tanks with storage volume larger than 1000 L
EN 14398-2	2008	Cryogenic vessels – Large transportable non-vacuum insulated vessels – Part 2: Design, fabrication, inspection and testing	Tank design criteria Fabrication requirements Procedures for inspecting and testing	Transportable non-vacuum-insulated tanks with storage volume larger than 1000 L
EN 14398-3	2003	Cryogenic vessels – Large transportable non-vacuum insulated vessels – Part 3: Operational requirements	Operational requirements Procedure for installing, putting into service, filling, and maintaining Emergency procedures	Transportable non-vacuum-insulated tanks with storage volume larger than 1000 L
EN 1251-1	2000	Cryogenic vessels – Transportable vacuum insulated vessels of not more than 1000 liters	Fundamental requirements	Vacuum-insulated pressure vessels with storage volume lower than 1000 L

		volume – Part 1: Fundamental requirements		
EN 1251-2	2000	Cryogenic vessels – Transportable vacuum insulated vessels of not more than 1000 liters volume – Part 2: Design, fabrication, inspection and testing	Tank design criteria Fabrication requirements Procedures for inspecting and testing	Vacuum-insulated pressure vessels with storage volume lower than 1000 L
EN 1251-3	2000	Cryogenic vessels – Transportable vacuum insulated vessels of not more than 1000 liters volume – Part 3: Operational requirements	Operational requirements Procedure for installing, putting into service, filling, and maintaining Emergency procedures	Vacuum-insulated pressure vessels with storage volume lower than 1000 L
EN 13458-1	2002	Cryogenic vessels – Static vacuum insulated vessels – Part 1: Fundamental requirements	Fundamental requirements	Fixed vacuum-insulated tanks with maximum operating pressure higher than 0.5 bar
EN 13458-2	2002	Cryogenic vessels – Static vacuum insulated vessels – Part 2: Design, fabrication, inspection and testing	Tank design criteria Fabrication requirements Procedures for inspecting and testing	Fixed vacuum-insulated tanks with maximum operating pressure higher than 0.5 bar
EN 13458-3	2005	Cryogenic vessels – Static vacuum insulated vessels – Part 3: Operational requirements	Operational requirements Procedure for installing, putting into service, filling, and maintaining Emergency procedures	Fixed vacuum-insulated tanks with maximum operating pressure higher than 0.5 bar
EN 14197-1	2003	Cryogenic vessels – Static non-vacuum insulated vessels – Part 1: Fundamental requirements	Fundamental requirements	Fixed non-vacuum-insulated tanks with maximum operating pressure higher than 0.5 bar
EN 14197-2	2003	Cryogenic vessels – Static non-vacuum insulated vessels – Part 2: Design, fabrication, inspection and testing	Tank design criteria Fabrication requirements Procedures for inspecting and testing	Fixed non-vacuum-insulated tanks with maximum operating pressure higher than 0.5 bar
EN 14197-3	2004	Cryogenic vessels – Static non-vacuum insulated vessels – Part 3: Operational requirements	Operational requirements Procedure for installing, putting into service, filling, and maintaining	Fixed non-vacuum-insulated tanks with maximum operating pressure higher than 0.5 bar

	Emergency procedures

6.2 Standards for ancillary components of LH_2 storage tanks

A liquid hydrogen storage system does not only consist of a super-insulated tank. Various additional components can be permanently attached or connected to the tank to enable filling and emptying procedures, control the flow rate of cryogenic fuel at the tank's inlet and outlet, and avoid overpressurization due to boil-off. This equipment is exposed to extremely low temperatures and, therefore, is designed and operated following specific criteria.

The CGA standard G-5.5 [302] establishes the minimum requirements for the safe design, installation, and operation of hydrogen venting systems. The National Fire Protection Association also references this document in NFPA 55 and NFPA 2. It includes the detailed sizing methodology, special requirements for PRVs equipped to cryogenic storage tanks, and design techniques to ensure the mechanical integrity in the case of hydrogen detonation and deflagration. In addition, it indicates where to locate the PRVs and how to drain water from stacks, avoid ice blockages, connect vent lines to stacks, and operate, inspect, maintain, and repair such components. Similarly, the industrial code EIGA 24/18 [303] defines the types of pressure protection devices used for cryogenic tanks (i.e., relief valves, pilot-operated relief valves, and bursting discs).

The standard ISO 21011 [258] indicates the requirements for the design, manufacturing, and testing of cryogenic valves connected with vacuum-insulated tanks. This document applies to vacuum-jacketed valves up to size DN 150 operating below –40 °C. The valves are designed and tested to satisfy the generally accepted nominal pressure PN 40 and attached to tanks with equal or lower maximum allowable pressure. Dedicated sections establish the requirements for the materials and the cleanliness level. The corresponding European standard EN 1626 [304] applies to valves operating below –10 °C but excludes the valves for liquified natural gas. Its applicability to LH_2 valves is not clear.

The standard ISO 21013 is dedicated explicitly to pressure relief accessories for cryogenic service. Part 1 [256] specifies the requirements for designing, manufacturing, and testing reclosable pressure relief valves operating with cryogenic fluids (i.e., below −10 °C) and at temperatures from ambient to cryogenic. The document's guidelines apply to components not exceeding the size of DN 150 designed to relieve fluids (vapors, single gases, or gas mixtures) in single-phase only. Part 2 [257] is dedicated to non-reclosable PRVs and applies to bursting discs and buckling-pin devices with sizes below DN 200 designed to relieve single-phase fluids. The calculation methods for determining the required mass flow to be relieved are indicated in Part 3 [305]. It considers both normal operating conditions, i.e., vessels with insulation system intact under normal vacuum, and abnormal operations, along with the cases of partial and total loss of vacuum with or without fire engulfment. Finally, Part 4 [306] specifies the design, manufacturing, and testing requirements for pilot-operated PRVs with DN 300 or lower. The European standard dedicated to safety devices for protection against excessive pressure for cryogenic applications is EN 13648. Unlike ISO 21013-1, Part 1 [307] of this standard is restricted to pressure relief valves not exceeding the size of DN 25 or DN 100 (depending on the valve category) and pressure designation up to PN 40. Part 2 [308] is dedicated to bursting discs with a maximum size of DN 100, while Part 3 [309] covers the same

cases of ISO 21013-3. In general, the European standards apply to equipment of smaller sizes compared to the corresponding international standards.

The standard ISO 21012 [310] specifies design, construction, testing, and marking requirements for non-insulated flexible hoses with sizes from DN 10 to DN 100 used to transfer cryogenic fluids at temperatures ranging from −270 to 65 °C. These hoses are commonly designed and tested to satisfy the rated pressure of 40 bar, but a maximum operating pressure is not established. Although this document addresses fittings and couplings, they are also subject to other dedicated standards. The corresponding European standard EN 12434 [311] applies to equipment of identical sizes operating under the same conditions. In contrast, the latter document indicates the maximum operating pressure of the flexible hoses (i.e., 80 bar). In addition, the standard EN 13371 [312] shows the requirements for designing, manufacturing, and testing couplings for temporary connecting flexible hoses to cryogenic vessels. It applies to equipment of the same size and operating in the same temperature range as the hoses but does not cover any permanent connections (e.g., flanges).

The standard ISO 24490 [250] indicates the minimum requirements for designing, manufacturing, testing, and installing centrifugal and reciprocating pumps for cryogenic service (i.e., below –10 °C). This document aims to meet the performance requirements, while guaranteeing the safety and reliability of this equipment. The operation and maintenance procedures are outside the scope of this document and covered by dedicated standards. The European standard EN 13275 [250] applies to the same equipment.

The standard ISO 28921 [313][314] establishes the criteria for the design and material selection, the fabrication and testing requirements for gate, globe, ball, and butterfly valves used as isolation and check valves operating at temperatures from –50 to –196 °C. The second part provides the testing procedures to verify the performance of these isolation valves when exposed to cold vapors. The performance of the actuators is not evaluated unless they are an integral part of the valve. The components covered by these documents have nominal sizes ranging from DN 10 to DN 1800, pressure designations from PN 16 to PN 400, and class from 150 to 2500 (indicating the maximum pressure and temperature the valve can safely handle). This document does not apply to the control valves used with cryogenic vessels (designed in accordance with ISO 21011) and the pressure relief devices for low-temperature applications (following the standard ISO 21013).

Table 20 collects the latest international and European standards for liquid hydrogen storage tanks' ancillary equipment. It covers various component, including valves, pressure relief devices, flexible hoses, couplings, and cryopumps.

Table 20: Standards for the ancillary components of liquid hydrogen storage tanks

Standard	Year	Title	Scope	Equipment type
CGA G-5.5	2021	Standard for hydrogen vent systems	Design criteria Methods for calculating the vented mass flow Installation, inspection, maintenance, and repair procedures	Hydrogen venting systems

			Safety measures	
EIGA 24/18	2018	Vacuum-insulated cryogenic storage tank systems pressure protection devices		Pressure protection devices for vacuum-insulated cryogenic storage tanks
ISO 21011	2008	Cryogenic vessels – Valves for cryogenic service	Design criteria Fabrication and testing requirements	Valves with DN 150 or lower for cryogenic service (temperatures below –40 °C) connected to a vacuum-insulated vessel
ISO 21013-1	2024	Cryogenic vessels – Pressure-relief accessories for cryogenic service – Part 1: Reclosable pressure-relief valves	Design criteria Fabrication and testing requirements	Reclosable pressure-relief valves with DN 150 or lower designed to relieve single-phase cryogenic fluids (temperatures below –10 °C)
ISO 21013-2	2018	Cryogenic vessels – Pressure-relief accessories for cryogenic service – Part 2: Non-reclosable pressure-relief valves	Design criteria Fabrication and testing requirements	Bursting discs and buckling-pin devices with DN 200 or lower designed to relieve single-phase cryogenic fluids (temperatures below –10 °C)
ISO 21013-3	2016	Cryogenic vessels – Pressure-relief accessories for cryogenic service – Part 3: Sizing and capacity determination	Sizing criteria Methods for calculating the vented mass flow	Pressure relief valves, bursting discs, and buckling-pin devices for cryogenic service Vacuum and non-vacuum-insulated vessels with insulation functioning at full potential, partially functioning, and totally lost with or without fire engulfment Vacuum-insulated vessels for fluids with saturation temperature below –198 °C at 1 bar with air or nitrogen in the insulation with or without fire engulfment
ISO 21013-4	2019	Cryogenic vessels – Pilot operated pressure relief devices – Part 4: Pressure-relief accessories for cryogenic service	Design criteria Fabrication requirements Testing requirements	Pilot-operated pressure-relief valves with DN 300 or lower designed to relieve single-phase cryogenic fluids (temperatures below –10 °C)
ISO 21012	2024	Cryogenic vessels – Hoses	Design criteria Fabrication , testing, and marking requirements	Non-insulated flexible hoses for the transfer of cryogenic fluids (temperatures ranging from –270 to 65 °C) with

				sizes from DN 10 to DN 100
ISO 24490	2016	Cryogenic vessels – Pumps for cryogenic service	Design criteria Fabrication, testing, and installation requirements	Centrifugal and reciprocating pumps for cryogenic service (temperatures below –10 °C)
ISO 28921-1	2022	Industrial valves – Isolating valves for low-temperature applications – Part 1: Design, manufacturing and production testing	Design criteria Material selection Fabrication and testing requirements	Isolation and check valves (gate, globe, ball, and butterfly valves) for cryogenic service (temperatures from –50 to –196 °C) with sizes from DN 10 to DN 1800, pressure designations from PN 16 to PN 400, and class from 150 to 2500
ISO 28921-2	2015	Industrial valves – Isolating valves for low-temperature applications – Part 2: Type testing	Procedures to verify the performance at cryogenic temperatures	Isolation and check valves (gate, globe, ball, and butterfly valves) for cryogenic service (temperatures from –50 to –196 °C) with sizes from DN 10 to DN 1800, pressure designations from PN 16 to PN 400, and class from 150 to 2500
EN 1626	2008	Cryogenic vessels – Valves for cryogenic service	Design criteria Fabrication and testing requirements	Valves with DN 150 or lower for cryogenic service (temperatures below –10 °C) connected to a vacuum-insulated vessel
EN 13648-1	2008	Cryogenic vessels – Safety devices for protection against excessive pressure – Part 1: Safety valves for cryogenic service	Design criteria Fabrication requirements Testing requirements	Pressure-relief valves with maximum size of DN 25 (type A) and DN 100 (type B) and pressure designation of PN 40, capable of relieving single-phase cryogenic fluids (temperatures below –10 °C)
EN 13648-2	2002	Cryogenic vessels – Safety devices for protection against excessive pressure – Part 2: Bursting disc safety devices for cryogenic service	Design criteria Fabrication and testing requirements	Bursting discs with maximum size of DN 100, capable of relieving single-phase cryogenic fluids (temperatures below –10 °C)
EN 13648-3	2002	Cryogenic vessels – Safety devices for protection against excessive pressure – Part 3: Determination of	Sizing criteria Methods for calculating the vented mass flow	Pressure relief valves and bursting discs for cryogenic service

		required discharge, capacity and sizing		Vacuum and non-vacuum-insulated vessels with insulation functioning at full potential, partially functioning, and totally lost with or without fire engulfment
EN 12434	2000	Cryogenic vessels – Cryogenic flexible hoses	Design criteria Fabrication, testing, and marking requirements	Non-insulated flexible hoses for the transfer of cryogenic fluids (temperatures ranging from –270 to 65 °C) with sizes from DN 10 to DN 100 and maximum operating pressure of 80 bar
EN 13275	2000	Cryogenic vessels – Pumps for cryogenic service	Design criteria Fabrication and testing requirements Installation requirements	Centrifugal and reciprocating pumps for cryogenic service (temperatures below –10 °C)

6.3 Standards for materials selection for cryogenic service

Defining compatibility requirements, minimum thermal and mechanical performances, and cleanliness levels for LH_2 handling equipment is crucial for guaranteeing their utilization under safe conditions. In addition, the resistance to cryogenic spillages should be covered by dedicated codes and standards.

The guideline ASTM C1774 [315] indicates how to measure insulation systems' thermal properties and heat flux under cryogenic conditions in a laboratory environment. The methods shown are suitable for highly anisotropic materials, such as MLI. The temperatures covered by this standard range from –269 to 127 °C, and the pressure ranges from approximately 10^{-9} to 1.3 bar. In addition, this guide specifies the design requirements to construct and operate test apparatuses. The standard ASTM C740 [316] covers the use of MLI systems operating at a maximum temperature of 177 °C and showing a thermal conductivity lower than 0.007 W/m·K. This document specifies the performance requirements, typical applications, manufacturing methods, material specifications, and safety considerations.

The EIGA guideline TB 11/114 [317] provides indications to limit the risks of failure due to differential thermal expansions between cryogenic tanks and piping and the occurrence of brittle fracture due to the impingement of cryogenic fluids onto the tank's outer jacket.

The international standard ISO 21010 [318] indicates the compatibility requirements (e.g., the chemical resistance) for storage vessels exposed to cryogenic gases and liquids. It establishes the testing methods to assess the material compatibility with oxygen and oxygen-enriched atmospheres that could form after air condensation. This document focuses on metallic and non-metallic materials commonly used for low-temperature applications, including structural and insulating materials. This standard does not cover the mechanical properties of steels in

cryogenic conditions. The European standard EN 1797 [319] has the same purpose and applies to liquid nitrogen, neon, hydrogen, and helium.

The standard ISO 21014 [320] defines practical methods for determining the thermal performance of cryogenic storage vessels in open and closed systems. Nevertheless, it does not indicate the minimum requirements for insulation systems, which can be specified during the component design. The European standard EN 12213 [321] aligns with the previous standard and has the same field of application.

ISO 21028-1 [322] specifies the toughness requirements for metallic materials exposed to temperatures below –80 °C, while ISO 21028-2 [322] applies to temperatures ranging from −20 to −80 °C. The former standard does not apply to unalloyed steels and cast materials since they are generally not used for cryogenic applications. The latter applies to fine-grain and low-alloyed steels with specified yield strength lower than 460 MPa, aluminum alloys, copper alloys, and austenitic stainless steels. The European standard EN 1252-1 [323] overlaps with ISO 21028-1 but does not apply to LNG tanks. EN 1252-2 [324] covers the same applications of ISO 21028-2.

ISO 23208 [325] establishes the minimum requirements for the cleanliness of the surfaces of tanks directly exposed to cryogenic fluids under any operating conditions. It indicates the maximum acceptable particle contamination to minimize the risk of malfunctioning and avoid the risk of ignition due to air condensation on the tank surface. The European standard EN 12300 [326] provides similar indications.

The International Organization for Standardization developed several standards for determining the resistance of cryogenic spillage protection systems (CSP) installed on carbon steel and exposed to cryogenic releases. ISO 20088-1 [327] is dedicated to liquid spillages and applicable to CPSs in contact with cryogenic fluids. As a reference, liquid nitrogen (nonflammable and with a low boiling point) is used for the experiments. ISO 20088-2 [328] is used to assess the resistance of CSP to vapors generated from cryogenic releases. This standard does not apply to high-pressure cryogenic liquid releases. Finally, ISO 20088-3 [329] focuses on jets resulting from pressurized releases of cryogenic fluids. The tests are conducted with liquid nitrogen at 8 bar, but the indications apply to LNG and LH_2. The loss of containment of an overpressurized LH_2 storage tank can cause a gaseous release with elevated momentum and extremely low temperature that can compromise the functionality of the CPS system.

Table 21 summarizes the standards related to the material compatibility and the evaluation of thermal and mechanical performances of structural and insulating materials for cryogenic service.

Table 21: Standards regarding the material compatibility, insulation performance, toughness and cleanliness requirements for liquid hydrogen handling equipment

Standard	Year	Title	Scope	Equipment type
ASTM C1774	2024	Standard Guide for Thermal Performance Testing of Cryogenic Insulation Systems	Methods for measuring thermal performance and heat flux Guidelines to construct and	Insulation materials for cryogenic service exposed to temperatures from –269 to 127 °C and the pressure from 10^{-9} to 1.3 bar

			operate test apparatuses	
ASTM C740	2019	Standard Practice for Evacuated Reflective Insulation In Cryogenic Service	Performance requirements, applications, manufacturing methods, material specifications, and safety considerations	MLI systems for cryogenic service operating at a maximum temperature of 177 °C and with thermal conductivity lower than 0.007 W/m·K
EIGA TB 11/114	2014	Recommendations for the Prevention of Brittle failure of the Outer Jacket of Vacuum Insulated Cryogenic Storage Tanks	Guidelines to prevent failures due to brittle fracture	Vacuum-insulated cryogenic storage tanks
ISO 21010	2017	Cryogenic vessels – Gas/material compatibility	Material compatibility requirements Testing methods to assess the compatibility with oxygen and oxygen-enriched atmospheres	Metallic and non-metallic materials for tanks and insulation systems for cryogenic applications
ISO 21014	2022	Cryogenic vessels – Cryogenic insulation performance	Testing methods to determine the thermal performance of insulation systems	Insulation systems for cryogenic applications
ISO 21028-1	2016	Cryogenic vessels – Toughness requirements for materials at cryogenic temperature – Part 1: Temperatures below -80 °C	Toughness requirements for materials used at temperatures below –80 °C	Fine-grain and low-alloyed steels with specified yield strength lower than 460 MPa, aluminum alloys, copper alloys, and austenitic stainless steels
ISO 21028-2	2018	Cryogenic vessels – Toughness requirements for materials at cryogenic temperature – Part 2: Temperatures between -80 °C and -20 °C	Toughness requirements for materials used at temperatures between –80 and –20 °C	Fine-grain and low-alloyed steels with specified yield strength lower than 460 MPa, aluminum alloys, copper alloys, and austenitic stainless steels
ISO 23208	2020	Cryogenic vessels – Cleanliness for cryogenic service	Requirements for the cleanliness of the surfaces directly exposed to cryogenic fluids	Storage tanks for cryogenic applications
ISO 20088-1	2016	Determination of the resistance to cryogenic spillage of insulation materials – Part 1: Liquid phase	Testing methods to determine the resistance to cryogenic liquid releases	Cryogenic spillage protection systems installed on carbon steel and exposed to cryogenic liquid releases
ISO 20088-2	2020	Determination of the resistance to cryogenic	Testing methods to determine the	Cryogenic spillage protection systems installed

		spillage of insulation materials – Part 2: Vapour exposure	resistance to cryogenic vapor releases	on carbon steel and exposed to cryogenic gaseous releases
ISO 20088-3	2018	Determination of the resistance to cryogenic spillage of insulation materials – Part 3: Jet release	Testing methods to determine the resistance to cryogenic gaseous releases at high-pressure	Cryogenic spillage protection systems installed on carbon steel and exposed to cryogenic and pressurized gaseous releases
EN 1797	2001	Cryogenic vessels – Gas/material compatibility	Material compatibility requirements Testing methods to assess the compatibility with oxygen and oxygen-enriched atmospheres	Metallic and non-metallic materials for tanks and insulation systems for cryogenic applications
EN 12213	1998	Cryogenic vessels – Methods for performance evaluation of thermal insulation	Testing methods to determine the thermal performance of insulation systems	Insulation systems for cryogenic applications
EN 1252-1	1998	Cryogenic vessels – Materials – Part 1: Toughness requirements for temperatures below -80 °C	Toughness requirements for materials used at temperatures below –80 °C	Fine-grain and low-alloyed steels with specified yield strength lower than 460 MPa, aluminum alloys, copper alloys, and austenitic stainless steels
EN 1252-2	2001	Cryogenic vessels – Materials – Part 2: Toughness requirements for temperatures between -80°C and -20°C	Toughness requirements for materials used at temperatures between –80 and –20 °C	Fine-grain and low-alloyed steels with specified yield strength lower than 460 MPa, aluminum alloys, copper alloys, and austenitic stainless steels
EN 12300	2006	Cryogenic vessels – Cleanliness for cryogenic service	Requirements for the cleanliness of the surfaces directly exposed to cryogenic fluids	Storage tanks for cryogenic applications

6.4 Standards for large-scale storage tanks for refrigerated liquified gases

Large-scale LH_2 storage tanks are currently not commercially available. As a result, the design and operational standards for refrigerated liquified gases (RLGs) storage are often adapted or referenced when dealing with LH_2. These standards are not optimized for hydrogen's unique properties, such as its higher diffusivity and lower storage temperature compared to other cryogenic fluids (e.g., LNG, LN_2 or LOX). Therefore, even if the standards for designing and operating large-scale LNG tanks provide a starting point, they cannot be directly applied on hydrogen systems. This underscores the need for further research and development.

The European standard EN 14620 is the technical specification for vertical, cylindrical tanks built aboveground. These large-scale tanks, whose primary liquid container is made of steel and secondary can be made of steel or concrete, are designed to store two-phase fluids with a boiling point below ambient temperature. The maximum design pressure of the tank is 0.5 barg, and the operating temperatures are between 0 and −196 °C. These tanks can store large quantities of refrigerated liquified gases, such as LNG, LPG, ammonia, nitrogen, oxygen, or argon. EN 14620-1 [32] indicates the system concept, selection, and general design considerations. In case of a conflict between the general requirements and the fluid-specific indications in other parts of the standard, the specific requirements prevail. EN 14620-2 [33] lays down the general materials, design, construction, and installation requirements for the metallic components of RLG storage tanks, while EN 14620-3 [34] is dedicated to concrete components. In addition, EN 14620-4 [35] addresses the requirements for the insulating materials commonly used in these storage tanks. The insulation system must maintain the boil-off below a specific limit, maintain the tank's outer wall at ambient temperature to prevent air condensation and icing, and limit the cool-down of the tank's foundations to avoid damage by frost heave. General guidance on selecting the proper insulation materials is provided. Finally, EN 14620-5 [36] specifies the requirements for testing, drying, purging, and cooling down the RLG storage tanks. Unlike Part 1, the other four parts of this standard cover a narrower range of operating temperatures (i.e., from 0 to –165 °C). In general, EN 14620 specifies the minimum performance requirements for the tank system, its foundation, and protection systems. It covers all the components permanently attached to the tank and located within the liquid or vapor, outside, inside, or between the two walls. Still, it does not address any ancillary components (e.g., cryopumps, valves, instrumentation, walkaways, platforms, and external pipe supports). Moreover, it does not cover any specifications for the operating procedures of these systems.

Table 22 collects the latest European standards for vertical, cylindrical tanks for storing refrigerated liquified gases at pressures slightly higher than atmospheric.

Table 22: Standards for vertical cylindrical, flat-bottomed tanks for the storage of refrigerated liquefied gases

Standard	Year	Title	Scope	Equipment type
EN 14620-1	2024	Design and manufacture of site built, vertical, cylindrical, flat-bottomed tank systems for the storage of refrigerated, liquefied gases with operating temperatures between 0 °C and -196 °C - Part 1: General	General design criteria Functioning principles	Vertical cylindrical, flat-bottomed tanks for the storage of refrigerated liquefied gases at temperatures between 0 and –196 °C and maximum pressure of 0.5 barg
EN 14620-2	2006	Design and manufacture of site built, vertical, cylindrical, flat-bottomed steel tanks for the storage of refrigerated, liquefied gases with operating temperatures between 0 °C and -165 °C - Part 2: Metallic components	Materials, design, construction, and installation requirements	Metallic components of vertical cylindrical, flat-bottomed tanks for the storage of refrigerated liquefied gases at temperatures between 0 and –165 °C and maximum pressure of 0.5 barg
EN 14620-3	2006	Design and manufacture of site built, vertical, cylindrical,	Materials, design, construction, and	Concrete components of vertical cylindrical, flat-

		flat-bottomed steel tanks for the storage of refrigerated, liquefied gases with operating temperatures between 0 °C and -165 °C - Part 3: Concrete components	installation requirements	bottomed tanks for the storage of refrigerated liquefied gases at temperatures between 0 and –165 °C and maximum pressure of 0.5 barg
EN 14620-4	2006	Design and manufacture of site built, vertical, cylindrical, flat-bottomed steel tanks for the storage of refrigerated, liquefied gases with operating temperatures between 0 °C and -165 °C - Part 4: Insulation components	Materials, design, construction, and installation requirements Material selection guidelines	Insulating components of vertical cylindrical, flat-bottomed tanks for the storage of refrigerated liquefied gases at temperatures between 0 and –165 °C and maximum pressure of 0.5 barg
EN 14620-5	2006	Design and manufacture of site built, vertical, cylindrical, flat-bottomed steel tanks for the storage of refrigerated, liquefied gases with operating temperatures between 0 °C and -165 °C - Part 5: Testing, drying, purging and cool-down	Testing, drying, purging, and cooling down procedures	Vertical cylindrical, flat-bottomed tanks for the storage of refrigerated liquefied gases at temperatures between 0 and –196 °C and maximum pressure of 0.5 barg

6.5 Standards for vacuum insulation panels

A limited number of international, European, and national standards indicate the minimum requirements for vacuum-insulation panels. The standard ISO 16478 [330] defines the requirements for VIPs with silica or glass fiber cores used as insulation systems for buildings, indicating the product properties, performances, testing methods, and guidelines for conformity evaluation and labeling. In addition, it defines the methodology to determine the aging factor for such systems and evaluate the influence of thermal bridges at the edges. Nevertheless, this document does not indicate any installation and application requirements and does not apply to industrial applications. As a result, ISO 16478 can only be used as a general indication rather than as a reference for designing insulation systems for liquid hydrogen storage tanks.

The European standard EN 17140 [331] specifies the characteristics of vacuum insulation panels for building applications (i.e., from –40 to 70 °C). This document defines the technical requirements, testing methods, inspection rules, marking, packaging, transportation, and storage procedures, and techniques for evaluating the aging of such systems. Unlike ISO 16478, it applies to all types of VIPs, regardless of the core material or type of envelope, with or without desiccants and with or without evacuation valves. Nevertheless, it does not cover any industrial applications. In addition, it does not consider VIPs with thermal conductivity higher than 2 $W/m^2 \cdot K$, those containing getters, and those with protective layers.

Finally, the Chinese standard GB/T 37608 [332] serves the same purpose as EN 17140 but also applies to VIPs in industrial applications and under operating conditions other than from –40 to 70 °C. Therefore, this document is the only potentially applicable standard to VIPs used as super-insulating materials for liquid hydrogen storage systems.

Table 23 summarizes the latest standards for vacuum insulation panels, highlighting their scopes and fields of applicability.

Table 23: Standards for vacuum insulation panels

Standard	Year	Title	Scope	Equipment type
ISO 16478	2023	Thermal insulation products – Vacuum insulation panels (VIPs) – Specification	Technical requirements Testing methods to evaluate the ageing effect Testing method to evaluate thermal bridges and edges Guidelines for conformity evaluation and labeling	Vacuum insulation panels with silica or glass fiber cores used for building applications
EN 17140	2020	Thermal insulation products for buildings – Factory-made vacuum insulation panels (VIP) – Specification	Technical requirements Testing methods to evaluate the ageing effect Inspection, marking, packaging, transportation, and storage procedures	Vacuum insulation panels used for building applications (i.e., from –40 to 70 °C) without getters and protective layers and with thermal conductivity lower than 2 $W/m^2 \cdot K$
GB/T 37608	2019	Vacuum insulation panels (VIP)	Technical requirements Testing methods to evaluate the ageing effect Inspection, marking, packaging, transportation, and storage procedures	Vacuum insulation panels used for building and industrial applications

7 Summary and conclusions

Deliverable D1.1 offers a comprehensive overview of large-scale liquid hydrogen storage tank technologies, their applications, technical characteristics, safety aspects, and considerations related to circularity and sustainability, along with the associated standards and regulations. The report emphasizes the critical role of efficient and safe LH_2 storage in transitioning to a sustainable hydrogen economy while highlighting the significant technological challenges associated with handling fuels under cryogenic conditions. The information collected in this document should inform the other work packages of the NICOLHy project, supporting their research toward more efficient, cost-effective, and safer large-scale storage systems for LH_2. For clarity and conciseness, the following section summarizes the main findings of the report and the resulting considerations.

7.1 Applications of large-scale LH_2 storage tanks

Large-scale liquid hydrogen storage tank applications can be broadly categorized into stationary and mobile (primarily referring to the maritime sector). Large-scale LH_2 storage tanks are essential for fueling rockets at launch complexes nowadays. Most of these tanks exhibit the conventional spherical, double-walled design and are insulated with perlite or hollow glass microspheres under high vacuum. These examples highlight the long-term reliability of some systems (e.g., those located at the Tanegashima Space Center) but also demonstrate the potential for insulation failure (e.g., perlite voids leading to increased boil-off in the tank at the Kennedy Space Center), prompting research into more robust insulation materials. The analysis covers newer and larger tanks under construction, incorporating more complex and integrated insulation systems to achieve zero boil-off storage. Large LH_2 tanks are also crucial for the energy sector, though specific examples are limited beyond discussing planned systems. This demonstrates the growing need for large-scale LH_2 storage beyond space applications.

Maritime transport plays a crucial role in the large-scale distribution of LH_2. Suiso Frontier remains the first and only LH_2 carrier currently operating. This maritime vessel uses a cylindrical, double-walled tank with multi-layer insulation under high vacuum and a boil-off condensation system. Several ongoing projects aim to develop large-scale naval vessels, including ships with capacities comparable to conventional LNG carriers. They will utilize new insulation systems to mitigate boil-off and incorporate dual-fuel propulsion systems. The development of large-scale LH_2 carriers emphasizes the increasing importance of maritime transport for long-distance delivery and underscores the need for further research in this sector.

7.2 Description and design of LH_2 storage tanks

The design requirements for LH_2 tanks show a clear trend toward increased reliance on stationary large-scale storage for industrial and energy use and maritime transport for long-distance delivery. In particular, the design of LH_2 storage tanks presents unique challenges due to the cryogenic temperatures and the exposure to hydrogen-rich environments. Despite the low pressure of the storage tanks during normal operations, there is no guarantee that these favorable conditions will be maintained in off-design or abnormal situations. Ad-hoc

design principles can ensure structural integrity and operational safety across various applications (stationary spherical LH_2 tanks, cylindrical flat-bottom LNG tanks, and maritime vessels). Spherical tanks are highlighted for their favorable thermal performance and stress distribution, although cylindrical designs are also considered, especially for large-scale applications. Each configuration presents advantages and disadvantages based on manufacturing cost and space requirements.

Careful operational procedures during filling and draining are crucial to managing thermal stresses, preventing cavitation, and maintaining safe pressure limits. Regular inspections allow tank integrity to be assessed and potential issues to be prevented. Additional safety measures are required to address the flammable nature of LH_2.

Material selection is critical due to the extremely low temperatures of liquid hydrogen. High yield strength, toughness, and ductility must be guaranteed at the normal operating conditions of LH_2 storage equipment. Additionally, low hydrogen permeability is crucial to prevent leakages and fuel losses. Austenitic stainless steels (primarily grades 304 and 316) are the most common choice due to their lack of ductile-to-brittle transition at cryogenic temperatures. However, the properties of 9 % nickel ferritic steels appear promising, as well as those of other alloys. These materials are potentially cost-effective alternatives for large-scale applications. The effects of hydrogen embrittlement on material properties should be thoroughly examined, focusing on factors such as temperature, hydrogen pressure, and microstructure.

7.3 Description of the thermal insulation systems

Thermal insulation systems are categorized as passive thermal barriers or active cooling systems. Passive systems rely on high-performance materials to minimize heat transfer and prevent boil-off, while active systems utilize energy-consuming components to remove heat and maintain cryogenic temperatures actively. Passive approaches commonly employ perlite, aerogel, spray-on foam insulation, glass microspheres, multi-layer insulation, and vacuum insulation panels.

Perlite’s thermal conductivity is highly dependent on the vacuum level. Under medium vacuum, the thermal conductivity is low but increases significantly at ambient pressure. Mechanically, perlite is prone to settling and compaction, especially under vibration or cyclic thermal loading, leading to reduced insulation performance over time. Perlite demonstrates good fire resistance, especially in slower-burning scenarios; however, high-heat exposure can degrade the material.

Aerogels exhibit exceptionally low thermal conductivity at low temperatures, even under relatively low vacuum conditions. This superior performance is linked to its unique nano-porous structure. Mechanically, aerogels are inherently fragile and brittle due to their low density and high porosity, limiting their load-bearing capacity. Aerogels are potentially fragile and need robust structural support, especially for mobile applications. While they generally demonstrate good fire resistance, the effect of other hazards needs further investigation.

The thermal performance of spray-on foam insulation depends on pressure and temperature. The thermal conductivity exhibits the lowest values under high vacuum conditions. However, performance degrades over time due to environmental exposure and moisture uptake. SOFI’s mechanical properties vary significantly depending on the type of foam, with closed-cell foams

generally showing superior strength and stability. Safety concerns include flammability, which can be mitigated through flame-retardant additives, and the risk of poor adhesion to substrates.

Glass microspheres have very low thermal conductivity, especially under high vacuum, making them ideal for cryogenic applications. Their mechanical properties vary depending on the type (solid, hollow, porous), size, and composition. Generally, they possess relatively high compressive strength and are resistant to settling and compaction, even under dynamic conditions. From a safety perspective, they demonstrate excellent fire resistance and produce minimal smoke and toxic gases during combustion.

Multi-layer insulation achieves exceptionally low thermal conductivity in high-vacuum environments due to the multiple layers of reflective material separated by vacuum spaces. However, its performance is sensitive to pressure; even minor vacuum loss or mechanical compression significantly increases thermal conductivity. Depending on the number and density of layers, MLI systems are relatively robust against external shock and vibration. Safety considerations focus on the risk of vacuum loss. MLI exhibits low fire resistance compared to perlite and other superinsulation materials for cryogenic applications.

Vacuum insulation panels achieve exceptionally low thermal conductivity thanks to combining a highly porous core material (often fumed silica or other low-conductivity materials) and a gas-tight envelope, maintaining a high vacuum. This minimizes conductive, convective, and radiative heat transfer. However, their thermal performance is significantly affected by internal pressure and moisture content. Edge effects and compression can also reduce thermal effectiveness. VIPs exhibit relatively low compressive strength and are sensitive to damage from external forces. The envelope material's strength and gas permeability influence mechanical performance and long-term durability. Safety considerations for VIPs center on the potential consequences of vacuum loss. While the core material often possesses good fire resistance, the envelope's integrity under fire conditions is not guaranteed. Additionally, the potential damage from impacts or vibrations needs careful assessment.

Active cooling systems, primarily used in aerospace applications, incorporate cryocoolers, heat exchangers, and circulating pumps to remove heat and achieve zero boil-off. A hybrid approach, utilizing vapor-cooled shields to leverage the sensible heat of boil-off gas, offers a pathway to enhance passive systems, particularly for large-scale storage.

7.4 Description and design of the ancillary components for LH_2 storage tanks

Various ancillary components are crucial to guarantee safe operations and efficient liquid hydrogen storage of transfer. They can be permanently attached to the storage tank or connected through flanges and joints, but in any case, they constitute an integral part of the LH_2 storage system. Cryogenic pumps are essential for transferring LH_2 between supply systems, storage tanks, and delivery terminals. Piston-driven cryopumps offer higher efficiency than diaphragm compressors (approximately 1.1 kWh/kg_{LH2} versus 3 kWh/kg_{H2}) thanks to the higher density of the liquid fuel. They enable rapid transfer operations. Nevertheless, managing cavitation and optimizing valve dynamics can be difficult, even though crucial to minimizing boil-off losses.

Ball, butterfly, and wedge gate valves can be either opened or closed, thus allowing or impeding the connection between the storage tank and transfer lines. Globe, needle, control,

and orbit valves are essential for controlling and managing the LH_2 flow rate. Pressure relief devices allow the tank's overpressurization to be avoided and the systems to operate safely. Safety valves are characterized by a rapid and complete opening at a set pressure, while pressure relief valves exhibit a gradual opening proportional to pressure increase. Pressure relief systems typically include resealable safety valves (Categories A and B, for continuous venting and emergency relief, respectively). Burst discs are non-resealable and generally considered a secondary safety measure. The optimal maintenance strategy for such equipment depends on the valve type and material.

Transferring LH_2 requires pipes with effective thermal insulation to minimize boil-off. Multi-layer vacuum insulation exhibits superior performance compared to other insulating materials, particularly where volume occupation is a constraint. In addition, flexible hoses can be used to load and unload LH_2 carriers while minimizing evaporation. Two main types of hoses are currently available for cryogenic service: corrugated metal hoses and cryogenic composite hoses. The former type is a mature technology with high reliability but is heavier and less flexible. The latter type is lightweight and more flexible but has challenges related to brittleness at low temperatures and hydrogen permeation.

As a general remark, proper design, material selection, and maintenance of these ancillary components are critical for ensuring the safe and efficient operation of LH_2 storage systems, highlighting the importance of adhering to relevant safety standards.

7.5 Standards for LH_2 storage

The regulatory framework for LH_2 storage is analyzed, emphasizing the critical need for comprehensive and up-to-date standards to ensure the safe design, installation, operation, inspection, and maintenance of such systems. This section identifies gaps in current standards, specifically for large-scale LH_2 tanks and certain ancillary components, emphasizing the need for further research and standardization efforts.

International and European standards and those from the Compressed Gas Association and the European Industrial Gases Association are highlighted as key resources. Standardization committees (e.g., ISO/TC 220, CEN/TC 268, and EIGA/WG-6) are fundamental in establishing best practices for liquid hydrogen storage systems' safety and operational efficiency. Specific standards outline the minimum design and performance requirements for vacuum-insulated LH_2 tanks, including dimensions, materials, insulation, and maintenance procedures. Nevertheless, these standards do not address transportable tanks, installation, or emergency procedures. Additional standards address the design and operation of ancillary equipment (e.g., valves, pressure relief devices, hoses, and cryopumps), indicating the design, testing, and maintenance requirements for each type of equipment.

Another important aspect is the selection of suitable materials for cryogenic service. ASTM C1774 and C740 indicate the methods of measuring thermal properties and performance, emphasizing the need to account for material anisotropy in composite insulation systems. The EIGA guideline TB 11/114 and the standard ISO 21010 offer guidance on material compatibility and prevention of brittle fracture at cryogenic temperatures.

The document notes the absence of specific standards for large-scale LH_2 storage tanks, emphasizing the need to adapt or reference existing guidelines for refrigerated liquefied gases.

EN 14620 is a relevant document for large-scale cylindrical storage tanks, but its limitations regarding hydrogen's unique properties are notable.

International, European, and national standards (e.g., ISO 16478, EN 17140, GB/T 37608) for vacuum insulation panels are primarily applicable to buildings but not industrial plants. In addition, these standards cover operating temperatures far higher than those of liquid hydrogen storage systems. Therefore, considering the purposes of the NICOLHy project, the rigorous application of these documents is not a viable option.

8 References

[1] International Energy Agency, “World Energy Outlook 2023,” 2023. [Online]. Available: https://www.iea.org/reports/world-energy-outlook-2023.

[2] NIST, “NIST Chemistry WebBook,” *NIST Standard Reference Database Number 69*, 2023. https://webbook.nist.gov/chemistry/ (accessed Feb. 22, 2023).

[3] Clean Hydrogen JU, “NICOLHy - Novel Insulation Concepts For Liquefied Hydrogen Storage Tanks,” 2024. https://nicolhy.eu/.

[4] L. Yin, H. Yang, and Y. Ju, “Review on the key technologies and future development of insulation structure for liquid hydrogen storage tanks,” *Int. J. Hydrogen Energy*, vol. 57, pp. 1302–1315, 2024, doi: 10.1016/j.ijhydene.2024.01.093.

[5] Japan Aerospace Exploration Agency, “Tanegashima Space Center,” 2024. https://global.jaxa.jp/about/centers/tnsc/.

[6] A. Naquash, N. Agarwal, and M. Lee, “A Review on Liquid Hydrogen Storage: Current Status, Challenges and Future Directions,” *Sustain.*, vol. 16, no. 18, 2024, doi: 10.3390/su16188270.

[7] J. E. Fesmire, J. P. Sass, Z. Nagy, S. J. Sojourner, D. L. Morris, and S. D. Augustynowicz, “Cost-Efficient Storage of Cryogens.” pp. 1–10, 2007.

[8] J. P. Sass, W. W. S. Cyr, T. M. Barrett, R. G. Baumgartner, J. W. Lott, and J. E. Fesmire, “Glass bubbles insulation for liquid hydrogen storage tanks,” *AIP Conf. Proc.*, vol. 1218, pp. 772–779, 2010, doi: 10.1063/1.3422430.

[9] J. E. Fesmire, S. D. Augustynowicz, Z. F. Nagy, S. J. Sojourner, and D. L. Morris, “Vibration and thermal cycling effects on bulk-fill insulation materials for cryogenic tanks,” *AIP Conf. Proc.*, vol. 823 II, no. April 2010, pp. 1359–1366, 2006, doi: 10.1063/1.2202556.

[10] J. P. Sass, J. E. Fesmire, Z. F. Nagy, S. J. Sojourner, D. L. Morris, and S. D. Augustynowicz, “Thermal Performance Comparison of Glass Mirospheres and Perlite Insulation Systems for Liquid Hydrogen Storage Tanks,” in *AIP Conference Proceedings*, 2008, pp. 1375–1382.

[11] J. Fesmire, A. Swanger, J. Jacobson, and W. Notardonato, “Energy efficient large-scale storage of liquid hydrogen,” *IOP Conf. Ser. Mater. Sci. Eng.*, vol. 1240, no. 1, p. 012088, 2022, doi: 10.1088/1757-899x/1240/1/012088.

[12] Kawasaki Heavy Industries Ltd., “CO2-free Hydrogen Energy Supply-Chain Technology Research Association Commences Operations —Multi-company effort takes a step toward the future of hydrogen energy,” 2016. .

[13] T. Ionomata, A. Hashimoto, S. Yamanouchi, K. Yamamoto, “Hydrogen Storage-Development of Liquefied Hydrogen Terminal,” 2021.

[14] A. Schiaroli, A. Campari, N. Paltrinieri, V. Cozzani, and F. Ustolin, “Consequence Analysis of a Bunkering Facility for Liquid Hydrogen Loading and Unloading,” in *Proceedings of the ASME 2024 43rd International Conference on Ocean, Offshore and Arctic Engineering*, 2024, pp. 1–10, doi: 10.1115/omae2024-126787.

[15] A. Campari, A. Schiaroli, A. Alvaro, F. Ustolin, V. Cozzani, and N. Paltrinieri, “Risk-Based Inspection and Maintenance of a Liquid Hydrogen Bunkering Facility,” in *Proceedings of the ASME 2024 43rd International Conference on Ocean, Offshore and Arctic Engineering*, 2024, pp. 1–9.

[16] Kawasaki Heavy Industries Ltd., “Kawasaki Completes Basic Design for World’s

Largest Class (11,200-cubic-meter) Spherical Liquefied Hydrogen Storage Tank," 2020. https://global.kawasaki.com/en/corp/newsroom/news/detail/?f=20201224_8018#:~:text=Tokyo%2C December.,world's largest of its kind.

[17] McDermott, "McDermott's CB&I Storage Solutions Completes Conceptual Design for World's Largest Liquid Hydrogen Sphere," 2021. https://www.mcdermott-investors.com/news/press-release-details/2021/McDermotts-CBI-Storage-Solutions-Completes-Conceptual-Design-for-Worlds-Largest-Liquid-Hydrogen-Sphere/default.aspx.

[18] McDermott, "Shell-Led Consortium Selected by DOE to Demonstrate Feasibility of Large-Scale Liquid Hydrogen Storage," 2021. Shell-Led Consortium Selected by DOE to Demonstrate Feasibility of Large-Scale Liquid Hydrogen Storage%0A.

[19] Kawasaki Heavy Industries Ltd., "Kawasaki Develops Cargo Containment System for Large Liquefied Hydrogen Carrier with World's Highest Carrying Capacity - AiP Obtained from ClassNK," 2021. https://global.kawasaki.com/en/corp/newsroom/news/detail/?f=20210506_9983.

[20] Kawasaki Heavy Industries Ltd., "Technological Development of Cargo Tank for Large Liquefied Hydrogen Carriers Completed," 2023. https://global.kawasaki.com/en/corp/newsroom/news/detail/?f=20230606_4159.

[21] J. Saul and H. Yang, "Korean Shipbuilder Sees Hydrogen Shipping Ready by 2025," *Reuters*, 2022. https://gcaptain.com/korean-shipbuilder-sees-hydrogen-shipping-ready-by-2025/.

[22] C-JOB, "New Class of Hydrogen Ship Design Will Revolutionize Renewables Market," 2024. https://c-job.com/new-class-of-hydrogen-ship-design-will-revolutionize-renewables-market/.

[23] J. Monteiro, L. Ribeiro, G. F. Pinto, B. Coutinho, and A. Baptista, "A Comparison of the Energy Expenditure in Different Storage Tank Geometries to Maintain H 2 in the Liquid State," *Energies*, vol. 17, no. 5557, pp. 1–17, 2024.

[24] Z. Wang and M. Walter, "Thermal performance of cylindrical and spherical liquid hydrogen tanks," *Int. J. Hydrogen Energy*, vol. 53, pp. 667–683, 2024, doi: 10.1016/j.ijhydene.2023.11.287.

[25] M. Taghavi, S. Sharma, and V. Balakotaiah, "International Journal of Heat and Mass Transfer Natural convection effects in insulation layers of spherical cryogenic storage tanks," *Int. J. Heat Mass Transf.*, vol. 220, no. March 2023, p. 124918, 2024, doi: 10.1016/j.ijheatmasstransfer.2023.124918.

[26] Y. Yu, F. Xie, M. Zhu, S. Yu, and Y. Li, "Design and Optimization of the Insulation Performance of a 4000 m3 Liquid Hydrogen Spherical Tank," *Processes*, vol. 11, no. 1778, pp. 1–20, 2023.

[27] A. M. Swanger, "World's Largest Liquid Hydrogen Tank Nearing Completion," 2022.

[28] Y. Ma, K. Zhu, Y. Li, and F. Xie, "Numerical investigation on chill-down and thermal stress characteristics of a LH2 tank during ground filling," *Int. J. Hydrogen Energy*, vol. 45, no. 46, pp. 25344–25356, 2020, doi: 10.1016/j.ijhydene.2020.06.056.

[29] N. Aeronautics, "Safety Standard for Hydrogen and Hydrogen Systems," *Natl. Aeronaut. Sp. Adm. NSS*, 2005.

[30] J. Wang, P. A. Webley, and T. J. Hughes, "Thermodynamic modelling of low fill levels in cryogenic storage tanks for application to liquid hydrogen maritime transport," *Appl. Therm. Eng.*, vol. 256, p. 124054, 2024, doi: 10.1016/j.applthermaleng.2024.124054.

[31] ASTM-C1774, “Standard Guide for Thermal Performance Testing of Cryogenic Insulation Systems,” *ASTM Int.*, vol. 13, no. Reapproved, pp. 1–23, 2013, doi: 10.1520/C1774-24.2.

[32] European Committee for Standardization, *EN 14620-1 - Design and manufacture of site built, vertical, cylindrical, flat-bottomed tank systems for the storage of refrigerated, liquefied gases with operating temperatures between 0 °C and -196 °C - Part 1: General*. 2024.

[33] European Committee for Standardization, *EN 14620-2 - Design and manufacture of site built, vertical, cylindrical, flat-bottomed steel tanks for the storage of refrigerated, liquefied gases with operating temperatures between 0 °C and -165 °C - Part 2: Metallic components*. 2006.

[34] European Committee for Standardization, *EN 14620-3 - Design and manufacture of site built, vertical, cylindrical, flat-bottomed steel tanks for the storage of refrigerated, liquefied gases with operating temperatures between 0 °C and -165 °C - Part 3: Concrete components*. 2006.

[35] European Committee for Standardization, *EN 14620-4 - Design and manufacture of site built, vertical, cylindrical, flat-bottomed steel tanks for the storage of refrigerated, liquefied gases with operating temperatures between 0 °C and -165 °C - Part 4: Insulation components*. 2006.

[36] European Committee for Standardization, *EN 14620-5 - Design and manufacture of site built, vertical, cylindrical, flat-bottomed steel tanks for the storage of refrigerated, liquefied gases with operating temperatures between 0 °C and -165 °C - Part 5: Testing, drying, purging and cool-down*. 2006.

[37] S. Barone and M. Sartori, “Seismic Isolation of LNG Storage Tabks in Italy with Curved Surface Sliders,” 2020.

[38] Kawasaki Heavy Industries Ltd., “Kawasaki Technical Review - Special Issue on Hydrogen Energy Supply Chain,” 2021.

[39] T. K. Drube, J. M. Gerlach, T. S. Leach, B. Vogel, and L. E. Klebanoff, “Exploring variations in the weight, size and shape of liquid hydrogen tanks for zero-emission fuel-cell vessels,” *Int. J. Hydrogen Energy*, vol. 80, no. April, pp. 1441–1465, 2024, doi: 10.1016/j.ijhydene.2024.06.420.

[40] A. N. Alkhaledi, S. Sampath, and P. Pilidis, “A hydrogen fuelled LH2 tanker ship design,” *Ships Offshore Struct.*, 2021, doi: https://doi.org/10.1080/17445302.2021.1935626.

[41] A. j. Colozza, *Hydrogen Storage for Aircraft*, no. September. 2002.

[42] A. Abe, M. Nakamura, I. Sato, H. Uetani, and T. Fujitani, “Studies of the large-scale sea transportation of liquid hydrogen,” *Int. J. Hydrogen Energy*, vol. 23, no. 2, pp. 115–121, Feb. 1998, doi: 10.1016/S0360-3199(97)00032-3.

[43] S. Kamiya, M. Nishimura, and E. Harada, “Study on Introduction of CO2 Free Energy to Japan with Liquid Hydrogen,” *Phys. Procedia*, vol. 67, pp. 11–19, Jan. 2015, doi: 10.1016/J.PHPRO.2015.06.004.

[44] J. R. Smith, S. Gkantonas, and E. Mastorakos, “Modelling of Boil-Off and Sloshing Relevant to Future Liquid Hydrogen Carriers,” *Energies*, vol. 15, no. 6, 2022, doi: 10.3390/en15062046.

[45] K. Maekawa, M. Takeda, Y. Miyake, and H. Kumakura, “Sloshing Measurements inside a Liquid Hydrogen Tank with External Heating-Type MgB2 Level Sensors during Marine Transportation by the Training Ship Fukae-Maru,” *Sensors*, vol. 18, p.

3694, 2018, doi: 10.3390/s18113694.

[46] A. Baeten and S. Baeten, “Numerical Analysis of Cryogenic H2 Sloshing Physics,” *Proc. Int. Offshore Polar Eng. Conf.*, pp. 2638–2645, 2023.

[47] Y. Qu, I. Noba, X. Xu, R. Privat, and J. N. Jaubert, “A thermal and thermodynamic code for the computation of Boil-Off Gas – Industrial applications of LNG carrier,” *Cryogenics (Guildf).*, vol. 99, no. September 2018, pp. 105–113, 2019, doi: 10.1016/j.cryogenics.2018.09.002.

[48] T. Banaszkiewicz *et al.*, “Liquefied natural gas in mobile applications—opportunities and challenges,” *Energies*, vol. 13, no. 21, pp. 1–35, 2020, doi: 10.3390/en13215673.

[49] M. Graczyk and T. Moan, “Structural response to sloshing excitation in membrane LNG tank,” *J. Offshore Mech. Arct. Eng.*, vol. 133, no. 2, pp. 1–9, 2010, doi: 10.1115/1.4001434.

[50] M. Miana, R. Legorburo, D. Díez, and Y. H. Hwang, “Calculation of Boil-Off Rate of Liquefied Natural Gas in Mark III tanks of ship carriers by numerical analysis,” *Appl. Therm. Eng.*, vol. 93, pp. 279–296, 2016, doi: 10.1016/j.applthermaleng.2015.09.112.

[51] J. W. Morris, “Steels: For Low Temperature Applications,” *Encyclopedia of Advanced Materials*. 1993.

[52] J. W. Morris and S. Mridha, “Cryogenic Steels,” *Ref. Modul. Mater. Sci. Mater. Eng.*, pp. 1–7, 2018, [Online]. Available: https://doi.org/10.1016/B978-0-12-803581-8.11227-5.

[53] W. M. Kimmel, N. S. Kuhn, R. F. Berry, and J. A. Newman, “Cryogenic Model Materials,” 2012, [Online]. Available: https://doi.org/10.2514/6.2001-757.

[54] D. A. Wigley, *Mechanical Properties of Materials at Low Temperatures*. New York, NY, USA: Springer, 1971.

[55] R. P. Walsh, “Tension and Compression Testing at Low Temperatures,” in *ASM Handbook Mechanical Testing and Evaluation*, H. Kuhn and D. Medlin, Eds. ASM International, 2000, pp. 164–171.

[56] G. Ventura and M. Perfetti, *Thermal Properties of Solids at Room and Cryogenic Temperatures*. 2014.

[57] R. Abbaschian, L. Abbaschian, and R. Reed-Hill, *Physical Metallurgy Principles*, 4th Editio. Cengage Learning, 2008.

[58] T. Flynn, *Cryogenic Engineering Revised and Expanded*, 2nd Editio. CRC Press Inc, 2004.

[59] S. Hany *et al.*, “Microstructural and mechanical properties of 9%Ni steels used for the construction of LNG storage tanks,” *Adv. Mater. Res.*, vol. 936, pp. 1953–1957, 2014, doi: 10.4028/www.scientific.net/AMR.936.1953.

[60] S. K. Kim, J. H. Kim, J. H. Kim, and J. M. Lee, “Numerical model for mechanical nonlinearities of high manganese steel based on the elastoplastic damage model,” *Metals (Basel).*, vol. 8, no. 9, 2018, doi: 10.3390/met8090680.

[61] C. R. Anoop *et al.*, *A review on steels for cryogenic applications*, vol. 10, no. 2. 2021.

[62] J. W. Morris, C. R. Krenn, D. Roundy, and M. L. Cohen, “Deformation of the limit of elastic stability,” *Mater. Sci. Eng. A*, vol. 309–310, pp. 121–124, 2001, doi: 10.1016/S0921-5093(00)01735-4.

[63] H. J. Kim, Y. H. Kim, and J. W. Morris, “Thermal mechanisms of grain and packet

refinement in a lath martensitic steel," *ISIJ Int.*, vol. 38, no. 11, pp. 1277–1285, 1998, doi: 10.2355/isijinternational.38.1277.

[64] Nickel Institute, "Low Temperature Properties of Nickel Alloy Steels," New York, NY, USA, 2021.

[65] S. K. Hwang and J. W. Morris, "The use of a boron addition to prevent intergranular embrittlement in Fe-12Mn," *Metall. Trans. A*, vol. 11, no. 7, pp. 1197–1206, 1980, doi: 10.1007/BF02668143.

[66] R. Palmer, S. Z. Xing, and E. W. Collings, "Structural Materials," in *Volume 2 of Cryogenic Materials, International Cryogenic Materials Conference*, 1988, pp. 557–565.

[67] A. M. El-Batahgy, A. Gumenyuk, S. Gook, and M. Rethmeier, "Comparison between GTA and laser beam welding of 9%Ni steel for critical cryogenic applications," *J. Mater. Process. Technol.*, vol. 261, no. June, pp. 193–201, 2018, doi: 10.1016/j.jmatprotec.2018.05.023.

[68] A. H. Eichelman and F. C. Hull, "The Effect of Composition on the Temperature of Spontaneous Transformation of Austenite to Martensite in 18-8 Type Stainless Steel," *Trans. ASM 45*, pp. 77–104, 1953.

[69] T. Angel, "Formation of Martensite in Austenitic Stainless Steel," *J. Iron Steel Inst.*, vol. 177, pp. 165– 174, 1954.

[70] B. T. Skoczeń, *Compensation Systems for Low Temperature Applications*. Berlin, Germany: Springer Berlin Heidelberg, 2004.

[71] M. Mc Guire, *Stainless Steels for Design Engineers*, 1st Editio. ASM International, 2008.

[72] P. G. Lapin, A. P. Gulyaev, and E. A. Ul'yanin, "The influence of the alloying elements on the properties of stainless maraging steels at low temperature," *Met. Sci. Heat Treat.*, vol. 14, no. 2, pp. 141–146, 1972, doi: 10.1007/BF00655765.

[73] R. P. Reed and T. Horiuchi, *Austenitic Steels at Low Temperatures*. Boston, MA: Springer US, 1983.

[74] A. Campari, F. Ustolin, A. Alvaro, and N. Paltrinieri, "A review on hydrogen embrittlement and risk-based inspection of hydrogen technologies," *Int. J. Hydrogen Energy*, vol. 48, no. 90, pp. 35316–35346, 2023, doi: 10.1016/j.ijhydene.2023.05.293.

[75] J. A. Shepic and F. R. Schwartzberg, "Fatigue Testing of Stainless Steel," in *Technical Reports-Materials Studies for Magnetic Fusion Energy Applications at Low Temperatures*, National Bureau of Standards, 1978, pp. 16–68.

[76] A. J. Nachtigall, "Strain-Cycling Fatigue Behavior of Ten Structural Metals Tested in Liquid Helium, Liquid Nitrogen, and Ambient Air," in *ASTM Properties of Materials for Liquefied Natural Gas Tankage*, ASTM International, 1975.

[77] R. J. Favor, D. N. Gideon, H. J. Grover, J. E. Hayes, and G. M. McClure, "WADD TR 61-132 - Investigation of Fatigue Behavior of Certain Alloys in the Temperature Range of Room Temperature to –423 °F," 1961.

[78] T. Yuri, T. Ogata, M. Saito, and Y. Hirayama, "Effect of welding structure and δ-ferrite on fatigue properties for TIG welded austenitic stainless steels at cryogenic temperatures," *Cryogenics (Guildf).*, vol. 40, no. 4, pp. 251–259, 2000, doi: 10.1016/S0011-2275(00)00033-3.

[79] R. L. Tobler and R. P. Reed, "Fatigue Crack Growth Resistance of Structural Alloys at Cryogenic Temperatures," *Adv. Cryog. Eng.*, pp. 82–90, 1978, doi: 10.1007/978-1-

4613-9853-0_7.

[80] R. Ogawa and J. W. Morris, “Fatigue Crack Growth Behavior in a Nitrogen-Strengthened High-Manganese Steel at Cryogenic Temperatures,” in *ASTM Fatigue at Low Temperatures*, 1985.

[81] T. Yokobori, I. Maekawa, Y. Tanabe, Z. Jin, and S. I. Nishida, “Fatigue Crack Propagation of 25Mn-5Cr-1Ni Austenitic Steel at Low Temperatures,” in *Fatigue at Low Temperatures*, West Conshohocken, PA: ASTM International, 1985, pp. 121–139.

[82] D. T. Read and R. P. Reed, “Fracture and strength properties of selected austenitic stainless steels at cryogenic temperatures,” *Cryogenics (Guildf).*, vol. 21, no. 7, pp. 415–417, 1981, doi: 10.1016/0011-2275(81)90175-2.

[83] J. H. Kim, S. W. Choi, D. H. Park, and J. M. Lee, “Charpy impact properties of stainless steel weldment in liquefied natural gas pipelines: Effect of low temperatures,” *Mater. Des.*, vol. 65, pp. 914–922, 2015, doi: 10.1016/j.matdes.2014.09.085.

[84] R. J. H. Wanhill, “Microstructural influences on fatigue and fracture resistance in high strength structural materials,” *Eng. Fract. Mech.*, vol. 10, no. 2, pp. 337–357, 1978, doi: 10.1016/0013-7944(78)90016-4.

[85] W. A. Logsdon, J. M. Wells, and R. Kossowsky, “Fracture Mechanics Properties ofAustenitic Stainless Steels for Advanced Cryogenic Applications,” in *Proceedings of the Second International Conference on Mechanical Behavior of Materials*, 1976, pp. 1283–1289.

[86] S. K. Dwivedi and M. Vishwakarma, “Hydrogen embrittlement in different materials: A review,” *International Journal of Hydrogen Energy*, vol. 43, no. 46. Elsevier Ltd, pp. 21603–21616, Nov. 15, 2018, doi: 10.1016/j.ijhydene.2018.09.201.

[87] D. E. Jiang and E. A. Carter, “Diffusion of interstitial hydrogen into and through bcc Fe from first principles,” *Phys. Rev. B - Condens. Matter Mater. Phys.*, vol. 70, no. 6, pp. 1–9, 2004, doi: 10.1103/PhysRevB.70.064102.

[88] A. Brocks Hagen and A. Alvaro, *Hydrogen Influence on Mechanical Properties in Pipeline Steel: State of the art*. 2020.

[89] Sandia National Laboratories, “Technical Database for Hydrogen Compatibility of Materials,” *H2 Tools*, 2023. https://h2tools.org/technical-database-hydrogen-compatibility-materials (accessed Jul. 14, 2023).

[90] ASTM International, *G229-00 Standard Practice for Slow Strain Rate Testing to Evaluate the Susceptibility of Metallic Materials to Environmentally Assisted Cracking*. 2000.

[91] ASTM International, *G142-98 Standard Test Method for Determination of Susceptibility of Metals to Embrittlement in Hydrogen Containing Environments at High Pressure , High Temperature, or Both*. 2022.

[92] A. Campari, F. Konert, O. Sobol, and A. Alvaro, “A comparison of vintage and modern X65 pipeline steel using hollow specimen technique for in-situ hydrogen testing,” *Eng. Fail. Anal.*, vol. 163, no. 108530, 2024.

[93] G. Rosenberg and I. Sinaiova, “Evaluation of hydrogen induced damage of steels by different test methods,” *Mater. Sci. Eng. A*, vol. 682, no. November 2016, pp. 410–422, 2017, doi: 10.1016/j.msea.2016.11.067.

[94] K. Christmann, “Hydrogen Adsorption on Metal Surfaces,” in *Atomistics of Fracture*, R. M. Latanision and J. R. Pickens, Eds. Boston: Springer US, 1983, pp. 363–389.

[95] J. A. Lee, “Hydrogen embrittlement NASA/TM-2016-218602,” 2016. doi:

10.1016/B978-044452787-5.00200-6.

[96] ASTM International, *ASTM E1820 - Standard Test Method for Measurement of Fracture Toughness*. 2018.

[97] International Organization for Standardization, *ISO 12135 - Metallic materials: Unified method of test for the determination of quasistatic fracture toughness*. 2021.

[98] International Organization for Standardization, *ISO 12108 - Metallic materials, Fatigue testing, Fatigue crack growth method*. 2018.

[99] ASTM International, *ASTM E 647-23 - Standard Test Method for Measurement of Fatigue Crack Growth Rates*. 2023.

[100] C. Borchers, T. Michler, and A. Pundt, “Effect of Hydrogen on the Mechanical Properties of Stainless Steels,” *Adv. Eng. Mater.*, vol. 10, no. 1–2, pp. 11–23, 2008, doi: 10.1002/adem.200700252.

[101] A. Campari, F. Ustolin, A. Alvaro, and N. Paltrinieri, “Inspection of hydrogen transport equipment: A data-driven approach to predict fatigue degradation,” *Reliab. Eng. Syst. Saf.*, vol. 251, p. 110342, 2024, doi: 10.1016/j.ress.2024.110342.

[102] Y. Ogawa, H. Matsunaga, J. Yamabe, M. Yoshikawa, and S. Matsuoka, “Fatigue limit of carbon and Cr–Mo steels as a small fatigue crack threshold in high-pressure hydrogen gas,” *Int. J. Hydrogen Energy*, vol. 43, no. 43, pp. 20133–20142, 2018, doi: 10.1016/j.ijhydene.2018.09.026.

[103] Y. Murakami and S. Matsuoka, “Effect of hydrogen on fatigue crack growth of metals,” *Eng. Fract. Mech.*, vol. 77, no. 11, pp. 1926–1940, 2010, doi: 10.1016/j.engfracmech.2010.04.012.

[104] R. P. Gangloff and B. P. Somerday, *Gaseous hydrogen embrittlement of materials in energy technologies: Volume 1*. Woodhead Publishing Ltd, 2011.

[105] R. P. Gangloff and B. P. Somerday, *Gaseous hydrogen embrittlement of materials in energy technologies: Volume 2*. Woodhead Publishing Ltd, 2011.

[106] S. Suresh and R. O. Ritchie, “Mechanistic dissimilarities between environmentally-influenced fatigue-crack propagation at near-threshold and higher growth rates in lower strength steels,” *Mater. Sci.*, vol. 16, no. 11, pp. 529–538, 1982.

[107] K. Shishime, M. Kubota, and Y. Kondo, “Effect of absorbed hydrogen on the near threshold fatigue crack growth behavior of short crack,” *Mater. Sci. Forum*, vol. 567–568, pp. 409–412, 2008, doi: 10.4028/www.scientific.net/msf.567-568.409.

[108] M. B. Djukic, G. M. Bakic, V. Sijacki Zeravcic, A. Sedmak, and B. Rajicic, “The synergistic action and interplay of hydrogen embrittlement mechanisms in steels and iron: Localized plasticity and decohesion,” *Eng. Fract. Mech.*, vol. 216, no. June, p. 106528, 2019, doi: 10.1016/j.engfracmech.2019.106528.

[109] H. Yang *et al.*, “Temperature Dependency of Hydrogen Embrittlement in Thermally H-precharged STS 304 Austenitic Stainless Steel,” *Met. Mater. Int.*, no. 0123456789, 2022, doi: 10.1007/s12540-022-01232-6.

[110] T. Michler and J. Naumann, “Hydrogen environment embrittlement of austenitic stainless steels at low temperatures,” *Int. J. Hydrogen Energy*, vol. 33, no. 8, pp. 2111–2122, 2008, doi: 10.1016/j.ijhydene.2008.02.021.

[111] T. Ogata, “Hydrogen Environment Embrittlement on Austenitic Stainless Steels from Room Temperature to Low Temperatures,” in *IOP Conference Series: Materials Science and Engineering*, 2015, vol. 102, pp. 1–8, doi: 10.1088/1757-899X/102/1/012005.

[112] C. San Marchi and B. P. Somerday, “Effects of high-pressure gaseous hydrogen on structural metals,” *SAE Tech. Pap. Ser.*, pp. 776–790, 2007, doi: 10.4271/2007-01-0433.

[113] A. W. Loginow and E. H. Phelps, “Steels for Seamless Hydrogen Pressure Vessels.,” *Trans. ASME*, pp. 274–282, 1974.

[114] H. G. Nelson and D. P. Williams, “Quantitative Observation of Hydrogen-Induced, Slow Crack Growth in a Low Alloy Steel,” 1973.

[115] H. G. Nelson, “On the mechanism of hydrogen-enhanced fatigue crack growth in ferritic steels,” 1976.

[116] P. Novak, R. Yuan, B. P. Somerday, P. Sofronis, and R. O. Ritchie, “A statistical, physical-based, micro-mechanical model of hydrogen-induced intergranular fracture in steel,” *J. Mech. Phys. Solids*, vol. 58, no. 2, pp. 206–226, 2010, doi: 10.1016/j.jmps.2009.10.005.

[117] W. Y. Choo and J. Y. Lee, “Effect of cold working on the hydrogen trapping phenomena in pure iron,” *Metall. Trans. A*, vol. 14, no. 7, pp. 1299–1305, 1983, doi: 10.1007/BF02664812.

[118] A. Campari, A. Alvaro, F. Ustolin, and N. Paltrinieri, “Calculation of the Damage Factor for the Hydrogen-Enhanced Fatigue in the RBI Framework,” in *Proceeding of the 33rd European Safety and Reliability Conference*, 2023, pp. 437–444, doi: 10.3850/978-981-18-8071-1_p022-cd.

[119] N. Yazdipour, D. Dunne, and E. Pereloma, “Effect of grain size on the hydrogen diffusion process in steel using cellular automaton approach,” *Mater. Sci. Forum*, vol. 706–709, pp. 1568–1573, 2012, doi: 10.4028/www.scientific.net/MSF.706-709.1568.

[120] K. S. Ghosh and D. K. Mondal, “Effect of grain size on mechanical electrochemical and hydrogen embrittlement behaviour of a micro-alloy steel,” *Mater. Sci. Eng. A*, vol. 559, pp. 693–705, 2013, doi: 10.1016/j.msea.2012.09.011.

[121] S. Chen, M. Zhao, and L. Rong, “Effect of grain size on the hydrogen embrittlement sensitivity of a precipitation strengthened Fe-Ni based alloy,” *Mater. Sci. Eng. A*, vol. 594, pp. 98–102, 2014, doi: 10.1016/j.msea.2013.11.062.

[122] J. F. Lancaster, *Metallurgy of welding*, Sixth Edit. Woodhead Publishing Ltd, 1999.

[123] N. Nanninga, J. Grochowsi, L. Heldt, and K. Rundman, “Role of microstructure, composition and hardness in resisting hydrogen embrittlement of fastener grade steels,” *Corros. Sci.*, vol. 52, no. 4, pp. 1237–1246, 2010, doi: 10.1016/j.corsci.2009.12.020.

[124] Y. Murakami, T. Kanezaki, Y. Mine, and S. Matsuoka, “Hydrogen Embrittlement Mechanism in Fatigue of Austenitic Stainless Steels,” *Metall. Mater. Trans. A Phys. Metall. Mater. Sci.*, vol. 39 A, no. 6, pp. 1327–1339, 2008, doi: 10.1007/s11661-008-9506-5.

[125] H. Matsunaga, O. Takakuwa, J. Yamabe, and S. Matsuoka, “Hydrogen-enhanced fatigue crack growth in steels and its frequency dependence,” *Philos. Trans. R. Soc. A Math. Phys. Eng. Sci.*, vol. 375, no. 2098, 2017, doi: 10.1098/rsta.2016.0412.

[126] A. M. Rashad, “A synopsis about perlite as building material - A best practice guide for Civil Engineer,” *Constr. Build. Mater.*, vol. 121, pp. 338–353, 2016, doi: 10.1016/j.conbuildmat.2016.06.001.

[127] E. Papa *et al.*, “Characterization of alkali bonded expanded perlite,” *Constr. Build. Mater.*, vol. 191, pp. 1139–1147, 2018, doi: 10.1016/j.conbuildmat.2018.10.086.

[128] K.D. Timmerhaus, Ed., *Advances in Cryogenic Engineering*, vol. 8. 1964.

[129] A. M. Swanger, J. E. Fesmire, J. Jacobson, M. Butts, and S. Cihlar, “Vacuum Pump-Down of the Annular Insulation Space for Large Field-Erected Liquid Hydrogen Storage Tanks,” *IOP Conf. Ser. Mater. Sci. Eng.*, vol. 1301, no. 1, p. 012066, 2024, doi: 10.1088/1757-899x/1301/1/012066.

[130] Sheth Insulations Pvt Ltd, “Perlite Insulation,” 2024. https://shethinsulations.in/perlite-insulation/.

[131] J. E. Fesmire, “Standardization in cryogenic insulation systems testing and performance data,” *Phys. Procedia*, vol. 67, pp. 1089–1097, 2015, doi: 10.1016/j.phpro.2015.06.205.

[132] J. P. Sass, J. E. Fesmire, Z. F. Nagy, S. J. Sojourner, D. L. Morris, and S. D. Augustynowicz, “Thermal Performance Comparison of Glass Microsphere and Perlite Insulation Systems for Liquid Hydrogen Storage,” in *AIP Conference Proceedings*, 2008, pp. 1375–1382.

[133] A. G. Krenn, R. C. Youngquist, and S. O. Starr, “Annular Air Leaks in a Liquid Hydrogen Storage Tank,” 2019.

[134] P. M. Angelopoulos, “Insights in the Physicochemical and Mechanical Properties and Characterization Methodology of Perlites,” *Minerals*, vol. 14, no. 1, 2024, doi: 10.3390/min14010113.

[135] M. Raji *et al.*, “Utilization of volcanic amorphous aluminosilicate rocks (perlite) as alternative materials in lightweight composites,” *Compos. Part B Eng.*, vol. 165, no. July 2018, pp. 47–54, 2019, doi: 10.1016/j.compositesb.2018.11.098.

[136] O. Çoban and T. Yilmaz, “Volcanic particle materials in polymer composites: a review,” *J. Mater. Sci.*, vol. 57, no. 36, pp. 16989–17020, 2022, doi: 10.1007/s10853-022-07664-0.

[137] N. Edres *et al.*, “Structural Characterization of Composites Based on Butadiene Rubber and Expanded Perlite,” *J. Compos. Sci.*, vol. 7, no. 12, pp. 1–18, 2023, doi: 10.3390/jcs7120487.

[138] A. M. Alghadi, S. Tirkes, and U. Tayfun, “Mechanical, thermo-mechanical and morphological characterization of ABS based composites loaded with perlite mineral,” *Mater. Res. Express*, vol. 7, no. 1, p. 15301, 2020, doi: 10.1088/2053-1591/ab551b.

[139] M. Mandic, B. Porankiewicz, and G. Danon, “An attempt at modelling of cutting forces in oak peripheral milling,” *BioResources*, vol. 10, no. 3, pp. 5476–5488, 2015, doi: 10.15376/biores.10.3.5476-5488.

[140] B. Szadkowski, A. Marzec, P. Rybinski, W. Zukowski, and M. Zaborski, “Characterization of ethylene-propylene composites filled with perlite and vermiculite minerals: Mechanical, barrier, and flammability properties,” *Materials (Basel).*, vol. 13, no. 3, 2020, doi: 10.3390/ma13030585.

[141] R. Kusiorowski, J. Witek, I. Majchrowicz, A. Kleta, and A. Jirsa-Ociepa, “Fire barrier based on expanded perlite composites,” *Sel. Pap. 13th Int. Conf. "Modern Build. Mater. Struct. Tech. MBMST 2019*, no. May, pp. 85–93, 2019, doi: 10.3846/mbmst.2019.047.

[142] R. Eberwein, A. Hajhariri, D. Camplese, G. E. Scarponi, V. Cozzani, and F. Otremba, “Experimental investigation on the behavior of thermal super insulation materials for cryogenic storage tanks in fire incidents,” *Process Saf. Environ. Prot.*, vol. 187, pp. 240–248, Jul. 2024, doi: 10.1016/j.psep.2024.04.131.

[143] R. Shigapov and O. Kovalchuk, “Investigation of Seismic Behaviour of Low-Temperature Tanks Taking into Account Loose Perlite Insulation,” *IOP Conf. Ser. Mater. Sci. Eng.*, vol. 661, no. 1, 2019, doi: 10.1088/1757-899X/661/1/012015.

[144] S. Füchsl, F. Rheude, and H. Röder, “Life cycle assessment (LCA) of thermal insulation materials: A critical review,” *Clean. Mater.*, 2022, [Online]. Available: https://doi.org/10.1016/j.clema.2022.100119.

[145] H. Hanna, “A Stir and Disinfect Technique to Recycle Perlite for Cost-Effective Greenhouse Tomato Production,” *J. Veg. Sci.*, 2006, [Online]. Available: https://doi.org/10.1300/J484v12n01_05.

[146] A. Sicakova, E. Kardosova, and M. Spak, “Perlite Application and Performance Comparison to Conventional Additives in Blended Cement,” *Eng. Technol. Appl. Sci. Res.*, 2020, [Online]. Available: https://doi.org/10.48084/etasr.3487.

[147] Z. Khoshraftar, H. Masoumi, and A. Ghaemi, “On the performance of perlite as a mineral adsorbent for heavy metals ions and dye removal from industrial wastewater: A review of the state of the art,” *Case Stud. Chem. Environ. Eng.*, 2023, [Online]. Available: https://doi.org/10.1016/j.cscee.2023.100385.

[148] Perlite Institute Inc, “Perlite: The Most Sustainable Insulation Solution for Buildings,” 2023. https://www.perlite.org/perlite-the-most-sustainable-insulation-solution-for-buildings/ (accessed Dec. 11, 2024).

[149] K. J. Jaya Kumar, “Heat transfer analysis of light weight cryogenic tank for space vehicles,” *Indian J. Sci. Technol.*, vol. 8, no. 4, pp. 314–319, 2015, doi: 10.17485/ijst/2015/v8i4/62291.

[150] B. E. Scholtens, J. E. Fesmire, J. P. Sass, S. D. Augustynowicz, and K. W.Heckle, “CRYOGENIC THERMAL PERFORMANCE TESTING OF BULK-FILL AND AEROGEL INSULATION MATERIALS,” 2007, pp. 1–10.

[151] J. E. Fesmire, J. B. Ancipink, A. M. Swanger, S. White, and D. Yarbrough, “Thermal conductivity of aerogel blanket insulation under cryogenic-vacuum conditions in different gas environments,” *IOP Conf. Ser. Mater. Sci. Eng.*, vol. 278, no. 1, 2017, doi: 10.1088/1757-899X/278/1/012198.

[152] R. Baetens, B. P. Jelle, and A. Gustavsen, “Aerogel insulation for building applications: A state-of-the-art review,” *Energy Build.*, vol. 43, no. 4, pp. 761–769, 2011, doi: 10.1016/j.enbuild.2010.12.012.

[153] J. E. Fesmire, S. D. Augustynowici, and S. Rouanetc, “AEROGEL BEADS AS CRYOGENIC THERMAL INSULATION SYSTEM,” p. 6, 2015.

[154] J. H. Kim, J. H. Ahn, J. D. Kim, D. H. Lee, S. K. Kim, and J. M. Lee, “Influence of silica-aerogel on mechanical characteristics of polyurethane-based composites: Thermal conductivity and strength,” *Materials (Basel).*, vol. 14, no. 7, 2021, doi: 10.3390/ma14071790.

[155] L. Edward and L. Filip, “Influence of vacuum level on insulation thermal performance for LNG cryogenic road tankers,” *MATEC Web Conf.*, vol. 240, 2018, doi: 10.1051/matecconf/201824001019.

[156] S. Salimian, A. Zadhoush, M. Naeimirad, R. Kotek, and S. Ramakrishna, “A review on aerogel: 3D nanoporous structured fillers in polymer-based nanocomposites,” *Polym. Compos.*, vol. 39, no. 10, pp. 3383–3408, 2018, doi: 10.1002/pc.24412.

[157] S. S. Sonu, N. Rai, and I. Chauhan, “Multifunctional Aerogels: A comprehensive review on types, synthesis and applications of aerogels,” *J. Sol-Gel Sci. Technol.*, vol. 105, no. 2, pp. 324–336, 2023, doi: 10.1007/s10971-022-06026-1.

[158] P. Qi, H. Zhu, F. Borodich, and Q. Peng, “A Review of the Mechanical Properties of Graphene Aerogel Materials: Experimental Measurements and Computer Simulations,” *Materials (Basel).*, vol. 16, no. 5, 2023, doi: 10.3390/ma16051800.

[159] X. Zhang, J. Yu, C. Zhao, and Y. Si, “Elastic SiC Aerogel for Thermal Insulation: A Systematic Review,” *Small*, vol. 20, no. 32, pp. 1–20, 2024, doi: 10.1002/smll.202311464.

[160] N. Buchtová, C. Pradille, J. L. Bouvard, and T. Budtova, “Mechanical properties of cellulose aerogels and cryogels,” *Soft Matter*, vol. 15, no. 39, pp. 7901–7908, 2019, doi: 10.1039/c9sm01028a.

[161] L. Wang *et al.*, “Enhancing aerogel mechanical properties with incorporation of POSS,” *Ceram. Int.*, vol. 45, no. 12, pp. 14586–14593, 2019, doi: 10.1016/j.ceramint.2019.04.176.

[162] X. Hou, R. Zhang, and B. Wang, “Novel self-reinforcing ZrO2–SiO2 aerogels with high mechanical strength and ultralow thermal conductivity,” *Ceram. Int.*, vol. 44, no. 13, pp. 15440–15445, 2018, doi: 10.1016/j.ceramint.2018.05.199.

[163] T. Liu *et al.*, “Aramid reinforced polyimide aerogel composites with high-mechanical strength for thermal insulation material,” *Polym. Adv. Technol.*, vol. 34, no. 5, pp. 1769–1776, 2023, doi: 10.1002/pat.5980.

[164] Z. Zhu, H. Yao, J. Dong, Z. Qian, W. Dong, and D. Long, “High-mechanical-strength polyimide aerogels crosslinked with 4, 4′-oxydianiline-functionalized carbon nanotubes,” *Carbon N. Y.*, vol. 144, pp. 24–31, 2019, doi: 10.1016/j.carbon.2018.11.057.

[165] A. K. Kasar, S. Tian, G. Xiong, and P. L. Menezes, “Graphene aerogel and its composites: synthesis, properties and applications,” *J. Porous Mater.*, vol. 29, no. 4, pp. 1011–1025, 2022, doi: 10.1007/s10934-022-01230-4.

[166] J. H. Lee and S. J. Park, “Recent advances in preparations and applications of carbon aerogels: A review,” *Carbon N. Y.*, vol. 163, pp. 1–18, 2020, doi: 10.1016/j.carbon.2020.02.073.

[167] R. Sankaran and P. L. Show, “Preliminary Investigation on Mechanical Properties of Hollow Glass Spheres,” *Mater. Sci. Forum*, vol. 1108, pp. 17–22, 2023, doi: 10.4028/p-a5ofga.

[168] M. Mahmoud, J. Kraxner, H. Elsayed, E. Bernardo, and D. Galusek, “Fabrication and environmental applications of glass microspheres: A review,” *Ceram. Int.*, vol. 49, no. 24, pp. 39745–39759, 2023, doi: 10.1016/j.ceramint.2023.10.040.

[169] I. G. Watkins and M. Prado, “Mechanical Properties of Glass Microspheres,” *Procedia Mater. Sci.*, vol. 8, pp. 1057–1065, 2015, doi: 10.1016/j.mspro.2015.04.168.

[170] T. Budtova, *Cellulose II aerogels: a review*, vol. 26, no. 1. Springer Netherlands, 2019.

[171] Z. A. Abdul Halim, M. A. Mat Yajid, M. H. Idris, and H. Hamdan, “Effects of silica aerogel particle sizes on the thermal–mechanical properties of silica aerogel–unsaturated polyester composites,” *Plast. Rubber Compos.*, vol. 46, no. 4, pp. 184–192, 2017, doi: 10.1080/14658011.2017.1306913.

[172] Y. Xu *et al.*, “High-strength, thermal-insulating, fire-safe bio-based organic lightweight aerogel based on 3D network construction of natural tubular fibers,” *Compos. Part B Eng.*, vol. 261, Jul. 2023, doi: 10.1016/j.compositesb.2023.110809.

[173] K. S. Liu, X. F. Zheng, C. H. Hsieh, and S. K. Lee, “The application of silica-based aerogel board on the fire resistance and thermal insulation performance enhancement

of existing external wall system retrofit," *Energies*, vol. 14, no. 15, Aug. 2021, doi: 10.3390/en14154518.

[174] I. Turhan Kara, B. Kiyak, N. Colak Gunes, and S. Yucel, "Life cycle assessment of aerogels: a critical review," *J. Sol-Gel Sci. Technol.*, vol. 111, no. 2, pp. 618–649, 2024.

[175] L. Huber, S. Zhao, W. J. Malfait, S. Vares, and M. M. Koebel, "Fast and Minimal-Solvent Production of Superinsulating Silica Aerogel Granulate," *Angew. Chemie Int. Ed.*, vol. 56, no. 17, pp. 4753–4756, 2017.

[176] C. A. Brühl and J. G. Zaller, "Biodiversity decline as a consequence of an inappropriate environmental risk assessment of pesticides," *Front. Environ. Sci.*, vol. 7, no. 464007, 2019.

[177] J. P. Vareda, C. A. García-González, A. J. Valente, R. Simón-Vázquez, M. Stipetic, and L. Durães, "Insights on toxicity, safe handling and disposal of silica aerogels and amorphous nanoparticles," *Environ. Sci. Nano*, vol. 8, no. 5, pp. 1177–1195, 2021.

[178] A. Dhawan, R. Shanker, M. Das, and K. C. Gupta, "Guidance for safe handling of nanomaterials," *J. Biomed. Nanotechnol.*, vol. 7, no. 1, pp. 218–224, 2011.

[179] J. E. Fesmire, B. E. Coffman, B. J. Meneghelli, and K. W. Heckle, "Spray-on foam insulations for launch vehicle cryogenic tanks," *Cryogenics (Guildf).*, vol. 52, no. 4–6, pp. 251–261, 2012, doi: 10.1016/j.cryogenics.2012.01.018.

[180] P. Foams, "Cryogenic Insulation — Towards Environmentally Friendly," 2024.

[181] J. E. Fesmire, "Layered composite thermal insulation system for nonvacuum cryogenic applications," *Cryogenics (Guildf).*, vol. 74, pp. 154–165, 2016, doi: 10.1016/j.cryogenics.2015.10.008.

[182] J. Wang, C. Zhang, Y. Deng, and P. Zhang, "A Review of Research on the Effect of Temperature on the Properties of Polyurethane Foams," *Polymers (Basel).*, vol. 14, no. 21, 2022, doi: 10.3390/polym14214586.

[183] S. Kalia and S. Y. Fu, *Polymers at Cryogenic Temperatures*. Springer Nature, 203–244, 2013.

[184] X. B. Zhang *et al.*, "Experimental study on cryogenic moisture uptake in polyurethane foam insulation material," *Cryogenics (Guildf).*, vol. 52, no. 12, pp. 810–815, 2012, doi: 10.1016/j.cryogenics.2012.10.001.

[185] U. Berardi, "The impact of aging and environmental conditions on the effective thermal conductivity of several foam materials," *Energy*, vol. 182, pp. 777–794, 2019, doi: 10.1016/j.energy.2019.06.022.

[186] U. Stirna, I. Beverte, V. Yakushin, and U. Cabulis, "Mechanical properties of rigid polyurethane foams at room and cryogenic temperatures," *J. Cell. Plast.*, vol. 47, no. 4, pp. 337–355, 2011, doi: 10.1177/0021955X11398381.

[187] P. Bartczak *et al.*, "Closed-cell polyurethane spray foam obtained with novel TiO2–ZnO hybrid fillers – mechanical, insulating properties and microbial purity," *J. Build. Eng.*, vol. 65, no. June 2022, 2023, doi: 10.1016/j.jobe.2022.105760.

[188] K. Singh, A. Ohlan, P. Saini, and S. K. Dhawan, "Polyurethane foam and fire safety," *Polym. Adv. Technol.*, no. November 2007, pp. 229–236, 2008, doi: 10.1002/pat.

[189] P. H. Schuerer, J. H. Ehl, and W. P. Prasthofer, "Cryogenic Insulation Strength and Bond Tester," Washington, D.C., 1985.

[190] M. Pailino and F. Teixeira-Dias, *On the use of polyurethane foam paddings to improve*

passive safety in crashworthiness applications. 2021.

[191] D. Rescigno, “Analysis of Environmental Factors and Operating Conditions on Degradation Patters of Aircraft Systems for Hydrogen-Based Power Generation,” 2024.

[192] Ecotelligent Homes, “Environmental impacts of spray foam insulation,” 2024. https://www.ecotelligenthomes.com/environmental-impacts-of-spray-foam-insulation/ (accessed Dec. 12, 2024).

[193] The Chemours Company FC, “Spray Foam Insulation Goes Green: Next Generation Spray Foam Continues to Provide Superior Insulation - Now With a Smaller Environmental Footprint,” 2018. https://www.opteon.com/en/-/media/files/opteon/opteon-spray-foam-insulation-goes-green-white-paper.pdf?rev=b9e8afb1e7864f81b2c113c6a24fb8f5&hash=0A3EE0795536701B8EC01DB22FCADFBB (accessed Dec. 12, 2024).

[194] S. Roy, “Applying Life Cycle Assessment (LCA) in Process Industry - The Chemours Experience,” in *Encyclopedia of Sustainable Technologies*, Elsevier, 2017, pp. 357–362.

[195] M. Wildnauer, M. Hegeman, T. Montalbo, and S. Murphy, “Life Cycle Assessment of Spray Polyurethane Foam Insulation - SPFA EPD Background Report,” 2018.

[196] GreenMatch, “Is Spray Foam Insulation Bad for the Environment?,” 2024. https://www.greenmatch.co.uk/blog/is-spray-foam-insulation-bad-for-the-environment (accessed Dec. 12, 2024).

[197] X. Qi, C. Gao, Z. Zhang, S. Chen, B. Li, and S. Wei, “Production and characterization of hollow glass microspheres with high diffusivity for hydrogen storage,” *Int. J. Hydrogen Energy*, vol. 37, no. 2, pp. 1518–1530, 2012, doi: 10.1016/j.ijhydene.2011.10.034.

[198] J. E. Fesmire, “Research and Development History of Glass Bubbles Bulk-Fill Thermal Insulation Systems for Large-Scale Cryogenic Liquid Hydrogen Storage Tanks,” 2017.

[199] S. Sankaran, B. N. Ravishankar, K. Ravi Sekhar, S. Dasgupta, and M. N. Jagdish Kumar, *Syntactic foams for multifunctional applications*. 2016.

[200] B. Karasu, İ. Demirel, A. Öztuvan, and B. Özdemir, “Glass Microspheres,” *El-Cezeri J. Sci. Eng.*, vol. 6, no. 3, pp. 613–641, 2019, doi: 10.31202/ecjse.562013.

[201] C. Jiao, H. Wang, S. Li, and X. Chen, “Fire hazard reduction of hollow glass microspheres in thermoplastic polyurethane composites,” *J. Hazard. Mater.*, vol. 332, pp. 176–184, 2017, doi: 10.1016/j.jhazmat.2017.02.019.

[202] R. W. Werlink, J. E. Fesmire, and J. P. Sass, “Vibration considerations for cryogenic tanks using glass bubbles insulation,” *AIP Conf. Proc.*, vol. 1434, no. 57, pp. 55–65, 2012, [Online]. Available: https://ntrs.nasa.gov/api/citations/20110014398/downloads/20110014398.pdf.

[203] J. E. Fesmire, “Research and Development History of Glass Bubbles Bulk-Fill Thermal Insulation Systems for Large-Scale Cryogenic Liquid Hydrogen Storage Tanks,” pp. 1–10, 2017.

[204] M. Delogu, L. Zanchi, S. Maltese, A. Bonoli, and M. Pierini, “Environmental and economic life cycle assessment of a lightweight solution for an automotive component: A comparison between talc-filled and hollow glass microspheres-reinforced polymer composites,” *J. Clean. Prod.*, pp. 548–560, 139AD, doi: 10.1016/j.jclepro.2016.08.079.

[205] R. D. Schlanbusch, B. P. Jelle, L. I. Christie Sandberg, S. M. Fufa, and T. Gao,

"Integration of life cycle assessment in the design of hollow silica nanospheres for thermal insulation applications," *Build. Environ.*, vol. 80, pp. 115–124, 2014, doi: 10.1016/j.buildenv.2014.05.010.

[206] 3M, "3M™ Glass Bubbles Compounding and Injection Molding Guidelines Performance under pressure." .

[207] D. Camplese *et al.*, "Modeling the performance of multilayer insulation in cryogenic tanks undergoing external fire scenarios," *Process Saf. Environ. Prot.*, vol. 186, no. April, pp. 1169–1182, 2024, doi: 10.1016/j.psep.2024.04.061.

[208] A. I. Plokhikh, D. V. Vlasova, K. B. Polikevich, and A. A. Minakov, "Mechanical properties of multilayer materials," *IOP Conf. Ser. Mater. Sci. Eng.*, vol. 525, no. 1, pp. 0–6, 2019, doi: 10.1088/1757-899X/525/1/012045.

[209] J. E. Fesmire and W. L. Johnson, "Cylindrical cryogenic calorimeter testing of six types of multilayer insulation systems," *Cryogenics (Guildf).*, vol. 89, no. November 2017, pp. 58–75, 2018, doi: 10.1016/j.cryogenics.2017.11.004.

[210] Y. Huang *et al.*, "Modeling and experimental study on combination of foam and variable density multilayer insulation for cryogen storage," *Energy*, vol. 123, pp. 487–498, 2017, doi: 10.1016/j.energy.2017.01.147.

[211] B. Wang, Y. H. Huang, P. Li, P. J. Sun, Z. C. Chen, and J. Y. Wu, "Optimization of variable density multilayer insulation for cryogenic application and experimental validation," *Cryogenics (Guildf).*, vol. 80, pp. 154–163, 2016, doi: 10.1016/j.cryogenics.2016.10.006.

[212] J. E. Fesmire, S. D. Augustynowicz, and B. E. Scholtens, "Robust multilayer insulation for cryogenic systems," *AIP Conf. Proc.*, vol. 985, no. April 2006, pp. 1359–1366, 2008, doi: 10.1063/1.2908494.

[213] B. Deng *et al.*, "Study of the thermal performance of multilayer insulation used in cryogenic transfer lines," *Cryogenics (Guildf).*, vol. 100, no. August 2018, pp. 114–122, 2019, doi: 10.1016/j.cryogenics.2019.01.005.

[214] R. Eberwein, A. Hajhariri, D. Camplese, G. E. Scarponi, V. Cozzani, and F. Otremba, "Experimental Research Of A Tank For A Cryogenic Fluid With a Wall Rupture In a Fire Scenario," 2024.

[215] F. Ustolin, T. Iannaccone, V. Cozzani, S. Jafarzadeh, and N. Paltrinieri, "Time to Failure Estimation of Cryogenic Liquefied Tanks Exposed to a Fire," in *31st European Safety and Reliability Conference*, 2021, pp. 935–942, doi: 10.3850/978-981-18-2016-8_182-cd.

[216] L. Swanstrom, H. Reiss, and O. Y. Troitsky, "Environmental Balances of Thermal Superinsulations," *Int. J. Thermophys.*, vol. 28, no. 5, pp. 1653–1667, 2005, doi: 10.1007/s10765-007-0148-4.

[217] M. Gonçalves, N. Simões, C. Serra, and I. Flores-Colen, "A review of the challenges posed by the use of vacuum panels in external insulation finishing systems," *Appl. Energy*, vol. 257, no. June 2019, p. 114028, 2020, doi: 10.1016/j.apenergy.2019.114028.

[218] R. Baetens *et al.*, "Vacuum insulation panels for building applications: A review and beyond," *Energy Build.*, vol. 42, no. 2, pp. 147–172, 2010, doi: 10.1016/j.enbuild.2009.09.005.

[219] D. Božiček, J. Peterková, J. Zach, and M. Košir, "Vacuum insulation panels: An overview of research literature with an emphasis on environmental and economic studies for building applications," *Renew. Sustain. Energy Rev.*, vol. 189, no.

September 2023, 2024, doi: 10.1016/j.rser.2023.113849.

[220] S. Verma and H. Singh, “Vacuum insulation panels for refrigerators,” *Int. J. Refrig.*, vol. 112, pp. 215–228, 2020, doi: 10.1016/j.ijrefrig.2019.12.007.

[221] P. Mukhopadhyaya, K. Kumaran, N. Normandin, D. van Reenen, and J. Lackey, “High-Performance Vacuum Insulation Panel: Development of Alternative Core Materials,” *J. Cold Reg. Eng.*, vol. 22, no. 4, pp. 103–123, 2008, doi: 10.1061/(asce)0887-381x(2008)22:4(103).

[222] S. E. Kalnæs and B. P. Jelle, “Vacuum insulation panel products: A state-of-the-art review and future research pathways,” *Appl. Energy*, vol. 116, no. 7465, pp. 355–375, 2014, doi: 10.1016/j.apenergy.2013.11.032.

[223] M. Davraz and H. C. Bayrakci, “Performance properties of vacuum insulation panels produced with various filling materials,” *Sci. Eng. Compos. Mater.*, vol. 21, no. 4, pp. 521–527, 2014, doi: 10.1515/secm-2013-0162.

[224] D. Kaushik, H. Singh, and S. A. Tassou, “Vacuum insulation panels for high-temperature applications – Design principles, challenges and pathways,” *Therm. Sci. Eng. Prog.*, vol. 48, no. October 2023, p. 102415, 2024, doi: 10.1016/j.tsep.2024.102415.

[225] D. H. Lee *et al.*, “Evaluation of Effective Thermal Conductivity of Vacuum Insulation System in Cryogenic Environment for Liquid Hydrogen Vessel Application,” *Proc. Int. Offshore Polar Eng. Conf.*, pp. 3478–3482, 2023.

[226] G. Volschenk, M. O’Shea, and B. Shaughnessy, “A novel approach to thermal insulation modelling in soft and medium vacuum insulation systems,” *Cryogenics (Guildf).*, vol. 144, no. May, p. 103946, 2024, doi: 10.1016/j.cryogenics.2024.103946.

[227] R. Zhang *et al.*, “Natural fibers as promising core materials of vacuum insulation panels,” *Constr. Build. Mater.*, vol. 453, no. November, 2024, doi: 10.1016/j.conbuildmat.2024.138890.

[228] F. E. Boafo, Z. Chen, C. Li, B. Li, and T. Xu, “Structure of vacuum insulation panel in building system,” *Energy Build.*, vol. 85, pp. 644–653, 2014, doi: 10.1016/j.enbuild.2014.06.055.

[229] Y. U. Kim, S. J. Chang, Y. J. Lee, H. No, G. S. Choi, and S. Kim, “Evaluation of the applicability of high insulation fire door with vacuum insulation panels: Experimental results from fire resistance, airtightness, and condensation tests,” *J. Build. Eng.*, vol. 43, Nov. 2021, doi: 10.1016/j.jobe.2021.102800.

[230] M. Dovjak, M. Košir, L. Pajek, N. Iglič, D. Božiček, and R. Kunič, “Environmental impact of thermal insulations: How do natural insulation products differ from synthetic ones?,” *IOP Conf. Ser. Earth Environ. Sci.*, 2017, [Online]. Available: https://doi.org/10.1088/1755-1315/92/1/012009.

[231] S. Resalati, T. Okoroafor, P. Henshall, N. Simões, M. Gonçalves, and M. Alam, “Comparative life cycle assessment of different vacuum insulation panel core materials using a cradle to gate approach,” *Build. Environ.*, vol. 188, p. 107501, 2021, [Online]. Available: https://doi.org/10.1016/j.buildenv.2020.107501.

[232] W. Jiang, P. Sun, P. Li, Z. Zuo, and Y. Huang, “Transient thermal behavior of multi-layer insulation coupled with vapor cooled shield used for liquid hydrogen storage tank,” *Energy*, vol. 231, p. 120859, 2021, doi: 10.1016/j.energy.2021.120859.

[233] R. B. Scott, “Thermal design of large storage vessels for liquid hydrogen and helium,” *J. Res. Natl. Bur. Stand. (1934).*, vol. 58, no. 6, p. 317, 1957, doi: 10.6028/jres.058.038.

[234] G. Cunnington, “Thermodynamic optimization of a cryogenic storage system for minimum boil-off,” 1982.

[235] J. C. Chato and J. M. Khodadadi, “Optimization of cooled shields in insulations,” *J. Heat Transfer*, vol. 106, no. 4, pp. 871–875, 1984, doi: 10.1115/1.3246766.

[236] T. Nast, D. Frank, and K. Burns, “Cryogenic propellant boil-off reduction approaches,” 2011.

[237] S. Y. Kim and B. H. Kang, “Thermal design analysis of a liquid hydrogen vessel,” *Int. J. Hydrogen Energy*, vol. 25, no. 2, pp. 133–141, 2000, doi: 10.1016/S0360-3199(99)00020-8.

[238] G. Babac, A. Sisman, and T. Cimen, “Two-dimensional thermal analysis of liquid hydrogen tank insulation,” *Int. J. Hydrogen Energy*, vol. 34, no. 15, pp. 6357–6363, 2009, doi: 10.1016/j.ijhydene.2009.05.052.

[239] Z. Liu, Y. Z. Li, and P. H. Gao, “Heat transfer analysis of cryogenic tank covered with vapor-cooled shield,” *J. Eng. Thermophys.*, vol. 40, pp. 629–634, 2019.

[240] W. B. Jiang, Z. Q. Zuo, Y. H. Huang, B. Wang, P. J. Sun, and P. Li, “Coupling optimization of composite insulation and vapor-cooled shield for on-orbit cryogenic storage tank,” *Cryogenics (Guildf).*, vol. 96, no. July, pp. 90–98, 2018, doi: 10.1016/j.cryogenics.2018.10.008.

[241] J. Zheng, L. Chen, J. Wang, Y. Zhou, and J. Wang, “Thermodynamic modelling and optimization of self-evaporation vapor cooled shield for liquid hydrogen storage tank,” *Energy Convers. Manag.*, vol. 184, no. December 2018, pp. 74–82, 2019, doi: 10.1016/j.enconman.2018.12.053.

[242] J. Zheng *et al.*, “Thermodynamic analysis and comparison of four insulation schemes for liquid hydrogen storage tank,” *Energy Convers. Manag.*, vol. 186, no. December 2018, pp. 526–534, 2019, doi: 10.1016/j.enconman.2019.02.073.

[243] J. Zheng, L. Chen, P. Wang, J. Zhang, J. Wang, and Y. Zhou, “A novel cryogenic insulation system of hollow glass microspheres and self-evaporation vapor-cooled shield for liquid hydrogen storage,” *Front. Energy*, vol. 14, no. 3, pp. 570–577, 2020, doi: 10.1007/s11708-019-0642-y.

[244] M. W. Liggett, “Space-based LH2 propellant storage system: subscale ground testing results,” *Cryogenics (Guildf).*, vol. 33, no. 4, pp. 438–442, 1993, doi: 10.1016/0011-2275(93)90174-M.

[245] D. Plachta, J. Stephens, W. Johnson, and M. Zagarola, “NASA cryocooler technology developments and goals to achieve zero boil-off and to liquefy cryogenic propellants for space exploration,” *Cryogenics (Guildf).*, vol. 94, no. July 2017, pp. 95–102, 2018, doi: 10.1016/j.cryogenics.2018.07.005.

[246] J. R. Feller *et al.*, “Analysis of Continuous Heat Exchangers for Cryogenic Boil-off Reduction,” in *AIP Conference Proceedings*, 2008, vol. 985, pp. 401–408.

[247] D. W. Plachta, R. J. Christie, E. Carlberg, and J. R. Feller, “Cryogenic propellant boil-off reduction system,” *AIP Conf. Proc.*, vol. 985, pp. 1457–1466, 2008, doi: 10.1063/1.2908506.

[248] G. Petitpas and S. M. Aceves, “Liquid hydrogen pump performance and durability testing through repeated cryogenic vessel filling to 700 bar,” *Int. J. Hydrogen Energy*, vol. 43, no. 39, pp. 18403–18420, Sep. 2018, doi: 10.1016/J.IJHYDENE.2018.08.097.

[249] G. Qiu *et al.*, “Numerical study on the dynamic process of reciprocating liquid hydrogen pumps for hydrogen refueling stations,” *Energy*, vol. 281, no. December

2022, 2023, doi: 10.1016/j.energy.2023.128303.

[250] International Organization for Standardization, *ISO 24490 - Cryogenic vessels – Pumps for cryogenic service*. 2016.

[251] K. Sotoodeh and O. Tobias, “Valve design considerations in liquid hydrogen systems to prevent failure,” pp. 1429–1441, 2023.

[252] K. Sotoodeh, “The Design of Pressure Safety and Relief Valves for Overpressure Protection : Essential considerations,” *Trans. Indian Natl. Acad. Eng.*, vol. 8, no. 2, pp. 273–287, 2023, doi: 10.1007/s41403-023-00396-w.

[253] R. Burgess, M. Post, W. Buttner, and C. Rivkin, “High Pressure Hydrogen Pressure Relief Devices : Accelerated Life Testing and Application Best Practices,” no. November, 2017.

[254] “International Organization for Standardization. Iso 21013- 1: cryogenic vessels - pressure relief accessories for cryogenic service: Part 1: reclosable pressure-relief valves.,” 2021.

[255] R. Meissner, P. Sieb, E. Wollenhaupt, S. Haberkorn, K. Wicke, and G. Wende, “Towards climate-neutral aviation : Assessment of maintenance requirements for airborne hydrogen storage and distribution systems,” *Int. J. Hydrogen Energy*, vol. 48, no. 75, pp. 29367–29390, 2023, doi: 10.1016/j.ijhydene.2023.04.058.

[256] International Organization for Standardization, *ISO 21013-1 - Cryogenic vessels – Pressure-relief accessories for cryogenic service – Part 1: Reclosable pressure-relief valves*. 2024.

[257] International Organization for Standardization, *ISO 21013-2 - Cryogenic vessels – Pressure-relief accessories for cryogenic service – Part 2: Non-reclosable pressure-relief valves*. 2018.

[258] International Organization for Standardization, *ISO 21011 - Cryogenic vessels – Valves for cryogenic service*. 2024.

[259] V. V. Osipov, M. J. Daigle, C. B. Muratov, M. Foygel, V. N. Smelyanskiy, and M. D. Watson, “Dynamical model of rocket propellant loading with liquid hydrogen,” *J. Spacecr. Rockets*, vol. 48, no. 6, pp. 987–998, 2011, doi: 10.2514/1.52587.

[260] K. Sotoodeh, “Soft material selection, application and the implications on valve design.” Valve World magazine, pp. 51–55, 2016.

[261] K. Sotoodeh, “A Review of Valve Stem Sealing to Prevent Leakage from the Valve and Its Effect on Valve Operation,” *J. Fail. Anal. Prev.*, vol. 21, no. 1, pp. 9–16, 2021, doi: 10.1007/s11668-020-01050-1.

[262] K. Sotoodeh, *Cryogenic valves for liquified natural gas plants*. USA: Elsevier (Gulf Professional Publishing), 2022.

[263] T. J. Peterson and J. G. Weisend II, *Properties of Fluids and Materials at Cryogenic Temperatures*. 2019.

[264] Z. Sápi and R. Butler, “Properties of cryogenic and low temperature composite materials – A review,” *Cryogenics (Guildf).*, vol. 111, no. November 2019, p. 103190, 2020, doi: 10.1016/j.cryogenics.2020.103190.

[265] A. De and I. Veris, *Fundamental Concepts of Liquid-Propellant Rocket Engines: Control Systems and Valves*. 2019.

[266] K. Sotoodeh, “Valve operability during a fire,” *J. Offshore Mech. Arct. Eng.*, vol. 141, no. 4, pp. 2–5, 2019, doi: 10.1115/1.4042073.

[267] J. Fydrych and G. Consogno, “A maintenance strategy for a multi-valve cryogenic distribution system,” *IOP Conf. Ser. Mater. Sci. Eng.*, vol. 278, no. 1, 2017, doi: 10.1088/1757-899X/278/1/012014.

[268] Y. S. Seo, S. M. Chung, and J. C. Park, “Multiphase-thermal flow simulation in a straight vacuum-insulated LH2 pipe: Cargo handling system in LH2 carrier,” *Ocean Eng.*, vol. 297, no. January, p. 117030, 2024, doi: 10.1016/j.oceaneng.2024.117030.

[269] J. H. Kim, D. K. Park, T. J. Kim, and J. K. Seo, “Thermal-Structural Characteristics of Multi-Layer Vacuum-Insulated Pipe for the Transfer of Cryogenic Liquid Hydrogen,” *Metals (Basel).*, vol. 12, no. 4, 2022, doi: 10.3390/met12040549.

[270] Q. Chen *et al.*, “Development and Recent Progress of Hoses for Cryogenic Liquid Transportation,” *Polymers (Basel).*, vol. 16, no. 7, 2024, doi: 10.3390/polym16070905.

[271] F. C. Bardi, H. Tang, M. Kulkarni, and X. Yin, “Structural analysis of cryogenic flexible hose,” *Proc. Int. Conf. Offshore Mech. Arct. Eng. - OMAE*, vol. 3, pp. 593–606, 2011, doi: 10.1115/OMAE2011-50238.

[272] J. Buitrago, S. T. Slocum, S. J. Hudak, and R. Long, “Cryogenic structural performance of corrugated pipe,” *Proc. Int. Conf. Offshore Mech. Arct. Eng. - OMAE*, vol. 6, pp. 331–342, 2010, doi: 10.1115/OMAE2010-21155.

[273] Y. Qiu, H. Yang, L. Tong, and L. Wang, “Research progress of cryogenic materials for storage and transportation of liquid hydrogen,” *Metals (Basel).*, vol. 11, no. 7, 2021, doi: 10.3390/met11071101.

[274] Compressed Gas Association, *CGA H-3 - Standard for cryogenic hydrogen storage*. 2024.

[275] European Industrial Gases Association, *EIGA 06/19 - Safety in storage, handling and distribution of liquid hydrogen*. 2019.

[276] European Industrial Gases Association, *EIGA 114/09 - Operation of static cryogenic vessels*. 2009.

[277] European Industrial Gases Association, *EIGA 119/04 - Periodic inspection of static cryogenic vessels*. 2004.

[278] European Industrial Gases Association, *EIGA PP 09/09 - Periodic Inspection and Reassessment of Static Cryogenic Vessels for use in the EU*. 2009.

[279] European Industrial Gases Association, *EIGA 151/05 - Prevention of Excessive Pressure during Filling of Cryogenic Vessels*. 2005.

[280] International Organization for Standardization, *ISO 13985 - Liquid hydrogen – Land vehicle fuel tanks*. 2006.

[281] International Organization for Standardization, *ISO 20421-1 - Cryogenic vessels – Large transportable vacuum-insulated vessels – Part 1: Design, fabrication, inspection and testing*. 2019.

[282] International Organization for Standardization, *ISO 20421-2 - Cryogenic vessels – Large transportable vacuum-insulated vessels – Part 2: Operational requirements*. 2017.

[283] European Committee for Standardization, *EN 13530-1 - Cryogenic vessels – Large transportable vacuum insulated vessels – Part 1: Fundamental requirements*. 2002.

[284] European Committee for Standardization, *EN 13530-2 - Cryogenic vessels – Large transportable vacuum insulated vessels – Part 2: Design, fabrication, inspection and testing*. 2002.

[285] European Committee for Standardization, *EN 13530-3 - Cryogenic vessels – Large transportable vacuum insulated vessels – Part 3: Operational requirements*. 2002.

[286] European Committee for Standardization, *EN 14398-1 - Cryogenic vessels – Large transportable non-vacuum insulated vessels – Part 1: Fundamental requirements*. 2003.

[287] European Committee for Standardization, *EN 14398-2 - Cryogenic vessels – Large transportable non-vacuum insulated vessels – Part 2: Design, fabrication, inspection and testing*. 2008.

[288] European Committee for Standardization, *EN 14398-3 - Cryogenic vessels – Large transportable non-vacuum insulated vessels – Part 3: Operational requirements*. 2003.

[289] International Organization for Standardization, *ISO 21029-1 - Cryogenic vessels – Transportable vacuum-insulated vessels of not more than 1000 liters volume – Part 1: Design, fabrication, inspection and tests*. 2019.

[290] International Organization for Standardization, *ISO 21029-2 - Cryogenic vessels – Transportable vacuum-insulated vessels of not more than 1000 liters volume – Part 2: Operational requirements*. 2015.

[291] European Committee for Standardization, *EN 1251-1 - Cryogenic vessels – Transportable vacuum insulated vessels of not more than 1000 liters volume – Part 1: Fundamental requirements*. 2000.

[292] European Committee for Standardization, *EN 1251-2 - Cryogenic vessels – Transportable vacuum insulated vessels of not more than 1000 liters volume – Part 2: Design, fabrication, inspection and testing*. 2000.

[293] European Committee for Standardization, *EN 1251-3 - Cryogenic vessels – Transportable vacuum insulated vessels of not more than 1000 liters volume – Part 3: Operational requirements*. 2000.

[294] International Organization for Standardization, *ISO 21009-1 - Cryogenic vessels – Static vacuum-insulated vessels – Part 1: Desing, fabrication, inspection and tests*. 2022.

[295] International Organization for Standardization, *ISO 21009-2 - Cryogenic vessels – Static vacuum-insulated vessels – Part 2: Operational requirements*. 2015.

[296] European Committee for Standardization, *EN 13458-1 - Cryogenic vessels – Static vacuum insulated vessels – Part 1: Fundamental requirements*. 2002.

[297] European Committee for Standardization, *EN 13458-2 - Cryogenic vessels – Static vacuum insulated vessels – Part 2: Design, fabrication, inspection and testing*. 2002.

[298] European Committee for Standardization, *EN 13458-3 - Cryogenic vessels – Static vacuum insulated vessels – Part 3: Operational requirements*. 2005.

[299] European Committee for Standardization, *EN 14197-1 - Cryogenic vessels – Static non-vacuum insulated vessels – Part 1: Fundamental requirements*. 2003.

[300] European Committee for Standardization, *EN 14197-2 - Cryogenic vessels – Static non-vacuum insulated vessels – Part 2: Design, fabrication, inspection and testing*. 2003.

[301] European Committee for Standardization, *EN 14197-3 - Cryogenic vessels – Static non-vacuum insulated vessels – Part 3: Operational requirements*. 2004.

[302] Compessed Gas Association, *CGA G-5.5 - Standard for hydrogen vent systems*. 2021.

[303] European Industrial Gases Association, *EIGA 24/18 - Vacuum-insulated cryogenic storage tank systems pressure protection devices*. 2018.

[304] European Committee for Standardization, *EN 1626 - Cryogenic vessels – Valves for cryogenic service*. 2008.

[305] International Organization for Standardization, *ISO 21013-3 - Cryogenic vessels – Pressure-relief accessories for cryogenic service – Part 3: Sizing and capacity determination*. 2016.

[306] International Organization for Standardization, *ISO 21013-4 - Cryogenic vessels – Pilot operated pressure relief devices – Part 4: Pressure-relief accessories for cryogenic service*. 2019.

[307] European Committee for Standardization, *EN 13648-1 - Cryogenic vessels – Safety devices for protection against excessive pressure – Part 1: Safety valves for cryogenic service*. 2008.

[308] European Committee for Standardization, *EN 13648-2 - Cryogenic vessels – Safety devices for protection against excessive pressure – Part 2: Bursting disc safety devices for cryogenic service*. 2002.

[309] European Committee for Standardization, *EN 13648-3 - Cryogenic vessels – Safety devices for protection against excessive pressure – Part 3: Determination of required discharge, capacity and sizing*. 2002.

[310] International Organization for Standardization, *ISO 21012 - Cryogenic vessels – Hoses*. 2024.

[311] European Committee for Standardization, *EN 12434 - Cryogenic vessels – Cryogenic flexible hoses*. 2000.

[312] European Committee for Standardization, *EN 13371 - Cryogenic vessels – Couplings for cryogenic service*. 2001.

[313] International Organization for Standardization, *ISO 28921-1 - Industrial valves – Isolating valves for low-temperature applications – Part 1: Design, manufacturing and production testing*. 2022.

[314] International Organization for Standardization, *ISO 28921-2 - Industrial valves – Isolating valves for low-temperature applications – Part 2: Type testing*. 2015.

[315] ASTM International, *ASTM C1774 - Standard Guide for Thermal Performance Testing of Cryogenic Insulation Systems*. 2024.

[316] ASTM International, *ASTM C740 - Standard Practice for Evacuated Reflective Insulation In Cryogenic Service*. 2019.

[317] European Industrial Gases Association, *EIGA TB 11/114 - Recommendations for the Prevention of Brittle failure of the Outer Jacket of Vacuum Insulated Cryogenic Storage Tanks*. 2014.

[318] International Organization for Standardization, *ISO 21010 - Cryogenic vessels – Gas/material compatibility*. 2017.

[319] European Committee for Standardization, *EN 1797 - Cryogenic vessels – Gas/material compatibility*. 2001.

[320] International Organization for Standardization, *ISO 21014 - Cryogenic vessels – Cryogenic insulation performance*. 2022.

[321] European Committee for Standardization, *EN 12213 - Cryogenic vessels – Methods*

for performance evaluation of thermal insulation. 1998.

[322] International Organization for Standardization, *ISO 21028-1 - Cryogenic vessels – Toughness requirements for materials at cryogenic temperature – Part 1: Temperatures below -80 °C*. 2016.

[323] European Committee for Standardization, *EN 1252-1 - Cryogenic vessels – Materials – Part 1: Toughness requirements for temperatures below -80 °C*. 1998.

[324] European Committee for Standardization, *EN 1252-2 - Cryogenic vessels – Materials – Part 2: Toughness requirements for temperatures between -80°C and -20°C*. 2001.

[325] International Organization for Standardization, *ISO 23208 - Cryogenic vessels – Cleanliness for cryogenic service*. 2020.

[326] European Committee for Standardization, *EN 12300 - Cryogenic vessels – Cleanliness for cryogenic service*. 2006.

[327] International Organization for Standardization, *ISO 20088-1 - Determination of the resistance to cryogenic spillage of insulation materials – Part 1: Liquid phase*. 2016.

[328] International Organization for Standardization, *ISO 20088-2 - Determination of the resistance to cryogenic spillage of insulation materials – Part 2: Vapour exposure*. 2020.

[329] International Organization for Standardization, *ISO 20088-3 - Determination of the resistance to cryogenic spillage of insulation materials – Part 3: Jet release*. 2018.

[330] International Organization for Standardization, *ISO 16478 - Thermal insulation products – Vacuum insulation panels (VIPs) – Specification*. 2023.

[331] European Committee for Standardization, *EN 17140 - Thermal insulation products for buildings – Factory-made vacuum insulation panels (VIP) – Specification*. 2020.

[332] Standardization Administration of the People's Republic of China, *GB/T 37608 - Vacuum insulation panels (VIP)*. 2019.